NOVEL PHASES AND FIELD THEORETICAL METHODS IN QUANTUM GASES

by

Xiaopeng Li

Bachelor of Science, University of Science and Technology of China, 2008

Master of Science, University of Pittsburgh, 2009

Submitted to the Graduate Faculty of

the Kenneth P. Dietrich School of Arts and Sciences in partial fulfillment

of the requirements for the degree of

Doctor of Philosophy

University of Pittsburgh

2013

UNIVERSITY OF PITTSBURGH

DEPARTMENT OF PHYSICS AND ASTRONOMY

This dissertation was presented

by

Xiaopeng Li

It was defended on

April 24, 2013

and approved by

W. Vincent Liu, Associate Professor, Department of Physics and Astronomy

Daniel Boyanovsky, Professor, Department of Physics and Astronomy

Andrew Daley, Assistant Professor, Department of Physics and Astronomy

Jeremy Levy, Professor, Department of Physics and Astronomy

Ira Rothstein, Professor, Department of Physics, Carnegie Mellon University

Dissertation Director: W. Vincent Liu, Associate Professor, Department of Physics and Astronomy

NOVEL PHASES AND FIELD THEORETICAL METHODS IN QUANTUM GASES

Xiaopeng Li, PhD

University of Pittsburgh, 2013

We study quantum phases and transitions in ultra-cold quantum gases, beyond the scope of conventional condensed matter systems. The study focuses on three major thrusts. The first thrust is the study of cold ensembles of bosonic or fermionic atoms in the higher orbital bands of optical lattices. Orbital and topological quantum physics is systematically explored for various lattice geometries, to be outlined below. The second is the low dimensional spin-imbalanced fermions in the Fulde-Ferrell-Larkin-Ovchinnikov (FFLO) phase. We analyze its thermal instability towards Berezinsky-Kosterlitz-Thouless (BKT) phase transitions driven by different topological defects at finite temperature. The third is the theoretical search for a mechanism to achieve a Bose-Einstein crystal phase for bosons in the ground state. A new class of two-body interactions characterized by strong momentum-dependence is found to give rise to such a quantum state. It is different than but related to the long-debated concept of supersolidity. The first thrust forms the main part of the dissertation. Meta-stable phases of high orbital bosons and fermions have been explored for different lattice geometries such as square and bipartite lattices. Exotic Mott and superfluid phases are studied in both one and two dimensions. Quantum and thermal phase transitions, associated with time reversal symmetry breaking and their experimental signatures are discussed. In particular a quantum "disordered" superfluid phase, beyond the mean field description, is found in one dimension. The challenging problem of probing time reversal symmetry breaking is solved. Besides, a one-dimensional fermionic optical ladder with coupled s- and p-orbitals is shown to mimic spin-orbit interactions and exhibit topological insulator and topological superconducting

phases. Charge fractionalization is shown to be realizable in such an sp-orbital ladder.

TABLE OF CONTENTS

LIST OF TABLES

LIST OF FIGURES

PREFACE

I would like to thank my supervisor Prof. W. Vincent Liu for his guidance and support during my PHD study. With his guidance, these five years working with Prof. Liu are delightful and productive for me. His insights strengthened my determination to be a theoretical physicist and will be constantly helpful in my whole career. I feel grateful and fortunate to be his student.

I enjoy collaborations with Prof. Erhai Zhao, Prof. Leon Balents, Prof. Arun Paramekanti, Dr. Zixu Zhang and Dr. Chungwei Lin. Prof. Erhai Zhao and Dr. Chungwei Lin were post-docs when I was a fresh graduate student. I benefited tremendously from discussions with them in my early stage. I am indebted to Prof. Leon Balents for his supervision during my visit in Kavli Institute for Theoretical Physics, University of California, Santa Barbara as a graduate fellow. My background is significantly broadened working with him on oxide heterostructures.

Also, I would like to thank my committee members Prof. Daniel Boyanovsky, Prof. Andrew Daley, Prof. Ira Rothstein and Prof. Jeremy Levy. I have benefited a lot from discussions with them. In particular, Prof. Daniel Boyanovsky and Prof. Andrew Daley's expert knowledge on phase transitions and dynamical stabilities are very helpful.

Finally, I thank my parents Zhixing Li and Lingzhi Li, and my wife Ranlan Lin for their constant support of my career.

1.0 INTRODUCTION

Starting from the first observation of Bose-Einstein condensation with ultracold atoms in 1995, the study of many-body physics in this field has exploded. With rapid experimental developments, ultracold bosons and fermions provide versatile and controllable systems to study correlated quantum condensed matter physics far beyond the scope of conventional systems [3, 4, 5], e.g., electron gases and liquid Helium. Despite the densities of the particles in the trapping potentials being dilute (more than five orders of magnitude less than air) [3], strong correlation effects can be observed in ultra-cold quantum gases, thanks to the strong interactions induced by Feshbach resonances [6].

Studying correlated physics of bosons is of particular interest in ultracold quantum gases [7, 8, 9, 10, 11]. Quantum phases and phase transitions of bosons in optical lattices were studied in recent years. The lowest band Mott insulating and superfluid phases have been observed. It was expected exotic stable phases (e.g., a Bose-Einstein condensate with a complex condensate wavefunction) for bosons are prohibited due to Feynman's "no-node" theorem [12], which states that the groundstate N-body wavefunction of a non-relativistic boson system has no nodes (see Appendix C). However, Bose-Einstein condensates with complex condensate wavefunctions have recently been reported in an optical lattice with high energy orbital bands loaded [13, 14, 15, 16]. Our work in Ref. [17, 18] is motivated by understanding the exotic phases with high orbital degrees of freedom involved.

In Ref. [18], a quantum orbital gas in a one-dimensional optical lattice is studied. The orbital degrees of freedom p_x and p_y, which are analogous to two spin-1/2 components, have been considered. With the matrix product state method, a rich phase diagram is established. The orbital ordering, a unique feature of the quantum orbital gas, provides new phases and phase transitions. Indeed, Mott and superfluid phases with and without orbital order are

found in numerical simulations. The system has a phase transition from the anti-ferro-orbital superfluid phase to the para-orbital superfluid phase. The para-orbital superfluid phase is a quantum "disorder" phase. This phase transition is related to the time reversal symmetry breaking. Experimental signatures of this phase transition are provided. Observing the time reversal symmetry breaking in one dimension is attracting growing interest of both experimentalists and theorists. Besides numerical methods, field-theoretical methods are also applied to understand the hidden mechanism leading to the orbital order in the superfluid phase. The phase transition in the superfluid from orbital order to disorder is found to be driven by quantum fluctuations of phase difference of two orbital components. Effective field theory predicts that the anti-ferro-orbital superfluid phase has one gapless mode, and that the para-orbital superfluid phase has two gapless modes. Across the phase transition from para-orbital to anti-ferro-orbital, the fluctuations of one gapless mode become locked. With field theory analysis, the stability and the possible localization transitions of the superfluid phases are also discussed.

The other subject I contribute to is to study high-Tc superconductivity in ultracold quantum gases [19, 20]. A system of attractive spin-imbalanced fermions (e.g., ^{6}Li) in optical lattices [21, 22, 23, 24] is carried out to simulate challenging High-Tc problems. With a well-known Lieb-Mattis transformation [25], the attractive Fermi Hubbard with spin-imbalance maps to the repulsive Hubbard model away from half filling [25]. The quantum simulator—the attractive spin-imbalanced fermion gas—will provide an answer to the long-standing question whether repulsive Hubbard model [26] with strong interaction supports d-wave superconductivity. The quantum simulator has the advantage of exploring the whole doping regime compared with high-Tc Cuprates. A method I contribute to in Ref. [20] based on the background field theory approach, includes thermal fluctuations of topological defects and estimates the transition temperature of stripe phases of spin-imbalanced fermions. Very recently, I find a quantum fluctuation induced superconducting phase with repulsive interaction in an orbital ladder system [19], opening new routes to study high-Tc superconductivity in quantum gases.

Besides the phases associated with symmetry breakings, searches for novel topological phases beyond Landau's symmetry breaking paradigm are also attracting growing interests

in the context of cold atoms in optical lattices. Previous theoretical proposals of engineering topological phases have been largely focused on systems with spin-orbit coupling, p-wave pairing or other variants, which may cause experimental complexity in optical lattices. Recently I showed that a standard double-well optical lattice exhibits a new paradigm of topological matter without resorting to any of the existing ideas [27]. A fermionic orbital ladder (with s and p orbitals) at half filling with weak interaction is shown to be in a Z_2 topological insulator phase with fermion zero modes (which features half charges) at the edges. The significant Z_2 topology arises directly from the complex phases of quantum tunneling between opposite parity orbitals and hence the present mechanism is parity. With strong interaction, the system undergoes a topological phase transition to a Mott insulator with ferro-orbital order, which is an analog of the ferro-magnetic phase in conventional magnetic materials. Away from half filling with weak s-wave cooper pairing, the orbital ladder is shown to enter a topological superconducting phase exhibiting protected Majorana fermions, which makes the system a promising candidate for topological quantum computing. This is totally unexpected of such a system without either spin-orbit coupling or p-wave pairing, an ingredient previously thought necessary for topological superconductivity. Remarkably, edge states of an array of such ladders form a zero-energy flat band in the presence of inter-ladder couplings, i.e., when crossing over to two dimensions. Past known examples suggest that edge states in a one-dimensional system would disperse in energy when extending to two dimensions. The unexpected flat band in 2D is an exact consequence of the p-orbital parity and hence is protected by symmetry. The flat band is reminiscent of that at the zigzag edge of graphene. The existence of a flat band opens a route to strongly correlated states fully controlled by interactions.

2.0 OPTICAL LATTICES AND MULTI-BANDS

Despite of the low density of ultra-cold atomic gases, strongly correlated physics can be studied with optical lattices, where Bose/Fermi Hubbard models can be simulated. In solid state materials, Fermi Hubbard models are expected to demonstrate many-body emergent phenomena such as high-Tc superconductivity and spin-charge separation. However, exact theoretical treatment of Fermi Hubbard models are quite challenging in most cases and approximate solutions are controversial. Quantum simulations of Fermi Hubbard model with atomic gases would help sort out controversies and provide concrete understandings of these models. In this chapter, we discuss the band structures of optical lattices and demonstrate how Hubbard models are reached in this context.

2.1 BAND STRUCTURES

In terms of field operators, the Hamiltonian of particles moving in optical lattices is

$$H = \int d\mathbf{x}\psi^{\dagger}(\mathbf{x}) \left(-\frac{\hbar^2}{2m}\vec{\nabla}^2 + V(\mathbf{x}) \right) \psi(\mathbf{x}), \tag{2.1}$$

where $\psi(\mathbf{x})$ is a field operator. It can be either bosonic or fermionic. We expand the operator $\psi(\mathbf{x})$ in the momentum basis

$$\psi(\mathbf{x}) = \frac{1}{\sqrt{A}} \sum_{\mathbf{K},\mathbf{k}} a_{\mathbf{K}}(\mathbf{k}) e^{i(\mathbf{K}+\mathbf{k})\cdot\mathbf{x}}, \tag{2.2}$$

where $\mathbf{k}$ labels the lattice momentum, $\mathbf{K}$ the reciprocal lattice vectors and A is the volume of the system. Optical lattice potentials $V(\mathbf{x})$, unlike the potentials in electronic materials, can typically be written as superpositions of just a few plane waves, i.e.,

$$V(\mathbf{x}) = \sum_{\mathbf{Q}} v(\mathbf{Q}) e^{i\mathbf{Q}\cdot\mathbf{x}},$$

with $\mathbf{Q}$ the reciprocal lattice vectors.

V_0/E_R	$4t^s_{nn}/E_R$	$4t^s_{nnn}/E_R$	W^s/E_R	$4t^p_{nn}/E_R$	$4t^p_{nnn}/E_R$	W^p/E_R
3	-0.4441	0.0449	0.4519	2.0074	0.3308	2.2803
5	-0.2631	0.0136	0.2642	1.6912	0.2914	1.8468
10	-0.07673	9.1E-4	0.07675	0.9741	0.1051	0.9965
20	-9.965E-3	1.2E-5	9.965E-3	0.2411	5.5E-3	0.2413

Table 1: Tunneling amplitudes in a one-dimensional optical lattice with potential $V(x) = V_0 \sin^2(kx)$. E_R is the recoil energy $\frac{\hbar^2 k^2}{2m}$. t^s_{nn} and t^s_{nnn} are nearest neighbor and next nearest neighbor tunnelings for the s (lowest) band. t^p_{nn} and t^p_{nnn} are nearest neighbor and next nearest neighbor tunnelings for the p (first excited) band. W^s and W^p are the band widths for the s and p bands, respectively.

The Hamiltonian in momentum space reads as

$$H = \sum_{\mathbf{K}_1,\mathbf{K}_2} \sum_{\mathbf{k}} \mathcal{H}_{\mathbf{k}}(\mathbf{K}_1, \mathbf{K}_2) a^\dagger_{\mathbf{K}_1}(\mathbf{k}) a_{\mathbf{K}_2}(\mathbf{k}), \tag{2.3}$$

with the matrix given by

$$\mathcal{H}_{\mathbf{k}}(\mathbf{K}_1, \mathbf{K}_2) = \frac{\hbar^2(\mathbf{K}_1 + \mathbf{k})^2}{2m} \delta_{\mathbf{K}_1\mathbf{K}_2} + v(\mathbf{K}_1 - \mathbf{K}_2). \tag{2.4}$$

Diagonalizing this matrix, we get the band structure $E_n(\mathbf{k})$ and the eigenvector $\lambda^{(n)}_{\mathbf{K}}(\mathbf{k})$, where n is the band index. The Hamiltonian in the eigen basis reads as

$$H = \sum_{n\mathbf{k}} E_n(\mathbf{k}) b^\dagger_n(\mathbf{k}) b_n(\mathbf{k}), \tag{2.5}$$

with $b_n(\mathbf{k}) = \sum_{\mathbf{K}} \lambda^{(n)*}_{\mathbf{K}}(\mathbf{k}) a_{\mathbf{K}}(\mathbf{k})$.

The Wannier basis is given by

$$\tilde{b}_n(\mathbf{R}) = \frac{1}{\sqrt{N_s}} \sum_{\mathbf{k}} b_n(\mathbf{k}) e^{i\mathbf{k}\cdot\mathbf{R}}, \tag{2.6}$$

with N_s the number of lattice sites. The corresponding Wannier wavefunction is given by

$$w_n(\mathbf{x}-\mathbf{R}) = \frac{1}{\sqrt{AN_s}} \sum_{\mathbf{K},\mathbf{k}} \lambda_{\mathbf{K}}^{(n)}(\mathbf{k}) e^{i\mathbf{K}\cdot\mathbf{x}} e^{i\mathbf{k}\cdot(\mathbf{x}-\mathbf{R})}. \tag{2.7}$$

The Hamiltonian can be rewritten in the Wannier basis as

$$H = \sum_{\mathbf{R}\mathbf{R}'} t^{(n)}(\mathbf{R}-\mathbf{R}') \tilde{b}_n^\dagger(\mathbf{R}) \tilde{b}_n(\mathbf{R}'), \tag{2.8}$$

with

$$t^{(n)}(\mathbf{R}-\mathbf{R}') = \frac{1}{N_s} \sum_{\mathbf{k}} E_n(\mathbf{k}) e^{i\mathbf{k}\cdot(\mathbf{R}-\mathbf{R}')}. \tag{2.9}$$

Typical values of tunnelings (tunnelings refer to tunneling matrix elements here) for s and p bands are listed in Table 1.

2.2 HARMONIC WAVEFUNCTION BASIS AND THE TIGHT BINDING MODEL

In the tight binding regime, optical lattices can be treated as individual harmonic oscillators, which are coupled by quantum tunneling. On each harmonic oscillator centered at lattice site $\mathbf{R}$, we have discrete energy levels with orbital wavefunctions $\phi_\nu(\mathbf{x}-\mathbf{R})$, with ν index the different levels. Associated with the localized orbital wavefunctions, we can define the lattice operators $a_\nu(\mathbf{R})$. To do this, it has to be enforced that the orbital wavefunctions are orthonormal. The simple eigen wavefunctions of harmonic oscillators do not satisfy the orthonorgonality condition, for the reason that there are overlaps between orbital wavefunctions on neighboring sites.

The procedure to construct the orthogonal basis from the localized harmonic oscillator wavefunctions is the following. We begin with the harmonic oscillator wavefunctions $\phi_\nu(\mathbf{x}-\mathbf{R})$ localized on site $\mathbf{R}$. These wavefunctions are already approximately orthogonal, i.e.,

$$\int d\mathbf{x}\phi_\nu(\mathbf{x}-\mathbf{R})\phi_{\nu'}(\mathbf{x}-\mathbf{R}') = \delta_{\nu\nu'}\delta_{\mathbf{R}\mathbf{R}'} + \epsilon,$$

where ϵ is some small number. We have restricted our discussion to wavefunctions ϕ_ν being real. Then we define

$$\tilde{\phi}_\nu(\mathbf{x}) = \phi_\nu(\mathbf{x}) - \frac{1}{2}\sum_{\nu'\mathbf{R}'}\left[1-\delta_{\nu\nu'}\delta_{\mathbf{R}\mathbf{R}'}\right]\phi_{\nu'}(\mathbf{x}-\mathbf{R}')\left[\int d\mathbf{x}'\phi_{\nu'}(\mathbf{x}'-\mathbf{R}')\phi_\nu(\mathbf{x}'-\mathbf{R})\right].$$

After that $\phi_\nu(\mathbf{x}-\mathbf{R})$ is renormalized as

$$\tilde{\phi}_\nu(\mathbf{x}) \to \tilde{\phi}_\nu(\mathbf{x})/\sqrt{\int d\mathbf{x}'\tilde{\phi}_\nu^2(\mathbf{x}')}.$$

The improved wavefunctions satisfy a better approximate orthogonal condition

$$\int d\mathbf{x}\tilde{\phi}_\nu(\mathbf{x}-\mathbf{R})\tilde{\phi}_{\nu'}(\mathbf{x}-\mathbf{R}') = \delta_{\nu\nu'}\delta_{\mathbf{R}\mathbf{R}'} + \mathcal{O}(\epsilon^2).$$

The above procedure can be iterated N times to get the orthonormal basis to the precision of $\mathcal{O}(\epsilon^{2^N})$.

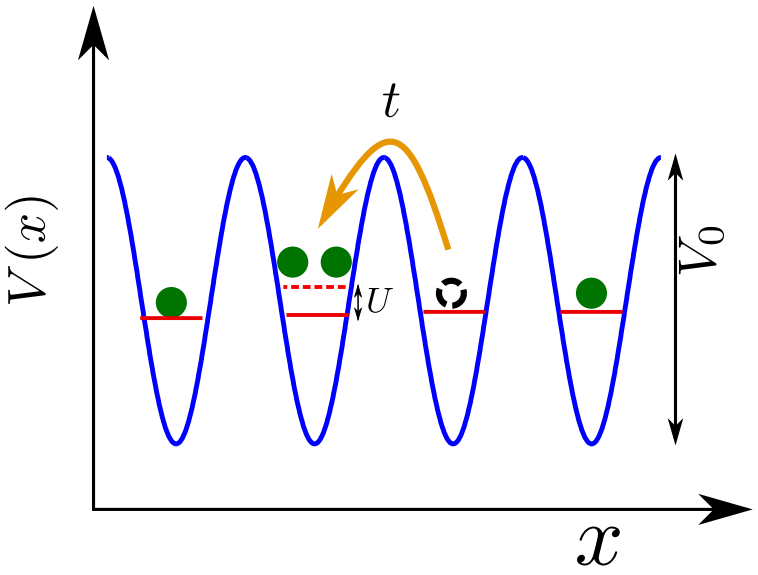

Figure 1: Illustration of Hubbard models from optical lattices. With deep lattices, atoms move in the lattices through quantum tunneling. The model describe atoms loaded into deep lattices is one-band Hubbard model.

Once we have the orthonormal basis, the hoppings between $\mathbf{R}$ and $\mathbf{R}'$ are calculated as

$$t_{\nu\nu'}(\mathbf{R}-\mathbf{R}') = \int d\mathbf{x}\tilde{\phi}_\nu(\mathbf{x}-\mathbf{R})H(\mathbf{x})\tilde{\phi}_{\nu'}(\mathbf{x}-\mathbf{R}'),$$

where $H(\mathbf{x})$ is the Hamiltonian in the first quantization form

$$H = -\frac{\hbar^2}{2m}\vec{\nabla}^2 + V(\mathbf{x}).$$

The lattice model Hamiltonian including tunnelings is given by

$$\hat{H} = \sum_{\nu\nu',\mathbf{R}\mathbf{R}'} t_{\nu\nu'}(\mathbf{R}-\mathbf{R}')a^\dagger_\nu(\mathbf{R})a_{\nu'}(\mathbf{R}'). \tag{2.10}$$

Without truncating the basis, the Hamiltonian is exact, from which the band structure can be calculated. If we only keep the lowest Harmonic wavefunctions, this lattice Hamiltonian gives qualitatively correct band structures.

2.3 MULTI-BAND HUBBARD MODEL

In the tight binding regime, the many-body physics of bosons/fermions loaded on the lowest band is described by a one-band Hubbard model given by

$$H = \sum_{<\mathbf{R}\mathbf{R}'>} -ta^\dagger(\mathbf{R})a(\mathbf{R}') + \frac{U}{2}\sum_{\mathbf{R}} a^\dagger(\mathbf{R})a(\mathbf{R})a^\dagger(\mathbf{R})a(\mathbf{R}), \tag{2.11}$$

assuming the interaction is weak compared with the band gap. For fermions, $a(\mathbf{R})$ has an additional pseudo-spin degrees of freedom. When the band gap is comparable with the interaction, the one-band Hubbard model is no longer valid. The physics will be described by a multi-band Hubbard model

$$\begin{aligned} H &= \sum_{\mathbf{R}\mathbf{R}'} t^{(n)}(\mathbf{R}-\mathbf{R}')a_n^\dagger(\mathbf{R})a_n(\mathbf{R}') \\ &\quad + \sum_{\mathbf{R}} V_{n_1n_2n_3n_4}a_{n_1}^\dagger(\mathbf{R})a_{n_2}^\dagger(\mathbf{R})a_{n_3}(\mathbf{R})a_{n_4}(\mathbf{R}). \end{aligned} \tag{2.12}$$

Due to strong interactions, calculations of $V_{n_1n_2n_3n_4}$ require careful treatments beyond tree-level estimates.

3.0 *P*-BAND MOTT INSULATORS AND SUPERFLUID TRANSITIONS

Quantum phase transitions have been extensively studied in lowest band Bose Hubbard models. For example, the zero-temperature Mott-superfluid transition [28, 8] , characterized by phase correlations has been observed [9]. In the Mott regime, atoms behave like localized particles; while in the superfluid regime, they become more "wave-like" demonstrating fundamental properties of quantum mechanics.

However, there is no evidence of phases beyond standard Mott and superfluid phases for lowest band bosons. Motivated by searching for non-standard phases, experiments on populating bosons on excited bands are put forward [29, 30]. And a more recent p-band boson experiment [13, 14] opens up a new thrust towards observing the exotic phases of bosons on higher bands with long life time. Given growing experimental progress on excited band bosons, probing detailed features of p-band Mott insulators and p-band superfluidity is attracting broader interests. There are numerous theoretical works on excited band bosons focusing on proposing exotic phases [31, 1, 32, 33, 12], which have demonstrated the fascinating physics associated with bosons on excited bands of optical lattices. The quantum phase transition from p-band Mott insulator to superfluid phase has been studied within the Gutzwiller mean field approach [31, 34]. For large interactions, the energy is minimized by an incompressible state with an orbital order. And for weak interactions the kinetic energy dominates over the interaction and drives the system into a superfluid with a feature of transversely staggered orbital current (TSOC) [1]. The competition between the kinetic energy and interaction energy is well described within the Gutzwiller approach, however the single particle spectra, the momentum distribution and finite temperature phase transitions are out of reach within this approach.

We apply the method of effective action beyond the Gutzwiller mean field [17], and

explore the single particle spectra in both of the p-band Mott insulator phase and the TSOC superfluid phase in a two dimensional square lattice. We have studied the phase coherence in the Mott insulator phase and found that sharp peaks rise at finite momenta ($(\pm\pi, 0)$ for the p_x band and $(0, \pm\pi)$ for the p_y band) when the Mott gap is small. This offers new approaches of preparing coherent matter waves from Mott insulators. From the p-band Mott insulator phase to the TSOC superfluid phase, the global U(1) symmetry and the time reversal T symmetry are broken. Away from the tip of the Mott lobe, we find two gapless modes at the critical point; while at the tip, we find four gapless modes due to the particle-hole symmetry. For TSOC superfluid phase we go beyond previous study in the weak coupling limit [1, 12] and consider the leading effect of Hubbard interaction in the strong coupling regime. Our theory is capable of capturing the main feature of TSOC superfluid phase in the strong coupling regime, where the critical point of Mott-superfluid transition is located. The isotropy of the sound velocity of the TSOC superfluid phase is explained. Finally, the finite temperature phase transitions of TSOC superfluid phase are discussed.

3.1 MODEL AND PHASE DIAGRAM

We start with a microscopic extended Bose-Hubbard model with p-orbital degrees of freedom on a square lattice [1, 31]

$$
\begin{aligned}
&H = H_t + H_{\text{onsite}}, \\
&H_t = \sum_{\mathbf{r}} -t \left[a_x^\dagger(\mathbf{r}) a_x(\mathbf{r}+\hat{x}) + a_y^\dagger(\mathbf{r}) a_y(\mathbf{r}+\hat{y}) + h.c.\right] \\
&-t_\perp \left[a_x^\dagger(\mathbf{r}) a_x(\mathbf{r}+\hat{y}) + a_y^\dagger(\mathbf{r}) a_y(\mathbf{r}+\hat{x}) + h.c.\right], \qquad (3.1) \\
&H_{\text{onsite}} = \sum_{\mathbf{r}} \frac{U}{2}((n(\mathbf{r})(n(\mathbf{r}) - \frac{2}{3}) - \frac{1}{3} L_z(\mathbf{r})^2) - \mu n. \qquad (3.2)
\end{aligned}
$$

Here, $a_x^\dagger(\mathbf{r})$ and $a_y^\dagger(\mathbf{r})$ are bosonic creation operators of p_x and p_y orbitals at $\mathbf{r}$. The discrete variable $\mathbf{r}$ labels the sites of a square lattice. The lattice constant a is set to be 1. t ($t_\perp$) is the longitudinal (transverse) hopping between nearest neighbor sites, U the on-site repulsion and the local angular momentum operator $L_z = -ia_y^\dagger a_x + ia_x^\dagger a_y$. The average occupation

number n of bosons per site is fixed by the chemical potential μ. For simplicity, we focus on a simple square lattice where p-band bosons have limited life-time. The life-time is significantly improved in the lattice created in experiments [14]. Nonetheless, experimental results of static phases agree with theoretical studies on simple square lattices [1]. We thus expect that our predictions here are relevant to the experiments [14].

Because $t < 0$ and $t_\perp > 0$, both of p_x band and p_y band show minima at finite momenta. It is inconvenient to take the long wavelength limit of the original lattice boson fields. To overcome this inconvenience we introduce the following staggered transformation

$$\begin{bmatrix} \psi_x^\dagger(\mathbf{r}) \\ \psi_y^\dagger(\mathbf{r}) \end{bmatrix} = \begin{bmatrix} (-1)^x a_x^\dagger \\ (-1)^y a_y^\dagger \end{bmatrix}, \begin{bmatrix} \psi_\uparrow^\dagger(\mathbf{r}) \\ \psi_\downarrow^\dagger(\mathbf{r}) \end{bmatrix} = \begin{bmatrix} \psi_x^\dagger + i\psi_y^\dagger \\ \psi_x^\dagger - i\psi_y^\dagger \end{bmatrix}. \tag{3.3}$$

$\psi_\uparrow^\dagger(\mathbf{r})$ and $\psi_\downarrow^\dagger(\mathbf{r})$ are lattice field operators for pseudo-spin $|\uparrow(\mathbf{r})\rangle = (-)^x|p_x\rangle + i(-)^y|p_y\rangle$ and $|\downarrow(\mathbf{r})\rangle = (-)^x|p_x\rangle - i(-)^y|p_y\rangle$ components, where $|p_x\rangle$ and $|p_y\rangle$ are local p_x and p_y orbital states.

In this pseudo-spin representation, the Hamiltonian reads

$$\begin{aligned} H &= \sum_{\mathbf{r},\mathbf{r}'} T_{\sigma\sigma'}(\mathbf{r}-\mathbf{r}')\psi_\sigma^\dagger(\mathbf{r})\psi_{\sigma'}(\mathbf{r}') \\ &+ \sum_{\mathbf{r}} \frac{U}{2}(n(\mathbf{r})^2 - \frac{2}{3}n(\mathbf{r}) - \frac{1}{3}L_z(\mathbf{r})^2) - \mu n(\mathbf{r}), \end{aligned} \tag{3.4}$$

with

$$\begin{aligned} T(\hat{x}) &= \begin{bmatrix} \frac{t-t_\perp}{2} & \frac{t+t_\perp}{2} \\ \frac{t+t_\perp}{2} & \frac{t-t_\perp}{2} \end{bmatrix}, \\ T(\hat{y}) &= \begin{bmatrix} \frac{t-t_\perp}{2} & -\frac{t+t_\perp}{2} \\ -\frac{t+t_\perp}{2} & \frac{t-t_\perp}{2} \end{bmatrix}, \end{aligned} \tag{3.5}$$

where $\sigma = \uparrow, \downarrow$, $n(\mathbf{r}) = \psi_\uparrow^\dagger(\mathbf{r})\psi_\uparrow(\mathbf{r}) + \psi_\downarrow^\dagger(\mathbf{r})\psi_\downarrow(\mathbf{r})$, and $L_z(\mathbf{r}) = (-1)^{x+y}[\psi_\uparrow^\dagger(\mathbf{r})\psi_\uparrow(\mathbf{r}) - \psi_\downarrow^\dagger(\mathbf{r})\psi_\downarrow(\mathbf{r})]$. The Fourier transform of $T_{\sigma\sigma'}$ gives

$$\epsilon(\mathbf{k}) = \begin{bmatrix} \epsilon_{\uparrow\uparrow}(\mathbf{k}) & \epsilon_{\uparrow\downarrow}(\mathbf{k}) \\ \epsilon_{\downarrow\uparrow}(\mathbf{k}) & \epsilon_{\downarrow\downarrow}(\mathbf{k}) \end{bmatrix}, \tag{3.6}$$

where $\epsilon_{\uparrow\uparrow}(\mathbf{k}) = \epsilon_{\downarrow\downarrow}(\mathbf{k}) = (t - t_\perp)(\cos(k_x) + \cos(k_y))$ and $\epsilon_{\uparrow\downarrow}(\mathbf{k}) = \epsilon_{\downarrow\uparrow}(\mathbf{k}) = (t + t_\perp)(\cos(k_x) - \cos(k_y))$.

It can be verified that the band structure given by $\epsilon(\mathbf{k})$ shows a minimum at zero momentum. Thus we have obtained a theory which is convenient for us to take the continuum limit. The internal symmetry group of the Hamiltonian is U(1) $\times$ T, where T denotes the time reversal symmetry ($\psi_{\uparrow(\downarrow)}(\mathbf{x}, t) \rightarrow \psi_{\downarrow(\uparrow)}(\mathbf{x}, -t)$) and U(1) denotes the global phase rotation symmetry ($\psi_\sigma \rightarrow e^{i\theta}\psi_\sigma$).

In the strong coupling limit, the system is in a Mott insulating phase for commensurate filling (filling factor ν is an integer), where the filling is defined as the occupation number of bosons loaded on p orbits per site. For filling factor ν larger than 1, the interaction term favors local orbital current states because of the $(-L_z^2)$ term in Hamiltonian (Eq. 3.4); these vortex-like states form a vortex-antivortex pattern due to super-exchange [31, 34]. For filling factor $\nu = 1$, the local vortex-like states are no longer favorable because the interaction term does not contribute on single particle states. Mathematically, the operator L_z^2 term is equal to identity, when acting on the single particle states, and thus does not favor vortex-like states. The Mott phase has an antiferro-orbital order, i.e., an alternating p_x-p_y pattern (FIG. 2), which breaks lattice translation symmetry [31]. We are interested in the long wavelength modes within this phase.

In the weak coupling limit, the system is in superfluid phase and the dispersion (obtained by diagonalizing $\epsilon(\mathbf{k})$) shows minima at zero momentum. The two minimal single particle states carry lattice momentum $\mathbf{k} = 0$ and pseudo-spin $\sigma = \uparrow, \downarrow$, and they are related by time reversal (T) transformation. Due to the $(-L_z^2)$ term in Hamiltonian, the T symmetry is spontaneously broken in the ground state, i.e., either $\langle\psi_\uparrow\rangle$ or $\langle\psi_\downarrow\rangle$ is finite. It is clear from Eq. (3.3) that the original particles form a staggered $p_x \pm ip_y$ pattern (FIG. 2) in this superfluid phase, which is named TSOC [1]. Thus going from the Mott insulator phase with filling $\nu = 1$ to the TSOC superfluid phase, the U(1) $\times$ T symmetry is spontaneously broken. The phase transition (FIG. 2) is confirmed by Gutzwiller mean field calculations [31]. However, the momentum distribution and the correlation functions in the Mott phase are out of reach within Gutzwiller mean field calculation. Motivated by this, we develop a theory valid in the strong coupling regime. With this theory we calculate the single particle

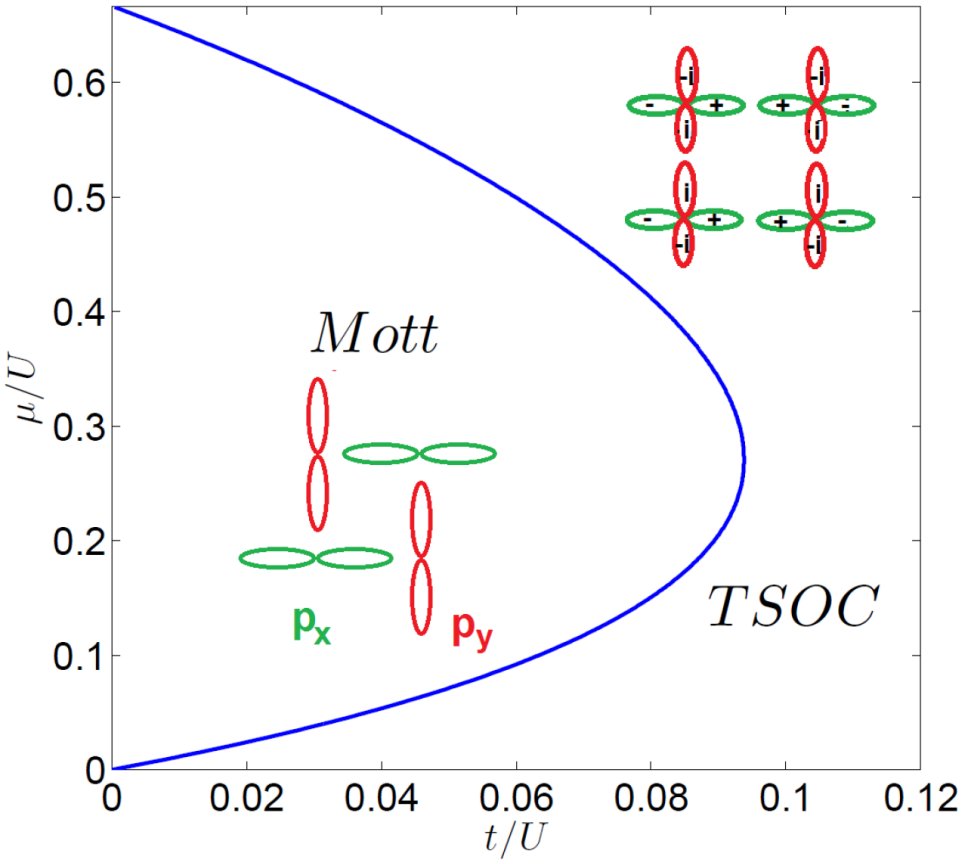

Figure 2: The phase diagram determined by the effective action method. The filling factor ν of the Mott regime shown is 1. $t_\perp$ is set to be $0.1t$. TSOC means the transversely staggered orbital current superfluidity[1]. The alternating p_x-p_y pattern shown in the Mott regime is the pattern of the Mott insulator with filling of $\nu = 1$ in the p-bands. The staggered $p_x \pm ip_y$ pattern in the TSOC regime illustrates the orbital current order in the TSOC phase.

spectrum for both of the Mott phase and the TSOC superfluid phase and discuss how the Mott gap closes at the critical point and how the phase coherence peak develops in the Mott phase, and we explain the isotropy of the sound velocity of the TSOC superfluid phase in the strong coupling regime.

3.2 SUPER-EXCHANGE AND ORBITAL ORDERING IN THE MOTT STATES

3.2.1 Mott states with filling factor larger than 1

In this section, we will derive the super-exchange in the Mott states with filling factor larger than 1. The procedure is to take the local interaction as the leading part and the hopping term as a perturbation. The local interaction is given by

$$H_U = \frac{U}{2}\left(n^2 - \frac{2}{3}n - \frac{1}{3}L_z^2\right). \tag{3.7}$$

It can be verified that the angular momentum operator L_z commutes with the local interaction, i.e.,

$$[L_z, H_u] = 0.$$

Thus the eigenstates of the local interaction can be chosen as states with definite angular momentum. For filling factor $\nu > 1$, the degenerate eigenstates with lowest energy are

$$\begin{aligned} |+\rangle &= |n_{p_x+ip_y} = \nu, n_{p_x-ip_y} = 0\rangle \\ |-\rangle &= |n_{p_x+ip_y} = 0, n_{p_x-ip_y} = \nu\rangle \end{aligned} \tag{3.8}$$

The lowest energy is $\frac{2}{3}U$. The states $|+\rangle$ and $|-\rangle$ have angular momentum $+\nu$ and $-\nu$, respectively.

We then restrict to the low energy sub Hilbert space spanned by the product states

$$|\{s(\mathbf{r})\}\rangle \equiv \otimes_{\mathbf{r}} |s(\mathbf{r})\rangle,$$

where $s(\mathbf{r}) = \pm$ and $\mathbf{r}$ runs all lattice sites. All the states in this subspace has the same energy to leading order in U and there is thus a huge degeneracy. The corrections due to the hopping term H_t will lift the degeneracy. The first order corrections vanish because H_t does not connect any states in the sub Hilbert space. The second order correction is calculated by the standard perturbation theory,

$$\Delta E(|\{s(\mathbf{r})\}\rangle) = \sum_m \frac{|\langle m|H_t|\{s(\mathbf{r})\}\rangle|^2}{E^{(0)}(|\{s(\mathbf{r})\}\rangle) - E^{(0)}(|m\rangle)}, \tag{3.9}$$

where $|m\rangle$ is some higher energy state perpendicular to the product states $|\{s(\mathbf{r}\}\rangle$, and $E^{(0)}$ is the leading order energy.

We restrict our discussion here on the nearest neighbor hoppings. In this case $\Delta E(|\{s(\mathbf{r})\}\rangle)$ simplifies as

$$\Delta E(|\{s(\mathbf{r})\}\rangle) = \sum_{\langle \mathbf{r},\mathbf{r}'\rangle} \Delta E(|s(\mathbf{r})s(\mathbf{r}')\rangle). \tag{3.10}$$

Now we only need to calculate the energy correction on a two-site state $|s(\mathbf{r})s(\mathbf{r}')\rangle$, which is straightforward. The energy corrections read

$$\begin{aligned}
\Delta E(|++\rangle) &= 2\times 2\times 3\frac{|t-t_\perp|^2/4}{-\frac{2}{3}U} + 2\times 2\frac{|t+t_\perp|^2/4}{-2U}, && (3.11)\\
\Delta E(|--\rangle) &= 2\times 2\times 3\frac{|t-t_\perp|^2/4}{-\frac{2}{3}U} + 2\times 2\frac{|t+t_\perp|^2/4}{-2U}, && (3.12)\\
\Delta E(|+-\rangle) &= 2\times 2\times 3\frac{|t+t_\perp|^2/4}{-\frac{2}{3}U} + 2\times 2\frac{|t-t_\perp|^2/4}{-2U}, && (3.13)\\
\Delta E(|-+\rangle) &= 2\times 2\times 3\frac{|t+t_\perp|^2/4}{-\frac{2}{3}U} + 2\times 2\frac{|t-t_\perp|^2/4}{-2U}, && (3.14)\\
& && (3.15)
\end{aligned}$$

The energy correction $\Delta E(|\{s(\mathbf{r})\}\rangle)$ is obtained as

$$\Delta E(|\{s(\mathbf{r})\}\rangle) = \sum_{\langle \mathbf{r},\mathbf{r}'\rangle} \left(-\frac{8tt_\perp}{U}\right) s(\mathbf{r})s(\mathbf{r}'). \tag{3.16}$$

Including this correction into the Hamiltonian, we get

$$\Delta\hat{H} = \sum_{\langle \mathbf{r},\mathbf{r}'\rangle} J\hat{L}_z(\mathbf{r})\hat{L}_z(\mathbf{r}'), \tag{3.17}$$

with the super-exchange interaction

$$J = -\frac{8tt_\perp}{U} > 0.$$

The orbital super-exchange makes the staggered angular momentum ordering favorable.

3.2.2 Mott state with filling factor 1

For Mott states with filling factor $\nu = 1$, the convenient basis to calculate the super-exchange interaction is the p_x, p_y basis. With similar argument as calculating super-exchange for Mott states with $\nu > 1$, we just need to calculate the second order correction of nearest neighbor product states, which are $|p_x p_x\rangle = p_x^\dagger(\mathbf{r})p_x^\dagger(\mathbf{r}')|0\rangle$, $|p_x p_y\rangle = p_x^\dagger(\mathbf{r})p_y^\dagger(\mathbf{r}')|0\rangle$, $|p_y p_y\rangle = p_y^\dagger(\mathbf{r})p_x^\dagger(\mathbf{r}')|0\rangle$, and $|p_y p_y\rangle = p_y^\dagger(\mathbf{r})p_y^\dagger(\mathbf{r}')|0\rangle$. The higher energy states that H_t will couple to are $p_x^\dagger(\mathbf{r})p_y^\dagger(\mathbf{r})|0\rangle$, $\frac{1}{\sqrt{2}}\left(p_x^\dagger(\mathbf{r})p_x^\dagger(\mathbf{r}) + p_y^\dagger(\mathbf{r})p_y^\dagger(\mathbf{r})\right)|0\rangle$, and $\frac{1}{\sqrt{2}}\left(p_x^\dagger(\mathbf{r})p_x^\dagger(\mathbf{r}) - p_y^\dagger(\mathbf{r})p_y^\dagger(\mathbf{r})\right)|0\rangle$, with corresponding energies $\frac{2}{3}U$, $\frac{4}{3}U$ and $\frac{2}{3}U$. For the $\hat{x}$ link defined by $\mathbf{r}' = \mathbf{r}+\hat{x}$, the second order energy corrections are given by $\Delta E(|p_x p_x\rangle) = -\frac{3t^2}{U}$, $\Delta E(|p_x p_y\rangle) = -\frac{3t^2}{U}$ and $\Delta E(|p_y p_y\rangle) = 0$. (Note that the transverse tunneling is neglected here, for the reason that the longitudinal tunneling is enough to lift the degeneracy.) For the $\hat{y}$ link defined by $\mathbf{r}' = \mathbf{r} + \hat{y}$, the energy corrections are given by $\Delta E(|p_x p_x\rangle) = 0$, $\Delta E(|p_x p_y\rangle) = -\frac{3t^2}{U}$ and $\Delta E(|p_y p_y\rangle) = -\frac{3t^2}{U}$. Including these energy corrections in the Hamiltonian, we get

$$\Delta H = \sum_{\mathbf{r}} J\left[\hat{\sigma}_z(\mathbf{r})\hat{\sigma}_z(\mathbf{r}+\hat{x}) + \hat{\sigma}_z(\mathbf{r})\hat{\sigma}_z(\mathbf{r}+\hat{y})\right], \tag{3.18}$$

with $J = \frac{3t^2}{4U}$, where the pseudo-spin components are p_x and p_y here. The super-exchange predict the orbital ordering shown in Fig. 2.

3.3 EFFECTIVE ACTION

3.3.1 Effective Action by double Hubbard-Stratonovich transformation

To capture the main feature of p-band Mott insulator and the TSOC superfluid in the strong coupling regime, we aim at a theory capable of incorporating the local Mott gap, which is the leading effect of the Hubbard interaction, in a non-perturbative manner. To do this, we follow the procedure in Ref. [35, 36, 37]. We first write the partition function Z as a functional integral over complex fields ψ_σ with the action $S[\psi^*,\psi] = \int_0^\beta d\tau \sum_{\sigma,\mathbf{r}} \{\psi_\sigma(\mathbf{r})\partial_\tau\psi_\sigma(\mathbf{r}) + H[\psi^*,\psi]\}$. We introduce an auxiliary field ϕ_σ to decouple the inter-site hopping term by means of a Hubbard-Stratonovich transformation and obtain

$$\begin{aligned} Z &= \int D[\psi^*_\sigma,\psi_\sigma,\phi^*_\sigma,\phi_\sigma] e^{\phi^*_\sigma T^{-1}_{\sigma\sigma'}\phi_{\sigma'} + [(\phi|\psi)+c.c.] - S_0[\psi^*,\psi]} \\ &= Z_0 \int D[\phi^*_\sigma,\phi_\sigma] e^{\phi^*_\sigma T^{-1}_{\sigma\sigma'}\phi_{\sigma'}} \langle \exp[(\phi|\psi)+c.c.]\rangle_0 \\ &\equiv Z_0 \int D[\phi^*_\sigma,\phi_\sigma] \exp\left(\phi^*_\sigma T^{-1}_{\sigma\sigma'}\phi_{\sigma'} + W[\phi^*_\sigma,\phi_\sigma]\right), \end{aligned} \tag{3.19}$$

where the shorthand notation $(\phi|\psi) = \sum_{\sigma,\mathbf{r}} \int_0^\beta d\tau \phi^*_\sigma(\mathbf{r})\psi_\sigma(\mathbf{r})$ and T^{-1} denotes the inverse of the hopping matrix. S_0 and Z_0 are the action and partition function in the local limit ($t, t_\perp = 0$). $\langle\ldots\rangle_0$ means averaging over the local action $S_0[\psi^*_\sigma,\psi_\sigma]$. The introduced generating function $W[\phi^*_\sigma,\phi_\sigma] = \ln\langle\exp\left((\phi|\psi)+c.c.\right)\rangle_0$. The local action S_0, which is equivalent to the original action without tunneling term, is invariant under a $U(1)\times U(1)$ transformation $\psi_\sigma \to e^{i\theta_\sigma}\psi_\sigma$. By definition, $W[\phi^*_\sigma,\phi_\sigma]$ is independent of hopping (t and $t_\perp$). Power expansion of $W[\phi^*_\sigma,\phi_\sigma]$ respecting this symmetry yields

$$\begin{aligned} W = &\int d\tau_1 d\tau_2 \sum_{\mathbf{r}} \mathrm{G}_\sigma(\mathbf{r},\tau_1-\tau_2)\phi^*_\sigma(\mathbf{r},\tau_1)\phi_\sigma(\mathbf{r},\tau_2) \\ &+\frac{1}{2!}\int \prod_{\alpha=1}^{4} d\tau_\alpha \sum_{\mathbf{r}} \\ &\quad \chi_{\sigma_1\sigma_2}(\mathbf{r},1234)\phi^*_{\sigma_1}(1)\phi_{\sigma_1}(2)\phi^*_{\sigma_2}(3)\phi_{\sigma_2}(4) \\ &+O(\phi^6), \end{aligned} \tag{3.20}$$

where the indices $1,2,3$, and 4 indicate time $\tau_1,\cdots,\tau_4$. And because of T (time reversal) symmetry, $\mathrm{G}_\uparrow = \mathrm{G}_\downarrow$, and $\chi_{\uparrow\uparrow} = \chi_{\downarrow\downarrow}$. In the transformed theory, the quadratic term of

T^{-1} in Eq. (3.19) is dominant in the strong coupling limit, $t/U \to 0$. We thus truncate the power expansion to quartic order. Now that the fluctuations of ϕ fields are controlled by T^{-1} (Eq. (3.19)), perturbative renormalization group (RG) analysis finds higher order terms are irrelevant [38]. From the definition, the coefficients are readily obtained as follows

$$\begin{aligned} \mathrm{G}_\sigma(\mathbf{r}, \tau_1 - \tau_2) &= \langle \psi_\sigma(\mathbf{r}, \tau_1) \psi^*_\sigma(\mathbf{r}, \tau_2) \rangle^c_0, \\ \chi_{\sigma_1\sigma_2}(\mathbf{r}; 1234) &= \langle \psi_{\sigma_1}(1) \psi^*_{\sigma_1}(2) \psi_{\sigma_2}(3) \psi^*_{\sigma_2}(4) \rangle^c_0. \end{aligned} \tag{3.21}$$

The effective action for ϕ fields is $S_{\text{eff}}[\phi^*_\sigma, \phi_\sigma] = \int d\tau \sum_{\mathbf{r},\mathbf{r}'} -\phi^*_\sigma(\mathbf{r}) T^{-1}_{\sigma\sigma'}(\mathbf{r}-\mathbf{r}') \phi_{\sigma'}(\mathbf{r}') - W[\phi^*_\sigma, \phi_\sigma]$, which can be used as a starting point to study the instability of Mott phase with respect to superfluidity by treating ϕ fields as superfluid order parameters [39]. However it is inconvenient to calculate the excitation spectrum and the momentum distribution from this action [35]. Also, the theory $S_{\text{eff}}[\phi^*_\sigma, \phi_\sigma]$ does not provide a clear picture of quasi particles. The above difficulties can be overcome by performing a second Hubbard-Stratonovich transform following the method of Ref. [35],

$$Z = \int D[\varphi^* \varphi \phi^* \phi] e^{-\varphi^*_\sigma T_{\sigma\sigma'} \varphi_{\sigma'} - [(\varphi|\phi) + c.c.] + W[\phi^*_\sigma, \phi_\sigma]}. \tag{3.22}$$

Integrating out ϕ fields gives the effective action $S_{\text{eff}}[\varphi^*_\sigma, \varphi_\sigma]$

$$S_{\text{eff}}[\varphi^*_\sigma, \varphi_\sigma] = -\tilde{W}[\varphi^*_\sigma, \varphi_\sigma] + \int d\tau \sum_{<\mathbf{r}_1, \mathbf{r}_2>} \mathcal{L}_0, \tag{3.23}$$

with

$$\begin{aligned} \mathcal{L}_0 &= \varphi^*_{\sigma_1}(\mathbf{r}_1, \tau) T_{\sigma_1\sigma_2}(\mathbf{r}_1 - \mathbf{r}_2) \varphi_{\sigma_2}(\mathbf{r}_2, \tau), \\ \tilde{W} &= \ln \langle \exp\left(-[(\varphi|\phi) + c.c.]\right) \rangle_W, \end{aligned} \tag{3.24}$$

where $\langle \ldots \rangle_W = \frac{\int D(\phi^*_\sigma, \phi_\sigma)(\ldots) \exp(W[\phi^*_\sigma, \phi_\sigma])}{\int D(\phi^*_\sigma, \phi_\sigma \exp(W[\phi^*_\sigma, \phi_\sigma])}$. Since the functional $W[\phi^*_\sigma, \phi_\sigma]$ is independent of hopping, $\tilde{W}[\varphi^*_\sigma, \varphi_\sigma]$ is also independent of hopping by definition.

Now the task is to calculate the functional $\tilde{W}$. The essence is to evaluate the expectation value of the exponential operator in a system described by the effective action W. Note that the action W (Eq. (3.20)) is a power expansion of the small parameter $1/U$ (strong coupling), so the perturbative field theoretical method is valid and powerful to compute the

expectation value. In this manner, we perform the power expansion of $\tilde{W}[\varphi^*_\sigma, \varphi_\sigma]$ respecting the $U(1) \times U(1)$ symmetry and obtain the effective theory for φ_σ as follows

$$
\begin{aligned}
&S_{\text{eff}}[\varphi^*_\sigma, \varphi_\sigma] = \\
&\int d\tau_1 d\tau_2 \sum_{\mathbf{r}} \varphi^*_\sigma(\mathbf{r}, \tau_1) \mathrm{G}^{-1}_\sigma(\tau_1 - \tau_2) \varphi_\sigma(\mathbf{r}, \tau_2) \\
&\quad + \int d\tau \sum_{<\mathbf{r}_1, \mathbf{r}_2>} \varphi^*_{\sigma_1}(\mathbf{r}_1, \tau) T_{\sigma_1\sigma_2}(\mathbf{r}_1 - \mathbf{r}_2) \varphi_{\sigma_2}(\mathbf{r}_2, \tau) \\
&\quad + \frac{1}{2} g_{\sigma_1\sigma_2} \int d\tau \sum_{\mathbf{r}} |\varphi_{\sigma_1}(\mathbf{r}, \tau)|^2 |\varphi_{\sigma_2}(\mathbf{r}, \tau)|^2.
\end{aligned} \tag{3.25}
$$

Here we have truncated the power expansion to quartic order. The vertex term can have a finite range behavior in τ space in principle, but we can take the static limit because the τ dependent corrections would be irrelevant in the RG sense, assuming that there are no other non-trivial fixed point other than Gaussian. The field ψ describes the bare (original) bosons with onsite interaction U, while the field φ describes quasi particle excitations which are greatly suppressed by the energy gap (of the order of U) in the strong coupling regime (this physical understanding comes from Eq. (3.28)). Thus the quasi particles are dilute, and we expect the three body scattering process is negligible, which further guarantees the validity of the truncation performed in Eq. (3.25). Here, we want to emphasize the quasi particles hop around through $T_{\sigma\sigma'}$ (Eq. (3.25)). The quasi particles are mobile instead of localized. The dispersion of the quasi particles is discussed in the next section.

Despite the difference of bare correlators of ψ and φ, it is proved that the correlators defined by the original action $S[\psi^*, \psi]$ are exactly equal to that defined by the infinite series of power expansion of this effective action $S_{\text{eff}}[\varphi^*_\sigma, \varphi_\sigma]$ (Sec. 3.3.3). With valid truncations, the connected correlators of φ reproduce the connected correlators of ψ approximately. In principle, one can follow the above procedure and get $\mathrm{G}^{-1}_{\sigma_1}(\tau_1 - \tau_2)$ and $g_{\sigma_1\sigma_2}$. It is straightforward to calculate these coefficients for the one component Bose-Hubbard Model. However it is inconvenient to proceed in this approach due to the complexity induced by the local degeneracy of ground states of the action S_0. Since these coefficients are *independent of hopping*, we decide to calculate the coefficients by identifying correlators of this effective action and the original correlators (defined by the original action) in the local limit $(t, t_\perp = 0)$. The derivation and the results are summarized in Sec. 3.3.2.

After the above manipulation, the leading effect of the Hubbard interaction, namely, generating a local energy gap in the quasi-particle spectrum, is included in the quadratic part of $S_{\text{eff}}[\varphi_\sigma^*, \varphi_\sigma]$, which makes the following Bogoliubov analysis valid in the strong coupling regime. With the effective theory $S_{\text{eff}}[\varphi_\sigma^*, \varphi_\sigma]$, the superfluid phase in the strong coupling regime is described as a superfluid phase of weakly interacting quasi particles. We want to emphasize that this physical picture is lacking in the theory $S_{\text{eff}}[\phi_\sigma^*, \phi_\sigma]$.

3.3.2 The coefficients of the effective action

We calculate the coefficients of the effective action in Eq. (3.25) by identifying the connected correlators of the effective action and that of the original Hamiltonian (Eq. 3.4). The connected correlators of the original local action is calculated in the operator representation in the occupation number basis.

$$\begin{aligned}
\mathrm{G}_\uparrow(\mathbf{r}, \tau) &= \frac{1}{Z_0}\mathrm{Tr}[T_\tau \hat{\psi}_\uparrow(\mathbf{r}, \tau)\hat{\psi}_\uparrow^\dagger(\mathbf{r}, 0)e^{-\beta H_0}], \\
&= \frac{1}{Z_0}\sum_{n,m}\langle nm|e^{-(\beta-\tau)H_0}\hat{\psi}_\uparrow(\mathbf{r})e^{-\tau H_0}\hat{\psi}_\uparrow^\dagger(\mathbf{r}, 0)|nm\rangle, \\
&= \frac{1}{Z_0}\sum_{n,m}(n+1)e^{-(\beta-\tau)\epsilon(n,m)}e^{-\tau\epsilon(n+1,m)}
\end{aligned} \tag{3.26}$$

where $|nm\rangle = \frac{(\hat{\psi}_\uparrow^\dagger)^n(\hat{\psi}_\downarrow^\dagger)^m}{\sqrt{n!m!}}|0\rangle$ are the eigenbasis of the local interaction H_0 with eigenvalues $\epsilon(n, m) = \frac{U}{2}\left((n+m)^2 - \frac{2}{3}(n+m) - \frac{1}{3}(n-m)^2\right) - \mu(n+m)$. The Fourier transform of this correlator gives

$$\begin{aligned}
\mathcal{G}_\uparrow(i\omega) &\equiv \int d\tau \mathrm{G}_\uparrow(\tau)e^{i\omega\tau}, \\
&= \frac{1}{Z_0}\sum_{n,m}(n+1)\left\{\frac{e^{-\beta\epsilon(n+1,m)}}{i\omega + \epsilon(n,m) - \epsilon(n+1,m)}\right. \\
&\qquad \left. - \frac{e^{-\beta\epsilon(n,m)}}{i\omega + \epsilon(n,m) - \epsilon(n+1,m)}\right\}.
\end{aligned} \tag{3.27}$$

In the low temperature limit ($\beta U \gg 1$), the exponential term selects out the local ground state, contributions from other states being suppressed. The double degenerate ground states are $|1\rangle \equiv |n_0, 0\rangle$ and $|2\rangle \equiv |0, n_0\rangle$, where n_0 is defined by minimizing $\epsilon(n, m)$. These two

ground states are related by time reversal symmetry. Because of the double degeneracy, we further define correlators with respect to one single ground state. $\mathcal{G}_{\uparrow}^{(1)}(i\omega)$ is defined corresponding to the ground state $|1\rangle$, while $\mathcal{G}_{\uparrow}^{(2)}(i\omega)$ is defined corresponding to the ground state $|2\rangle$. Thus,

$$\begin{aligned}
\mathcal{G}_{\uparrow}^{(1)}(i\omega) &= \frac{n_0}{i\omega+\epsilon(n_0-1,0)-\epsilon(n_0,0)} \\
&\quad -\frac{n_0+1}{i\omega+\epsilon(n_0,0)-\epsilon(n_0+1,0)}, \\
\mathcal{G}_{\uparrow}^{(2)}(i\omega) &= -\frac{1}{i\omega+\epsilon(0,n_0)-\epsilon(1,n_0)}, \\
\mathcal{G}_{\uparrow}(i\omega) &= \frac{\mathcal{G}_{\uparrow}^{(1)}+\mathcal{G}_{\uparrow}^{(2)}}{2}.
\end{aligned} \tag{3.28}$$

It can be verified that $\mathcal{G}_{\uparrow}^{(1)}=\mathcal{G}_{\downarrow}^{(2)}$ and $\mathcal{G}_{\uparrow}^{(2)}=\mathcal{G}_{\downarrow}^{(1)}$. Up to this point, the quadratic part of the effective action in Eq. (3.25) is obtained. In the following, we always split the correlators into two parts (labeled by superindices 1,2) according to two ground states $|1\rangle$ and $|2\rangle$. Here we focus on the Mott insulator with filling $\nu=1$ for which the time reversal symmetry is not broken. For the vortex-antivortex Mott insulator with filling $\nu>1$, the local ground state will spontaneously choose either $|1\rangle$ or $|2\rangle$. And thus one can calculate all the correlators assuming that the ground state is $|1\rangle$ or $|2\rangle$ instead of taking the average.

The four point function is given as

$$\begin{aligned}
&\chi_{\sigma_1\sigma_2}(\tau_1,\tau_2,\tau_3,0)=\langle\psi_{\sigma_1}(\tau_1)\psi^*_{\sigma_1}(\tau_2)\psi_{\sigma_2}(\tau_3)\psi^*_{\sigma_2}(0)\rangle_0^c, \\
= &\frac{1}{Z_0}\mathrm{Tr}\Big[e^{-\beta H_0}T_\tau(e^{\tau_1 H_0}\hat{\psi}_{\sigma_1}e^{-\tau_1 H_0})(e^{\tau_2 H_0}\hat{\psi}^\dagger_{\sigma_1}e^{-\tau_2 H_0}) \\
&\qquad (e^{\tau_3 H_0}\hat{\psi}_{\sigma_2}e^{-\tau_3 H_0})\hat{\psi}^\dagger_{\sigma_2}\Big]^c.
\end{aligned} \tag{3.29}$$

To calculate the coefficients $g_{\sigma_1\sigma_2}$ in the static limit, we are only interested in the time average of χ.

$$\begin{aligned}
\bar{\chi}_{\sigma_1\sigma_2} &= \int_0^\beta d\tau_1 d\tau_2 d\tau_3 \chi_{\sigma_1\sigma_2}(\tau_1,\tau_2,\tau_3,0) \\
&\equiv \frac{\bar{\chi}^{(1)}_{\sigma_1\sigma_2}+\bar{\chi}^{(2)}_{\sigma_1\sigma_2}}{2}.
\end{aligned} \tag{3.30}$$

The diagonal part is calculated as

$$\begin{aligned}\bar{\chi}^{(1,2)}_{\uparrow\uparrow} &= \frac{1}{Z_0}\mathrm{Tr}_{1,2}\left[e^{-\beta H_0}T_\tau(e^{\tau_1 H_0}\psi_\uparrow e^{-\tau_1 H_0})\right. \\ &\quad \left.(e^{\tau_2 H_0}\psi^\dagger_\uparrow e^{-\tau_2 H_0})(e^{\tau_3 H_0}\psi_\uparrow e^{-\tau_3 H_0})\psi^\dagger_\uparrow\right] \\ &- 2\beta|\mathcal{G}^{(1/2)}_\uparrow(0)|^2 \ , \end{aligned} \tag{3.31}$$

where $\mathrm{Tr}_{1,2}$ means taking the trace with respect to the ground state $|1\rangle$ or $|2\rangle$. After somewhat tedious calculation we get

$$\begin{aligned}\bar{\chi}^{(1)}_{\uparrow\uparrow} &= \frac{-4(n_0+1)(n_0+2)}{[\epsilon(n_0,0)-\epsilon(n_0+1,0)]^2[\epsilon(n_0,0)-\epsilon(n_0+2,0)]} \\ &+ \frac{-4(n_0-1)n_0}{[\epsilon(n_0,0)-\epsilon(n-1,0)]^2[\epsilon(n_0,0)-\epsilon(n_0-2,0)]} \\ &+ \frac{-4n_0(n_0+1)}{[\epsilon(n_0-1,0)-\epsilon(n_0,0)]^2[\epsilon(n_0+1,0)-\epsilon(n_0,0)]} \\ &+ \frac{+4n_0(n_0+1)}{[\epsilon(n_0,0)-\epsilon(n_0+1,0)]^2[\epsilon(n_0,0)-\epsilon(n_0-1,0)]} \\ &+ \frac{-4n_0^2}{[\epsilon(n_0-1,0)-\epsilon(n_0,0)]^3} \\ &+ \frac{4(n_0+1)^2}{[\epsilon(n_0,0)-\epsilon(n_0+1,0)]^3} \quad , \end{aligned} \tag{3.32}$$

$$\begin{aligned}\bar{\chi}^{(2)}_{\uparrow\uparrow} &= \frac{-8}{[\epsilon(0,n_0)-\epsilon(1,n_0)]^2[\epsilon(0,n_0)-\epsilon(2,n_0)]} \\ &+ \frac{4}{[\epsilon(0,n_0)-\epsilon(1,n_0)]^3} \quad . \end{aligned} \tag{3.33}$$

Because of time reversal symmetry other four point correlators are readily obtained by $\bar{\chi}^{(1)}_{\downarrow,\downarrow} = \bar{\chi}^{(2)}_{\uparrow,\uparrow}$, $\bar{\chi}^{(2)}_{\downarrow,\downarrow} = \bar{\chi}^{(1)}_{\uparrow,\uparrow}$.

Similarly the off-diagonal part is calculated as follows

$$\begin{aligned}\bar{\chi}^{(1,2)}_{\uparrow\downarrow} &= \frac{1}{Z_0}\mathrm{Tr}_{1,2}\left[e^{-\beta H_0}T_\tau(e^{\tau_1 H_0}\psi_\uparrow e^{-\tau_1 H_0})\right. \\ &\quad \left.(e^{\tau_2 H_0}\psi^\dagger_\uparrow e^{-\tau_2 H_0})(e^{\tau_3 H_0}\psi_\downarrow e^{-\tau_3 H_0})\psi^\dagger_\downarrow\right] \\ &- \beta\mathcal{G}^{(1)}_\uparrow(0)\mathcal{G}^{(1)}_\downarrow(0), \end{aligned} \tag{3.34}$$

where $\mathrm{Tr}_{1,2}$ means taking the trace with respect to the ground state $|1\rangle$ or $|2\rangle$. After some straightforward calculation,

$$\bar{\chi}^{(1)}_{\uparrow\downarrow} = n_0 f_0 + (n_0+1) f_1, \tag{3.35}$$

with

$$\begin{aligned} f_0 &= \frac{-1}{[\epsilon(n_0,0)-\epsilon(n_0-1,0)]^2[\epsilon(n_0,0)-\epsilon(n_0-1,1)]} \\ &+ \frac{1}{[\epsilon(n_0,0)-\epsilon(n_0-1,0)]^2[\epsilon(n_0,0)-\epsilon(n_0,1)]} \\ &+ \frac{1}{[\epsilon(n_0,0)-\epsilon(n_0,1)]^2[\epsilon(n_0,0)-\epsilon(n_0-1,0)]} \\ &+ \frac{-1}{[\epsilon(n_0,0)-\epsilon(n_0,1)]^2[\epsilon(n_0,0)-\epsilon(n_0-1,1)]} \\ &+ \frac{-2/[\epsilon(n_0,0)-\epsilon(n_0-1,1)]}{[\epsilon(n_0,0)-\epsilon(n_0-1,0)][\epsilon(n_0,0)-\epsilon(n_0,1)]}, \end{aligned} \tag{3.36}$$

and

$$\begin{aligned} f_1 &= \frac{1}{[\epsilon(n_0,0)-\epsilon(n_0,1)]^2[\epsilon(n_0,0)-\epsilon(n_0+1,0)]} \\ &+ \frac{1}{[\epsilon(n_0,0)-\epsilon(n_0+1,0)]^2[\epsilon(n_0,0)-\epsilon(n_0,1)]} \\ &+ \frac{-1}{[\epsilon(n_0,0)-\epsilon(n_0,1)]^2[\epsilon(n_0,0)-\epsilon(n_0+1,1)]} \\ &+ \frac{-1}{[\epsilon(n_0,0)-\epsilon(n_0+1,0)]^2[\epsilon(n_0,0)-\epsilon(n_0+1,1)]} \\ &+ \frac{-2/[\epsilon(n_0,0)-\epsilon(n_0+1,1)]}{[\epsilon(n_0,0)-\epsilon(n_0+1,0)][\epsilon(n_0,0)-\epsilon(n_0,1)]}. \end{aligned} \tag{3.37}$$

$\bar{\chi}^{(2)}_{\uparrow\downarrow}$ is obtained from $\bar{\chi}^{(1)}_{\uparrow\downarrow}$ with $\epsilon(n,m)$ substituted by $\epsilon(m,n)$. For $n_0 > 1$, one can safely let $\bar{\chi}^{(2)}_{\uparrow\downarrow} = \bar{\chi}^{(1)}_{\uparrow\downarrow}$ and thus $\bar{\chi}_{\uparrow\downarrow} = \bar{\chi}^{(1)}_{\uparrow\downarrow}$ because $\epsilon(n,m) = \epsilon(m,n)$. However for $n_0 = 1$, both $\bar{\chi}^{(2)}_{\uparrow\downarrow}$ and $\bar{\chi}^{(1)}_{\uparrow\downarrow}$ are singular because $\epsilon(1,0) = \epsilon(0,1)$; while the average of these two is finite by taking the proper limit $\epsilon(1,0) = \epsilon(0,1) + 0^+$.

Up to this point, we have obtained the four point correlators from the original Hamiltonian in Eq. (3.4). In order to calculate $g_{\sigma_1\sigma_2}$, we still need the time average of the four point correlator defined by the effective action in Eq. (3.25). Since the local ground state of this theory is not unique, one should not naively apply the Feynman rules of the usual ϕ^4 field

theory. Similar to the approach we used above, we calculate the correlators on each ground state and then take the average. Thus we have

$$\begin{aligned}
\bar{\chi}_{\sigma_1\sigma_2} &= \int d\tau_1 d\tau_2 d\tau_3 \chi_{\sigma_1\sigma_2}(\tau_1,\tau_2,\tau_3,0) \\
&= \frac{\bar{\chi}^{(1)}_{\sigma_1\sigma_2} + \bar{\chi}^{(2)}_{\sigma_1\sigma_2}}{2} \\
&= -g_{\sigma_1\sigma_2} \left\{ [(\mathcal{G}^{(1)}_{\sigma_1}(0)\mathcal{G}^{(1)}_{\sigma_2}(0))^2 + (\mathcal{G}^{(1)}_{\sigma_1})^4 \delta_{\sigma_1,\sigma_2}] \right. \\
&\left. + [(\mathcal{G}^{(2)}_{\sigma_1}(0)\mathcal{G}^{(2)}_{\sigma_2}(0))^2 + (\mathcal{G}^{(2)}_{\sigma_1})^4 \delta_{\sigma_1,\sigma_2}] \right\} /2. \qquad (3.38)
\end{aligned}$$

Then $g_{\sigma_1\sigma_2}$ is obtained,

$$\begin{aligned}
g_{\sigma_1\sigma_2} &= -2\bar{\chi}_{\sigma_1\sigma_2} / \left\{ [(\mathcal{G}^{(1)}_{\sigma_1}(0)\mathcal{G}^{(1)}_{\sigma_2}(0))^2 + (\mathcal{G}^{(1)}_{\sigma_1})^4 \delta_{\sigma_1,\sigma_2}] \right. \\
&+ \left. [(\mathcal{G}^{(2)}_{\sigma_1}(0)\mathcal{G}^{(2)}_{\sigma_2}(0))^2 + (\mathcal{G}^{(2)}_{\sigma_1})^4 \delta_{\sigma_1,\sigma_2}] \right\}. \qquad (3.39)
\end{aligned}$$

We verify that these coefficients satisfy $g_{\uparrow\downarrow} > g_{\uparrow\uparrow}$.

3.3.3 Validity of the double Hubbard-Stratonovich transformation

The connected correlators of the original boson fields ψ_σ can be obtained from the generating functional

$$Z[J^*, J] \equiv e^{-\psi^*_\sigma T_{\sigma\sigma'}\psi_{\sigma'} - S_0[\psi^*,\psi] + [(J|\psi) + c.c.]}. \qquad (3.40)$$

For example,

$$\langle \psi_\sigma(x)\psi^*_{\sigma'}(x') \rangle_{S[\psi^*,\psi]} = \lim_{J\to 0} \frac{\delta \log Z[J^*, J]}{\delta J^*_\sigma(x)\delta J_{\sigma'}(x')}, \qquad (3.41)$$

where $x \equiv (\vec{r}, \tau)$ and $\langle \dots \rangle_{S[\psi^*,\psi]}$ means an average defined by the action $S[\psi^*, \psi] = \psi^*_\sigma T_{\sigma\sigma'}\psi_{\sigma'} + S_0[\psi^*, \psi]$. Introducing the first Hubbard-Stratonovich transformation,

$$\begin{aligned}
Z[J^*, J] &= \int D[\psi^*, \psi; \phi^*, \phi] \exp \left\{ \phi^*_\sigma T^{-1}_{\sigma\sigma'} \phi_{\sigma'} - S_0[\psi^*_\sigma, \psi_\sigma] \right. \\
&\left. + [(\phi|\psi) + c.c.] + [(J|\psi) + c.c.] \right\}. \qquad (3.42)
\end{aligned}$$

After a shift $\phi_\sigma \to \phi_\sigma - J_\sigma$, we get

$$\begin{aligned} Z[J^*, J] \quad &= \int D[\psi^*, \psi, \phi^*, \phi] e^{[(\phi|\psi)+c.c.]-S_0[\psi^*_\sigma, \psi_\sigma]} \\ &\times \exp\left\{(\phi_\sigma - J_\sigma)^* T^{-1}_{\sigma\sigma'}(\phi_{\sigma'} - J_{\sigma'})\right\}. \end{aligned} \tag{3.43}$$

After integrating out the ψ_σ fields, we get

$$\begin{aligned} Z[J^*, J] \quad &= Z_0 \int D[\phi^*, \phi] \exp\left\{(\phi_\sigma - J_\sigma)^* T^{-1}_{\sigma\sigma'}(\phi_{\sigma'} - J_{\sigma'})\right. \\ &\left. + W[\phi^*_\sigma, \phi_\sigma]\right\}. \end{aligned} \tag{3.44}$$

Now we introduce the second Hubbard-Stratonovich transformation

$$\begin{aligned} &Z[J^*, J] \\ &= Z_0 \int D[\varphi^*, \varphi; \phi^*, \phi] \exp\left\{-\varphi^*_\sigma T_{\sigma\sigma'}\varphi_{\sigma'} + [(\varphi|J) + c.c.]\right\} \\ &\times \exp\left\{-[(\varphi|\phi) + c.c.] + W[\phi^*_\sigma, \phi_\sigma]\right\}. \end{aligned} \tag{3.45}$$

Integrating out the ϕ_σ fields, we get

$$\begin{aligned} Z[J^*, J] \quad &= Z_0 \int D[\varphi^*, \varphi] \exp\left\{-\varphi^*_\sigma T_{\sigma\sigma'}\varphi_{\sigma'} + \tilde{W}[\varphi^*_\sigma, \varphi_\sigma]\right. \\ &\left. + [(\varphi|J) + c.c.]\right\}. \end{aligned} \tag{3.46}$$

The generating functional for φ_σ fields is equal to the generating functional of ψ_σ (up to a constant independent of the sources J). And this proves the connected correlators of φ_σ are the same as that of ψ_σ, although the action of φ_σ is very different from that of ψ_σ. For example,

$$\begin{aligned} &\langle \varphi_\sigma(x)\varphi^*_{\sigma'}(x')\rangle_{S_{\rm eff}[\varphi^*,\varphi]} = \lim_{J\to 0} \frac{\delta \log Z[J^*, J]}{\delta J^*_\sigma(x)\delta J_{\sigma'}(x')}, \\ &= \langle \psi_\sigma(x)\psi^*_{\sigma'}(x')\rangle_{S[\psi^*,\psi]}. \end{aligned} \tag{3.47}$$

where $\langle \dots \rangle_{S_{\rm eff}[\varphi^*,\varphi]}$ means an average defined by the action $S_{\rm eff}[\varphi^*, \varphi] = \varphi^*_\sigma T_{\sigma\sigma'}\varphi_{\sigma'} - \tilde{W}[\varphi^*_\sigma, \varphi_\sigma]$.

3.4 ZERO AND FINITE TEMPERATURE PHASE TRANSITIONS

Here, we focus on the lowest Mott lobe regime ($\nu = 1$) for which time reversal T symmetry is not broken. We start our analysis from the effective action (Eq. (3.25)). We use the correlators of quasi particle fields φ, which can be calculated within Bogoliubov theory, to approximate the correlation functions and momentum distribution of the bare particles. (The reason is explained in Sec. 3.3.3.) The method, we apply here, yields results [35] that agree with for example the RPA calculation [37], when calculating the momentum distribution of the s-band Bose-Hubbard model.

First, let us determine the ground state which is homogeneous and static after the staggered transformation (Eq. (3.3)). The free energy functional is

$$\frac{S}{N\beta} = (\mathcal{G}_\sigma^{-1}(0) + \epsilon_{\sigma\sigma}(\mathbf{k}=0))n_{s,\sigma} + \frac{1}{2}g_{\sigma_1\sigma_2}n_{s,\sigma_1}n_{s,\sigma_2}, \tag{3.48}$$

where N is the number of lattice sites, $\mathcal{G}_\sigma(i\omega)$ is the Fourier transform of $\mathrm{G}_\sigma(\tau)$ and $n_{s,\sigma} = |\langle\varphi_\sigma\rangle|^2$ is the superfluid density of the pseudo-spin σ component. By minimizing the free energy functional, we get

$$n_{s,\sigma} = \begin{cases} -\frac{\mathcal{G}_\sigma^{-1}(0)+\epsilon_{\sigma\sigma}(\mathbf{k}=0)}{g_{\sigma\sigma}} & \text{if } \mathcal{G}_\sigma^{-1}(0) + \epsilon_{\sigma\sigma}(\mathbf{k}=0) < 0; \\ 0 & \text{otherwise.} \end{cases} \tag{3.49}$$

In the Mott regime, $n_{s,\sigma}$ vanishes. In the superfluid regime, only one component is finite, i.e., either $n_{s,\uparrow}$ or $n_{s,\downarrow}$ is finite and the other vanishes, because the off-diagonal part $g_{\uparrow\downarrow}$ is greater than the diagonal part $g_{\uparrow\uparrow}$ ($= g_{\downarrow\downarrow}$). Thus $U(1) \times T$ is spontaneously broken across the Mott-superfluid phase transition in this model for filling $\nu = 1$. The phase boundary is shown in FIG. 2. The phase diagram is consistent with Ref. [31]. The Mott regime determined by our approach is larger. (When applied to calculate the phase boundary of s-band Bose-Hubbard model, the method adopted here yields results that agree with other mean field theories [35].) In the following part, we assume the superfluid component is the '↑' component. The superfluid density scales as $n_{s,\uparrow} \sim |n-\nu|^\zeta$ away from the Mott tip when the mean particle number per site, n, is not equal to ν, whereas it scales as $n_{s,\uparrow} \sim (t-t_c)^{\zeta'}$ at the Mott tip where $n = \nu$.

Next, we explore the fluctuations $\tilde{\varphi}_\sigma(\mathbf{r},\tau) = \varphi_\sigma(\mathbf{r},\tau) - \sqrt{n_{s,\sigma}}$. Expanding the action to the quadratic order of the fluctuation fields $\tilde{\varphi}_\sigma$, we get

$$S[\tilde{\varphi}^*_\sigma, \tilde{\varphi}_\sigma] = \frac{1}{2}\sum_{\mathbf{k},\omega} \Psi^\dagger(\mathbf{k}, i\omega)[h(\mathbf{k}, i\omega)]\Psi(\mathbf{k}, i\omega), \tag{3.50}$$

with

$$\Psi^\dagger(\mathbf{k}, i\omega) = \left[\tilde{\varphi}^*_\uparrow(\mathbf{k}, i\omega), \tilde{\varphi}_\uparrow(-\mathbf{k}, -i\omega), \tilde{\varphi}^*_\downarrow(\mathbf{k}, i\omega), \tilde{\varphi}_\downarrow(-\mathbf{k}, -i\omega)\right] \tag{3.51}$$

and

$$\begin{aligned}
h_{11} &= \epsilon_{\uparrow\uparrow}(\mathbf{k}) + \mathcal{G}^{-1}_\uparrow(i\omega) + 2g_{\uparrow\uparrow}n_s \quad , \\
h_{12} &= h_{21} = g_{\uparrow\uparrow}n_s \quad , \\
h_{13} &= h_{31} = \epsilon_{\uparrow\downarrow}(\mathbf{k}) \quad , \\
h_{22} &= \epsilon_{\uparrow\uparrow}(-\mathbf{k}) + \mathcal{G}^{-1}_\uparrow(-i\omega) + 2g_{\uparrow\uparrow}n_s \quad , \\
h_{24} &= h_{42} = \epsilon_{\downarrow\uparrow}(-\mathbf{k}) \quad , \\
h_{33} &= \epsilon_{\downarrow\downarrow}(\mathbf{k}) + \mathcal{G}^{-1}_\downarrow(i\omega) + g_{\uparrow\downarrow}n_s \quad , \\
h_{44} &= \epsilon_{\downarrow\downarrow}(-\mathbf{k}) + \mathcal{G}^{-1}_\downarrow(-i\omega) + g_{\uparrow\downarrow}n_s \quad ,
\end{aligned} \tag{3.52}$$

where $\tilde{\varphi}_\sigma(\mathbf{k}, i\omega)$ is the Fourier transform of $\tilde{\varphi}_\sigma(\mathbf{r},\tau)$. Only non-zero $[h]$ matrix elements are listed above. Using the quadratic action for fluctuations, we calculate the Bogoliubov spectrum.

3.4.1 Mott phase

In this part, we study the momentum distribution of p-band Mott insulator phase and we show that diverging peaks for bosons on p_x and p_y bands rise at finite momenta when the Mott gap closes. This offers new approaches of preparing coherent matter waves in experiments.

In the Mott phase, superfluid density $n_s = 0$. The Green function $\mathscr{G}_{\sigma_1\sigma_2}(\mathbf{k}, i\omega) = \langle\psi_{\sigma_1}(\mathbf{k}, i\omega)\psi^*_{\sigma_2}(\mathbf{k}, i\omega)\rangle = \langle\varphi_{\sigma_1}(\mathbf{k}, i\omega)\varphi^*_{\sigma_2}(\mathbf{k}, i\omega)\rangle$ is readily obtained as $\mathscr{G}^{-1}_{\sigma_1\sigma_2}(\mathbf{k}, i\omega) = \epsilon_{\sigma_1\sigma_2}(\mathbf{k}) + \mathcal{G}^{-1}_{\sigma_1}(i\omega)\delta_{\sigma_1\sigma_2}$. Solving the equation $\det[\mathscr{G}^{-1}(\mathbf{k}, \omega)] = 0$, we get the single particle spectra shown in FIG. 3 and FIG. 4. Deep in the Mott regime, all single particle excitations are

fully gapped. It can be verified that the Green function $\mathscr{G}_{\sigma_1,\sigma_2}(\mathbf{k}, i\omega)$ is diagonal in the $\{\psi_x(\mathbf{k}, i\omega),\ \psi_y(\mathbf{k}, i\omega)\}$ basis. Thus we can label the spectra by $E_x^{\pm}$ and $E_y^{\pm}$. The $E_x^+(E_x^-)$ branch is the p_x band of particle (hole) excitations; while $E_y^+(E_y^-)$ branch is the p_y band of particle (hole) excitations. Upon the phase transition point, the gap at $\mathbf{k} = 0$ drops and approaches zero. Away from the Mott tip, two particle branches (E_x^+ and E_y^+) touch zero first (FIG. 3), which causes the instability of the Mott insulator phase and drives the phase transition from Mott insulator to TSOC superfluid. For a more physical case in which the density is fixed to be an integer, both of particle and hole branches close simultaneously when increasing hopping because of the particle-hole symmetry at the Mott tip (FIG. 4). For both cases the gap closes right at the phase transition point determined by minimizing the free energy functional in Eq. (3.49).

At zero temperature, we obtain the momentum distribution $n(\mathbf{k}) \equiv \mathrm{Tr}\langle\psi^*_{\sigma_1}(\mathbf{k})\psi_{\sigma_2}(\mathbf{k})\rangle$ of the p-band Mott insulator phase from the Green function as $n(\mathbf{k}) = \frac{1}{2\pi}\int_{-\infty}^{+\infty} d\omega e^{i\omega 0^+}\mathscr{G}_{\sigma_1\sigma_2}(\mathbf{k}, i\omega)$. Extending the integration to a contour in the upper complex plane of ω, the momentum distribution measures the spectral weight of the negative pole of Green function $[\mathscr{G}(\mathbf{k}, \omega)]$ (the negative pole refers to the real part of the energy spectrum being negative). Deep in the Mott regime, the momentum distribution is very flat (FIG. 5). Approaching the phase transition point from Mott insulator side, a peak at zero momentum develops, and the peak diverges right at the critical point where the Mott gap closes(FIG. 5). The continuous development of the peak of the momentum distribution at $\mathbf{k} = 0$ means the phase coherence ($\langle\hat{\psi}_x^\dagger(\mathbf{r})\hat{\psi}_x(\mathbf{r}')\rangle$ and $\langle\hat{\psi}_y^\dagger(\mathbf{r})\hat{\psi}_y(\mathbf{r}')\rangle$) develops continuously when increasing hopping in the Mott regime. However, we do not see the phase coherence of ψ_x and ψ_y components, i.e., $\langle\hat{\psi}_x^\dagger(\mathbf{r})\hat{\psi}_y(\mathbf{r}')\rangle$ always vanishes in the Mott regime even when $\mathbf{r} = \mathbf{r}'$. To compare with experiments, we also obtain the Green function for the original bosons and get the momentum distribution of original bosons shown in FIG. 6. Near phase transition point in the p-band Mott insulator phase, the momentum distribution for p_x bosons shows a peak at $(\pm\pi, 0)$ and the momentum distribution for p_y bosons shows a peak at $(0, \pm\pi)$. This offers possibilities of observing coherent matter waves from p-band Mott insulator.

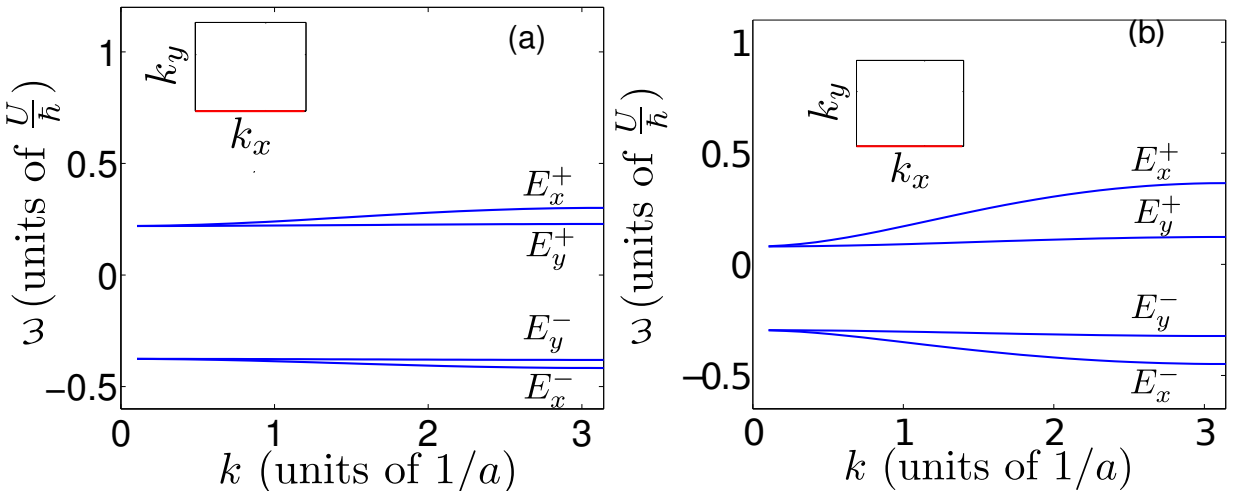

Figure 3: (a) The single particle spectra along the k_x axis deep in the Mott regime with parameters $\mu/U = 0.4, t/U = 0.02, t_\perp = 0.1t$. (b) The single particle spectra along the k_x axis in the Mott regime near the critical point with parameters $\mu/U = 0.4, t/U = 0.065, t_\perp = 0.1t$. The Mott gap drops when increasing hopping and the gap of particle branches closes at the critical point for $\mu/U = 0.4$. The insets indicate the k_x axis in the Brillouin zone.

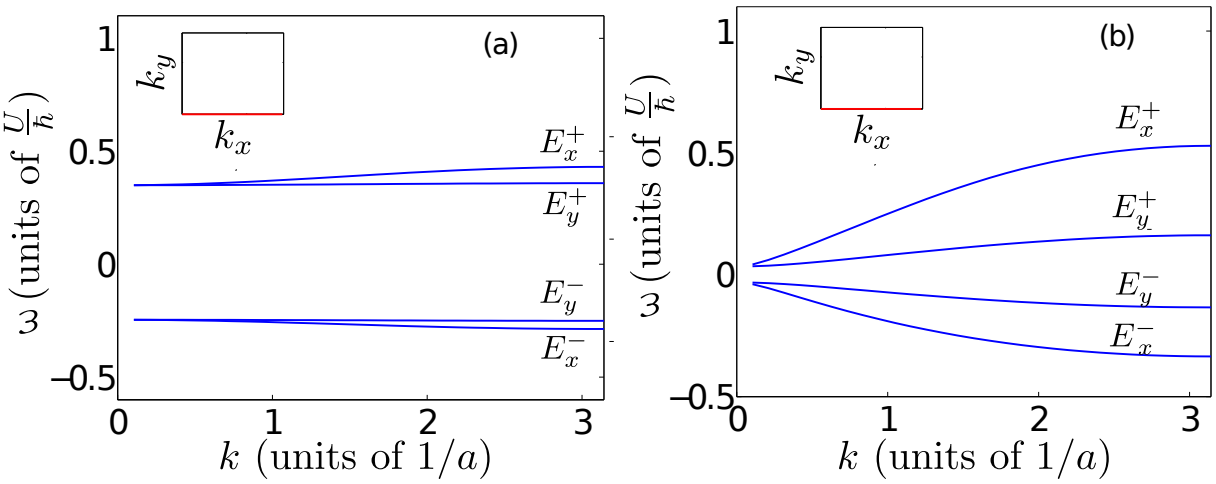

Figure 4: (a) The single particle spectra along k_x axis deep in the Mott regime with parameters $\mu/U = 0.27, t/U = 0.02, t_\perp = 0.1t$. (b) The single particle spectra along the k_x axis in the Mott regime near the critical point with parameters $\mu/U = 0.27, t/U = 0.09, t_\perp = 0.1t$. The Mott gap for both of the particle and hole branches closes at the critical point at the Mott tip regime. The insets indicate the k_x axis in the Brillouin zone.

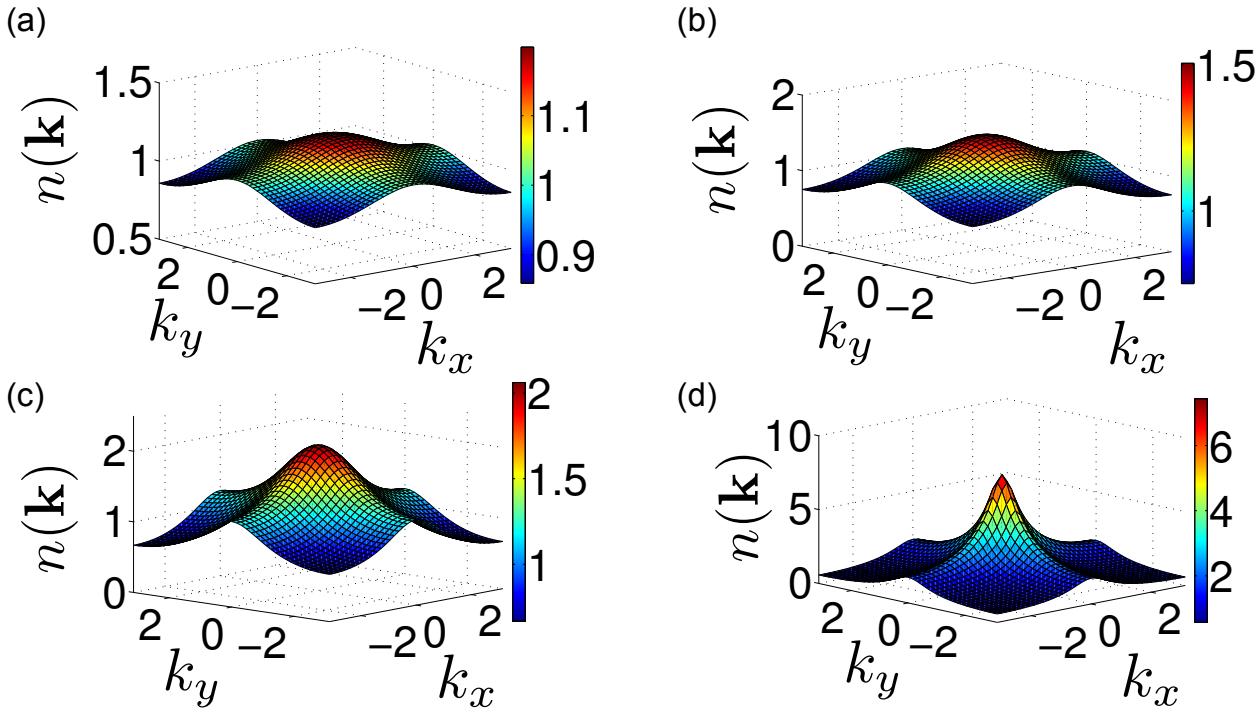

Figure 5: The momentum distribution defined by $\mathrm{Tr}\langle\psi^*_{\sigma_1}(\mathbf{k})\psi_{\sigma_2}(\mathbf{k})\rangle$ in the Mott regime with parameters $\mu/U = 0.3, t_\perp = 0.1t$. For (a) through (d), the parallel hopping t/U is 0.02, 0.04, 0.06 and 0.09 respectively. A coherent peak rises continuously when approaching the Mott-superfluid transition point from the Mott insulator side. The unit for lattice momentum k is a^{-1} with a the lattice constant.

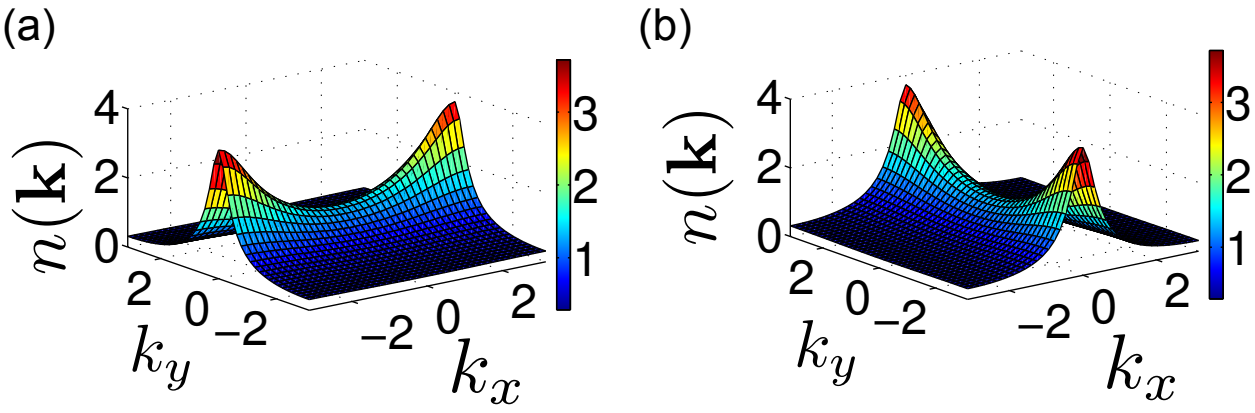

Figure 6: The momentum distribution (a) for p_x band boson and (b) for p_y band boson in the p-band Mott insulator phase near the Mott-superfluid phase transition point. The parameters we use are $\mu/U = 0.3$, $t/U = 0.09$ and $t_\perp = 0.1t$. The unit for lattice momentum k is a^{-1} with a the lattice constant.

3.4.2 Superfluid phase

The single particle excitation spectrum of the TSOC superfluid is calculated within Bogoliubov theory. Solving the equation $\det[h(\mathbf{k}, i\omega)] = 0$, the spectrum is obtained. Deep in the TSOC superfluid phase, there are four branches, one of which is gapless and linear around momentum $\mathbf{k} = 0$ (FIG. 7). The spectra can no longer be understood in the same way as in the Mott regime, since the time reversal symmetry is broken. For momentum $k_x = \pm k_y$, the excitations have definite pseudo-spin, while for generic momenta, the excitations do not carry definite pseudo-spin. The $\uparrow$ and $\downarrow$ components are actually mixed unless $k_x = \pm k_y$. The physical reason for this is that the dispersion $\epsilon_{\sigma_1\sigma_2}(\mathbf{k})$ is not diagonal for generic momenta.

Deep in the superfluid regime, the off-diagonal term $\epsilon_{\uparrow\downarrow}$ does not affect the U(1) phase mode for the reason that the mode of flipping pseudo-spin is fully gapped (the gap is $g_{\uparrow\downarrow}n_s$) in that regime (FIG. 7(b)). And the spectrum of the phase mode ($\omega_{U(1)}(\mathbf{k})$) of TSOC superfluid is fully determined by h_{11}, h_{12}, h_{21} and h_{22} in Eq. (3.52), all of which are isotropic to the quadratic order of momentum $\mathbf{k}$. The sound velocity defined by $\partial_{\mathbf{k}}\omega_{U(1)}(\mathbf{k})|_{\mathbf{k}\to 0}$ is thus isotropic in the weak coupling regime as derived in Ref. [12]. In the strong coupling regime,

the gap of flipping pseudo-spin becomes smaller near the phase transition point (FIG. 7(a)), and the coupling ($\epsilon_{\uparrow\downarrow}(\mathbf{k})$) between $\psi_\uparrow$ and $\psi_\downarrow$ will modify $\omega_{U(1)}(\mathbf{k})$. However, the correction to $\omega_{U(1)}(\mathbf{k})$ in the limit of $\mathbf{k} \to 0$ is to the order of $(t+t_\perp)^2 \frac{(k_x^2-k_y^2)^2}{g_{\uparrow\downarrow} n_s}$, so $\partial_{\mathbf{k}} \omega_{U(1)}(\mathbf{k})|_{\mathbf{k}\to 0}$ is unaffected. Thus the sound velocity of TSOC superfluid is isotropic in the strong coupling regime.

3.4.3 Finite temperature phase transitions of TSOC superfluid phase.

Strong coupling regime.— In the TSOC superfluid phase, we can neglect the temporal fluctuations of the fields. Thus we have

$$\begin{bmatrix} \varphi_x(\mathbf{r}) \\ \varphi_y(\mathbf{r}) \end{bmatrix} = \sqrt{n_s/2} \begin{bmatrix} e^{i\theta(\mathbf{r})}(-)^{s_x(\mathbf{r})} \\ e^{i\theta(\mathbf{r})+\frac{\pi}{2}}(-)^{s_y(\mathbf{r})} \end{bmatrix}, \tag{3.53}$$

where $s_{x/y}(\mathbf{r}) = 0$ or 1. This substitution captures the thermal fluctuations of the TSOC superfluid phase in the strong coupling regime. And the energy functional describing the fluctuations of θ and s fields is

$$\begin{aligned} E = & -J_\theta \sum_{\mathbf{r}} \left[\cos(\theta(\mathbf{r}) - \theta(\mathbf{r}+\hat{x})) + \cos(\theta(\mathbf{r}) - \theta(\mathbf{r}+\hat{y}))\right] \\ & + \sum_{\mathbf{r}} \left[-J_1 e^{i\pi s_y(\mathbf{r})} e^{i\pi s_y(\mathbf{r}+\hat{y})} - J_2 e^{i\pi s_y(\mathbf{r})} e^{i\pi s_y(\mathbf{r}+\hat{x})}\right] \\ & + \sum_{\mathbf{r}} \left[-J_1 e^{i\pi s_x(\mathbf{r})} e^{i\pi s_x(\mathbf{r}+\hat{x})} - J_2 e^{i\pi s_x(\mathbf{r})} e^{i\pi s_x(\mathbf{r}+\hat{y})}\right], \end{aligned} \tag{3.54}$$

where $J_\theta = (|t| + |t_\perp|)n_s/2$, $J_1 = |t|n_s/2$ and $J_2 = |t_\perp|n_s/2$. The θ part is an isotropic XY model and the s_x s_y parts are anisotropic Ising model. Considering the thermal fluctuations of $\theta(\mathbf{r})$, $s_x(\mathbf{r})$ and $s_y(\mathbf{r})$ separately, we can define two transition temperatures—the Kosterlitz Thouless (KT) transition temperature $\mathrm{T_{KT}}$ and the Ising transition temperature $\mathrm{T_{Ising}}$. $\mathrm{T_{KT}}$ is well approximated by $\mathrm{T_{KT}} \approx \frac{\pi}{2} J_\theta$ [40]. The Ising temperature is $\mathrm{T_{Ising}} = \frac{2}{\log(1+\sqrt{2})} J_{\mathrm{eff}}$, where J_{eff} is determined by $\sinh(2J_1/\mathrm{T_{Ising}})\sinh(2J_2/\mathrm{T_{Ising}}) = \sinh^2(2J_{\mathrm{eff}}/\mathrm{T_{Ising}})$ [41]. For $|t_\perp| \ll |t|$, $\mathrm{T_{Ising}} \ll \mathrm{T_{KT}}$ because $J_{\mathrm{eff}} \to 0$ when $t_\perp \to 0$. At temperature lower than $\mathrm{T_{Ising}}$, the TSOC superfluid phase has an algebraic U(1) ordering and a long range Ising ordering (orbital order). At temperature higher than $\mathrm{T_{Ising}}$, the orbital ordering disappears. Because of the existence of free Ising kinks (flips of pseudo-spin), half vortices with boundary condition

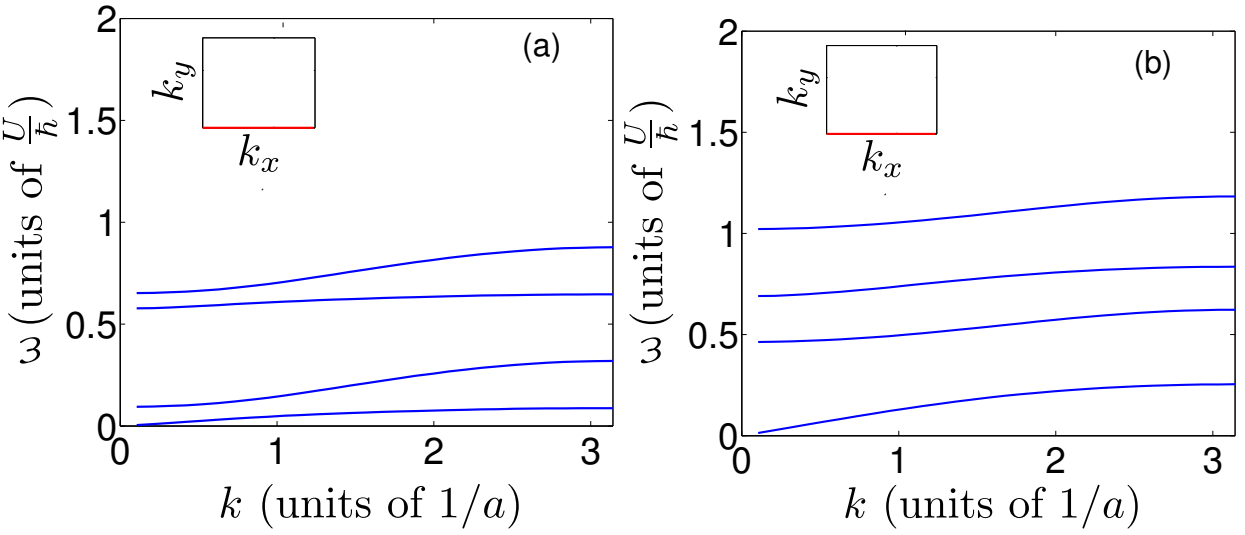

Figure 7: The Bogoliubov spectra in the TSOC superfluid phase. (a) shows the spectra along k_x axis near critical point with parameters $\mu/U = 0.5$, $t/U = 0.065$, $t_\perp = 0.1t$. (b) shows the spectra along k_x axis deep in the superfluid phase with parameters $\mu/U = 0.5, t/U = 0.1, t_\perp = 0.1t$. The insets indicate the k_x axis in the Brillouin zone.

$\oint d\theta = \pi$ are possible, which will modify the KT transition temperature. The modified KT transition temperature is $\mathrm{T_{KT}} \approx \frac{\pi}{8} J_\theta$ when $|t_\perp| \ll |t|$. The schematic finite temperature phase diagram is shown in FIG. 8.

Weak coupling regime.— In the weak coupling regime, the substitution

$$\begin{bmatrix} \varphi_x(\mathbf{r}) \\ \varphi_y(\mathbf{r}) \end{bmatrix} = \sqrt{n_s/2} \begin{bmatrix} e^{i\theta_x(\mathbf{r})} \\ e^{i\theta_y(\mathbf{r})} \end{bmatrix}, \tag{3.55}$$

captures the leading thermal fluctuations. We only consider infinitesimal interaction strength. The energy functional describing the fluctuations is

$$E = \int d^2\mathbf{x} \frac{1}{4} t n_s \left((\partial_x \theta_x)^2 + (\partial_y \theta_y)^2 \right) + \frac{1}{4} t_\perp n_s \left((\partial_y \theta_x)^2 + (\partial_x \theta_y)^2 \right). \tag{3.56}$$

The system is in a normal phase above the KT transition temperature $T_{\mathrm{KT}} = \frac{n_s \pi}{2} \sqrt{t t_s}$. Below the KT transition temperature the vortex fluctuations are negligible. The inter-orbital interaction generates a sine-Gordon term $g \cos(2\Delta)$ ($\Delta = \theta_x - \theta_y$). With the field $\theta_x + \theta_y$ integrated out, the energy functional describing Δ is

$$E = \int d^2\mathbf{x} \frac{1}{4} n_s t_\perp (\vec{\nabla} \Delta)^2 + g \cos(2\Delta). \tag{3.57}$$

The sine-Gordon term is relevant below the temperature $T_{\mathrm{SG}} = \frac{n_s \pi}{4} t_\perp$ in the sense of renormalization group. This is the transition temperature from orbital disordered superfluid phase to the orbital ordered TSOC phase.

Figure 8: The schematic plot of finite temperature phase diagram in the TSOC superfluid regime. Tc_1 is the Ising transition temperature. Below Tc_1, the orbital order and the superfluid order coexist for the TSOC superfluid phase. Tc_2 is the KT transition temperature. For temperature above Tc_1 and below Tc_2, the orbital order no longer exists but the superfluid order still survives. Above Tc_2, no order exists and the lattice bose gas is in the normal phase.

3.5 CONCLUSION

We have developed a theory of an extended Bose-Hubbard model with p-orbital degrees of freedom, which is valid in the strong coupling regime. With this theory, we explored the single particle spectra in the Mott insulator phase and the Bogoliubov quasi-particle spectra in the TSOC superfluid phase. We studied how the momentum distribution develops in the Mott insulator phase when increasing the inter-site hopping and found that diverging peaks rise in momentum distribution at finite momenta when the Mott gap closes. We explained the isotropy of the sound velocity of the TSOC superfluid phase. The finite temperature phase transitions of the TSOC superfluid phase are discussed. Finally we mention here that the checkerboard lattice in experiments [14] has advantages in preparing long life-time p-band phases. Given the consistency of the experimental results with previous theoretical studies on a simple square lattice [1], our predictions are expected to be relevant to experimental lattices.

4.0 TIME REVERSAL SYMMETRY BREAKING IN P-ORBITAL BOSONS IN ONE-DIMENSIONAL OPTICAL LATTICE

Theoretical studies on high orbital band bosons have predicted the quantum phases are beyond standard [31, 1, 32, 33, 42, 43, 44, 17], and there has been experimental evidence [13, 14, 16, 15] which is consistent with the theoretical predictions. However concrete evidence is still lacking, and it is still challenging to distinguish the non-standard phases of high orbital bosons from the standard phases. Probing the time reversal symmetry (TRS) breaking in the superfluid (SF) and Mott insulating phases of p-orbital bosons is a demanding task for both theorists and experimentalists. A phase-sensitive scheme of detecting the TRS breaking of the TSOC superfluid phase [1, 17, 13] has been proposed very recently [45].

Our work [18] has proposed a 'smoking gun' feature of TRS breaking in the Mott phases, which is probable in experiments. A system of bosons loaded in p_x and p_y orbits of a one dimensional (1D) optical lattice at zero temperature, has been studied with both numerical simulations and field-theoretical methods. We find two SF phases distinguished by an orbital order—an anti-ferro-orbital (AFO) SF and a para-orbital (PO) SF, and two Mott insulating phases—an AFO Mott and a p_x Mott phase (FIG. 9). The AFO order is a staggered orbital current ($p_x \pm ip_y$) order [31, 1]. In the AFO SF phase, the inter-band phase difference is locked at $\pm\frac{\pi}{2}$ and the spontaneous AFO ($p_x \pm ip_y$) order in this phase breaks the TRS, whereas the fluctuations of the relative phase restore the TRS in the PO SF phase. Based on our results, we propose an experimental method to distinguish different phases by measuring momentum distribution (MD) (FIG. 10), instead of directly measuring the local current flow resulting from TRS breaking. In this way the PO to AFO quantum phase transition, associated with TRS breaking, can be observed in experiments. The finite momentum peaks in the MD of the AFO SF phase require less experimental efforts to measure than the zero momentum

peaks of the conventional 1D SF phases [46]. In the AFO Mott phase the quantum noise measurement will be able to provide a concrete evidence of spontaneous TRS breaking.

4.1 EXPERIMENTAL PROPOSAL

The system we shall propose is a one dimensional lattice elongated along the x direction, and each lattice site has a rotation symmetry in the x-y plane (FIG. 9). In other words, the p_x and p_y orbits are locally degenerate, but the hopping differs significantly. Such a 1D system can be realized from a 2D optical lattice. Suppose the 2D optical lattice is formed by different laser beams in the x and y directions and the lattice potential reads $V = V_x \sin^2(k_x x) + V_y \sin^2(k_y y)$, where V_x and k_x (V_y and k_y) are the strength and wave numbers of the laser beams in the x (y) direction. In tight binding approximation, we can use the harmonic wavefunctions to approximate the Wannier functions. In the harmonic approximation, the local isotropy (rotation symmetry of each site in the x-y plane) requires $V_x k_x^2 = V_y k_y^2$. This relation, which guarantees the (approximate) two-fold orbital degeneracy at each lattice site, can be somewhat surprisingly well held in the 1D limit by taking the lattice potential depth $V_y \gg V_x$ and simultaneously the lattice constants a_y ($= \frac{\pi}{k_y}$) $\gg a_x$ ($= \frac{\pi}{k_x}$). As a result, the local isotropy is maintained, but the system has stronger potential and larger lattice spacing in the y direction than x, which makes the hopping in the y direction smaller than that in the x direction. The system becomes approximately 1D, when the hopping in the y direction is much smaller than that in the x direction. As an example, we take $V_x/E_{R,x} = 16$, $V_y/E_{R,y} = 32$ and $a_y/a_x = 2^{1/4}$, where $E_{R,\alpha} \equiv \hbar^2 k_\alpha^2/2m$ is the recoil energy in the α direction. Such a system is locally isotropic, while the hopping of p_y orbital in the y direction is about $1/40$ of the hopping of p_x orbital in the x direction, and the system is dynamically 1D. With the technique in Ref. [14], bosons can be loaded in the p-orbits of optical lattices. And this meta-stable state has fairly long life time [14]. The key ingredient of suppressing loss from p-orbital bands in experiments is mismatching band gaps, that is making the gap between p-bands to d-bands different from that between the lowest s band and p-bands.

4.2 MODEL AND METHOD

4.2.1 Model

In the 1D limit, the Hamiltonian describing bosons loaded in these p_x and p_y orbits reads [1]

$$\begin{aligned} H = & \sum_{<jj'>} -t_x \hat{a}_x^\dagger(j)\hat{a}_x(j') - t_y \hat{a}_y^\dagger(j)\hat{a}_y(j') \\ & + \sum_j \frac{U}{2}\left[\hat{n}(j)(\hat{n}(j)-\frac{2}{3}) - \frac{1}{3}\hat{L}_z^2(j) - \mu\hat{n}(j)\right]. \end{aligned} \tag{4.1}$$

Here $\hat{a}_x(j)$ ($\hat{a}_y(j)$) is the annihilation operator for p_x (p_y) orbital at site j. The discrete variable j labels the sites of the 1D chain, with the lattice constant a_x. The local particle number operator $\hat{n}(j)$ is defined as $\sum_{\alpha=x,y}\hat{a}_\alpha^\dagger(j)\hat{a}_\alpha(j)$, and the local angular momentum operator $\hat{L}_z(j)$ is defined as $\sum_{\alpha,\beta}\epsilon_{\alpha\beta}(-i\hat{a}_\alpha^\dagger(j)\hat{a}_\beta(j))$, where the superscripts α and β run over x and y. t_x (<0) is the longitudinal hopping of p_x bosons, and t_y (>0) is the transverse hopping of p_y bosons (FIG. 9). U (>0) is the repulsive Hubbard interaction. The average number of bosons per site is fixed by chemical potential μ. In this chapter the ratio $|t_x/t_y|$ is fixed as 9.

The hopping term has a U(1)×U(1) symmetry, which is $\hat{a}_\alpha(j) \to [e^{i\sigma_0\theta}e^{i\sigma_z\phi}]_{\alpha\beta}\hat{a}_\beta(j)$, with $\sigma_0 = \begin{bmatrix} 1 & 0 \\ 0 & 1 \end{bmatrix}$ and $\sigma_z = \begin{bmatrix} 1 & 0 \\ 0 & -1 \end{bmatrix}$. It appears that the particle numbers of p_x and p_y components, $N_x = \sum_j n_x(j)$ and $N_y = \sum_j n_y(j)$ are separately conserved. However the pair hopping term $\hat{a}_y^\dagger\hat{a}_y^\dagger\hat{a}_x\hat{a}_x$ from $\hat{L}_z^2$ does not conserve N_x and N_y separately, and thus breaks the U(1)×U(1) symmetry. Only the total particle number $N = N_x + N_y$ is conserved. The U(1)×U(1) symmetry is reduced to U(1)×Z_2 defined as $\hat{a}_\alpha(j) \to [e^{i\sigma_0\theta}e^{i\sigma_z\frac{\pi}{2}}]_{\alpha\beta}\hat{a}_\beta(j)$.

4.2.2 Methods

We use a matrix product state (MPS) to represent the ground state [47], which is

$$|\psi\rangle = \sum_{\sigma_1\ldots\sigma_L} \mathrm{Tr}\left[A^{\sigma_1}[1]\ldots A^{\sigma_L}[L]\right]|\sigma_1\ldots\sigma_L\rangle, \tag{4.2}$$

where $A^{\sigma_j}[j]$ is a rank χ matrix defined at site j. $|\sigma_j\rangle$ represents the basis of local Hilbert space at site j. The ground state is obtained by optimizing the A matrices iteratively [47]. The method is equivalent to the single site DMRG method [48]. Because of the large local Hilbert space, this method is more efficient than the two site DMRG method [49] in our problem. To avoid potential trapping in the iterative optimization procedure, we implement White's correction [48], which protects reasonably against trapping. An open boundary condition is adopted in this work. The good quantum number we used in our numerical calculation is the total particle number $\sum_j n(j)$.

The chemical potential is calculated as the energy it takes to add a particle or hole to the many-body state [50, 51]. Numerical errors of energies are estimated from $\sqrt{\langle H^2\rangle - \langle H\rangle^2}$. The largest system studied has 120 sites, which is large enough to compare with experiments on 1D quantum gases [46]. With the numerical method the ground state phase diagram of Hamiltonian in Eq. (4.1) is mapped out and shown in FIG. 9. The Mott gaps and error bars in Fig. 9 are determined by extrapolating to the thermodynamic limit with least squares fitting. The phase boundary of the Mott insulating phase is determined by the vanishing of Mott gap. The phase boundary between the AFO and PO SF phases is determined by the vanishing of the Z_2 order parameter, defined as $\tilde{L}_z \equiv \frac{1}{L}\sum_j \langle e^{iQj}\hat{L}_z(j)\rangle$, with $Q = \pi$. We use a system of 40 sites to determine this phase boundary. The existence of the AFO and PO SF phases is verified for a system with up to 100 sites. The central focus of this paper is the finding of unexpected quantum orbital phases in a 1D optical lattice. A more accurate calculation of phase boundaries is left for future study.

4.3 PHASE DIAGRAM

With the variational MPS method the ground state phase diagram of Hamiltonian in Eq. (4.1) is mapped out and shown in FIG. 9. The phase boundary of the Mott insulating phase is determined by the vanishing of Mott gap. The phase boundary between the AFO and PO SF phases is determined by the vanishing of the Z_2 order parameter, defined as $\tilde{L}_z \equiv \frac{1}{L}\sum_j \langle e^{iQj}\hat{L}_z(j)\rangle$, with $Q = \pi$.

Mott phases.— For the Mott phases (FIG. 9), the filling factor $\nu = \langle \hat{n}(j) \rangle$ at each site is commensurate. The occupation number for each orbit, both $\langle \hat{a}_x^\dagger \hat{a}_x \rangle$ and $\langle \hat{a}_y^\dagger \hat{a}_y \rangle$ are incommensurate. For filling ν greater than 1, the Mott phase features a complex order

$$\langle \hat{a}_x^\dagger(j) \hat{a}_y(j) \rangle \sim e^{iQj} e^{i\zeta \frac{\pi}{2}}$$

with $\zeta = \pm$ spontaneously chosen, which breaks the U(1)×Z_2 symmetry down to U(1). Equivalently this Mott state has a staggered angular momentum order $\langle \hat{L}_z(j) \rangle \sim e^{iQj}$. The order parameter $\tilde{L}_z$ is finite. Without loss of generality, we have assumed $\tilde{L}_z$ is positive. This Z_2 order also breaks the TRS, because finite $\tilde{L}_z$ means a finite local vortex-like current flow. For filling ν equal to 1, the Z_2 order does not exist for $|t_y| \ll |t_x|$. We call it p_x Mott since p_x boson dominates this Mott phase, i.e., $\langle \hat{a}_x^\dagger \hat{a}_x \rangle \gg \langle \hat{a}_y^\dagger \hat{a}_y \rangle$ for $|t_x| \gg |t_y|$. In these Mott phases, the phase correlations $\langle a_{\nu_1}^\dagger(j) a_{\nu_2}(j') \rangle$ decay exponentially, signifying finite charge charge gaps.

AFO superfluid phase.— By increasing the hopping the system goes into the SF phase when the Mott gap closes. The system has a phase transition from the AFO Mott phase to the AFO SF phase (FIG. 9). Since the Z_2 symmetry is broken in this SF phase, it behaves like a single component SF phase far from the Z_2 critical point. This AFO SF phase is thus characterized by an algebraic correlation

$$\langle \hat{a}_\uparrow^\dagger(j') \hat{a}_\uparrow(j) \rangle \sim |j - j'|^{-K/2},$$

where $\hat{a}_\uparrow^\dagger(j) = e^{iQj} \hat{a}_x^\dagger(j) + i\xi \hat{a}_y^\dagger(j)$, with $\xi \in (0, 1]$. $\xi = 1$ in the limit of $t_x/U \to 0$. The phase correlations of original boson operators, defined as $G_{\alpha\beta}(j, j') = \langle \hat{a}_\alpha^\dagger(j) \hat{a}_\beta(j') \rangle$, are given by

$$\begin{aligned} G_{xx}(j, j') &\sim e^{iQ(j-j')} |j - j'|^{-K/2} \\ G_{xy}(j, j') &\sim i e^{iQj} |j - j'|^{-K/2} \\ G_{yy}(j, j') &\sim |j - j'|^{-K/2} \end{aligned} \tag{4.3}$$

in the AFO SF phase. We emphasize that the TRS is broken in this phase, because the off-diagonal correlation $G_{xy}(j, j')$ is complex. The key feature is that the power law decay ($|j - j'|^{-K/2}$) correlations (G_{xx} G_{xy} and G_{yy}) exhibit the same power exponent $K/2$. In this phase, the relative phase (φ_-) between the p_x and p_y SF components is locked. The two

components share the same $U(1)$ phase φ_+ at low energy. The Lagrangian describing phase fluctuations is

$$\mathcal{L}[\varphi_+] = \frac{1}{2\pi K}\left[\frac{1}{v_+}(\partial_\tau\varphi_+)^2 + v_+(\partial_x\varphi_+)^2\right]. \tag{4.4}$$

The Bose liquid is completely characterized by the sound velocity v_+ and Luttinger parameter K. For $K < \frac{1}{2}$, the AFO SF phase is stable against the periodic lattice potential; for $K > \frac{1}{2}$ at commensurate filling, this phase is unstable and undergoes a localization transition towards the Mott phase [52, 28]. The AFO order is preserved across the localization transition in our system.

PO superfluid phase.— The AFO order disappears for larger hopping, and the AFO SF gives way to the PO SF. The behavior of the Z_2 order parameter $\tilde{L}_z$ and occupation numbers of p_x and p_y bosons across the phase transition is shown in FIG. 11. The Z_2 order is destroyed by quantum fluctuations of φ_- and thus the TRS is restored in the PO SF phase. The phase correlations of the original bosons in this phase are given by

$$\begin{aligned} G_{xx}(j,j') &\sim e^{iQ(j-j')}|j-j'|^{-K_x/2} \\ G_{yy}(j,j') &\sim |j-j'|^{-K_y/2}. \end{aligned} \tag{4.5}$$

The phase coherence between p_x and p_y components—$G_{xy}(j,j')$—vanishes in this phase. By numerical simulations, we find $K_x \ll K_y$. Following Haldane [53], an analytic expression estimating K_x/K_y is derived, $\frac{K_x}{K_y} \approx \sqrt{|\frac{t_y n_y}{t_x n_x}|}$, where n_x (n_y) is the filling of p_x (p_y) bosons. This is in qualitative agreement with the numerical results. The Lagrangian describing this PO SF phase is

$$\begin{aligned} \mathcal{L}[\varphi_x,\varphi_y] &= \sum_{\alpha=x,y}\frac{1}{2\pi K_\alpha}\left[\frac{1}{v_\alpha}(\partial_\tau\varphi_\alpha)^2 + v_\alpha(\partial_x\varphi_\alpha)^2\right] \\ &\quad +\lambda(\partial_\tau\varphi_x)(\partial_\tau\varphi_y), \end{aligned} \tag{4.6}$$

where φ_x (φ_y) is the phase of p_x (p_y) SF component. The mixing term (λ) is much smaller than the kinetic term ($\frac{1}{2\pi K_\alpha v_\alpha}$) in our system.

Quantum phase transition from AFO to PO in the superfluid phases.— The phase transition from the AFO SF to the PO SF is described by a sine-Gordon model of the relative phase φ_-. The Lagrangian is

$$\mathcal{L}[\varphi_-] = \frac{1}{2\pi K_-}\left[\frac{1}{v_-}(\partial_\tau\varphi_-)^2 + v_-(\partial_x\varphi_-)^2\right] + m\cos(2\varphi_-), \tag{4.7}$$

where m is estimated as $m \approx \frac{1}{3}Un_xn_y$. When m is greater than some critical $m_c(K_-)$, the sine-Gordon theory is in a gapped phase [54], and therefore φ_- field is locked at one minimum of $m\cos(2\varphi_-)$. Such an orbital gapped phase is the AFO SF phase. When $m < m_c(K_-)$, the sine-Gordon term $m\cos(2\varphi_-)$ is irrelevant in the sense of renormalization group, and the theory is in a gapless phase for which φ_- is no longer locked. This orbital-gapless phase is the PO SF phase. We emphasize here the sine-Gordon term is not perturbative in our model.

4.4 EXPERIMENTAL SIGNATURES

Since the quantum phases we have found are characterized by distinct phase correlations, measuring the MDs by TOF will distinguish different phases. The MDs are shown in FIG. 10. The advantage of the AFO SF over conventional 1D SF phases is that the finite momentum peaks require less experimental efforts to measure. For conventional 1D SF phases, the dominant peak of MD is at $\mathbf{k} = \mathbf{0}$, which implies long expansion time to measure the peak in MD [46]. In the AFO SF phases, the strong peaks at finite momenta provide possibilities of precise measurement of MD near the peaks, say $k_x = \pm\pi/a_x$. The Luttinger parameter can be obtained by precisely measuring MD, because $\log(n_{1d}(k_x)) \sim (\frac{K}{2} - 1)\log(|k_x \pm \pi/a_x|)$ for k_x near $\pm\pi/a_x$.

In the Mott regime, the AFO order will have experimental signatures in the quantum noise measurement. The quantum noise is defined as

$$C(\mathbf{d}) = \int d^2\mathbf{X}\langle n_{\text{tof}}(\mathbf{X} + \frac{1}{2}\mathbf{d})n_{\text{tof}}(\mathbf{X} - \frac{1}{2}\mathbf{d})\rangle - \langle n_{\text{tof}}(\mathbf{X} + \frac{1}{2}\mathbf{d})\rangle\langle n_{\text{tof}}(\mathbf{X} - \frac{1}{2}\mathbf{d})\rangle, \tag{4.8}$$

with $\mathbf{X} = (X, Y)$, $\mathbf{d} = (d_x, d_y)$. $n_{\rm tof}$ is the density obtained from a single absorption image and the brackets $\langle\,\rangle$ denote statistical averages of independently acquired images [55]. Since our proposed experimental setup is in 2D, we derived the quantum noise in the 2D x-y plane. In Mott phases with p-orbital degrees of freedom $C(\mathbf{d})$ is given by

$$\begin{aligned} C(\mathbf{d}) &= N_s \int d^2\mathbf{X} \left\{ \sum_{\mathbf{K}} \delta^{(2)} \left(\frac{m}{\hbar t}\mathbf{d} - \mathbf{K} \right) \left(\zeta_{xx} n_x + \zeta_{yy} n_y \right)^2 \right. \\ &\left. + N_s \sum_{\mathbf{K}} \delta^{(2)} \left(\frac{m}{\hbar t}\mathbf{d} - \mathbf{K} + \mathbf{Q}_x + \mathbf{Q}_y \right) \left(\zeta_{xy} G_{xy}(0,0) + \zeta_{yx} G^*_{xy}(0,0) \right)^2 \right\}, \quad (4.9) \end{aligned}$$

where t is the time of flight. Here, $\zeta_{xx} \sim (X + \frac{1}{2}d_x)(X - \frac{1}{2}d_x)$, $\zeta_{xy} \sim (X + \frac{1}{2}d_x)(Y - \frac{1}{2}d_y)$, $\zeta_{yx} \sim (Y + \frac{1}{2}d_y)(X - \frac{1}{2}d_x)$ and $\zeta_{yy} \sim (Y + \frac{1}{2}d_y)(Y - \frac{1}{2}d_y)$, up to a smooth Gaussian profile, which is typically approximated by a constant function independent of $\mathbf{X}$ and $\mathbf{d}$ in quantum noise measurement [55]. N_s is the number of lattice sites. $\mathbf{Q}_x = (\frac{\pi}{a_x}, 0)$, $\mathbf{Q}_y = (0, \frac{\pi}{a_y})$ and $\mathbf{K} = 2j_1\mathbf{Q}_x + 2j_2\mathbf{Q}_y$ (j_1 and j_2 are integers). The center of the trapped cold gas is taken as the origin of coordinates here. The feature that $C(\mathbf{d})$ has sharp dips (peaks) at $\mathbf{d} = \mathbf{d}_0 \equiv \frac{\hbar t}{m}\left(\mathbf{K} - \mathbf{Q}_x - \mathbf{Q}_y\right)$ signifies $G_{xy}(0,0)$ is imaginary (real). G_{xy} being imaginary tells a local vortex-like current flow, which is a concrete evidence for the TRS breaking. For the p_x Mott state, there are no peaks or dips at $\mathbf{d}_0$, whereas there are sharp dips for AFO Mott state. If there is a PO Mott state, for which $G_{xy}(0,0)$ is finite and real, $C(\mathbf{d})$ will develop peaks instead of dips at $\mathbf{d}_0$.

4.5 DETAILS OF EFFECTIVE FIELD THEORY ANALYSIS

In this section, we will apply the field theoretical approach and discuss the phase transitions discovered by numerical calculations. Since superfluid phases are critical in one dimension, i.e., the correlation length diverges, the underlying lattice is irrelevant. Thus the superfluid phases are described by the continuum limit of the original theory for lattice bosons. The

action of the continuous theory is

$$\begin{aligned} L &= \int dx d\tau \mathcal{L}(x,\tau) \\ \mathcal{L} &= \sum_{\alpha=x,y} [\psi^*_\alpha(x,\tau)(r_\alpha + \partial_\tau - \mu)\psi_\alpha(x,\tau)] \\ &+ \sum_\alpha \frac{1}{2} K_\alpha |\nabla\psi_\alpha(x,\tau)|^2 + \sum_\alpha g_1 |\psi_\alpha|^4 \\ &+ \sum_{\alpha\neq\beta} g_2 |\psi_\alpha|^2 |\psi_\beta|^2 + g_3 \psi^*_\alpha \psi^*_\alpha \psi_\beta \psi_\beta, \end{aligned} \tag{4.10}$$

where $\psi_x(x,\tau)$ is the path integral representation of $e^{iQx}a_x(x)$ and $\psi_y(x,\tau)$ is the representation of $a_y(x)$. The coefficients are related to the original theory by

$$\begin{aligned} &r_\alpha = -2|t_\alpha|,\ K_\alpha = 2|t_\alpha|, \\ &g_1 = \frac{1}{2}U,\ g_2 = \frac{1}{3}U,\ g_3 = \frac{1}{6}U. \end{aligned} \tag{4.11}$$

These coefficients are obtained by taking the trivial continuous limit of the lattice model in Eq. (4.1). The coefficients will be renormalized considering the effect of the lattice potential. We neglect this effect, and focus on a framework of understanding the key features qualitatively in this section.

Following Haldane [53], the boson fields are expressed in terms of the density $\rho_\alpha(x,\tau)$ and phase $\varphi_\alpha(x,\tau)$ as $\begin{bmatrix} \psi_x(x,\tau) \\ \psi_y(x,\tau) \end{bmatrix} = \begin{bmatrix} \sqrt{\rho_x(x,\tau)}e^{i\varphi_x(x,\tau)}e^{i\Delta^0/2} \\ \sqrt{\rho_y(x,\tau)}e^{i\varphi_y(x,\tau)}e^{-i\Delta^0/2} \end{bmatrix}$. The density fields are written as $\rho_\alpha(x,\tau) = [\rho^0_\alpha + \delta\rho_\alpha(x,\tau)]\sum_m e^{2im\theta_\alpha(x,\tau)}$, with $\theta_\alpha(x,\tau)$ defined as $\partial_x\theta_\alpha(x,\tau) = \pi[\rho^0_\alpha + \delta\rho_\alpha]$. Here the $\delta\rho_\alpha(x,\tau)$ and $\varphi_\alpha(x,\tau)$ fields are slowing varying in space and imaginary time and the $\sum_m e^{2im\theta}$ term accounts for the particles' discreteness and is crucial for studying the instabilities of localization of bosons. Δ^0 and ρ^0_α are saddle point solutions defined by minimizing

$$\begin{aligned} L^0 &\equiv \frac{g_1+g_2}{2}(\rho^0_x + \rho^0_y)^2 + \frac{g_1-g_2}{2}(\rho^0_x - \rho^0_y)^2 \\ &+ \frac{g_2}{2}\cos(2\Delta^0)[(\rho^0_x + \rho^0_y)^2 + (\rho^0_x - \rho^0_y)^2] \\ &+ \frac{r_x + r_y - 2\mu}{2}(\rho^0_x + \rho^0_y) + \frac{r_x - r_y}{2}(\rho^0_x - \rho^0_y). \end{aligned} \tag{4.12}$$

Δ^0 is obviously $\pi/2$ for non-vanishing $\sum_\alpha \rho_\alpha^0$. We now proceed by defining $\varphi_\pm$ as $\varphi_\pm = \frac{1}{2}(\varphi_x \pm \varphi_y)$ and $\delta\rho_\pm$ as $\delta\rho_\pm = \frac{1}{2}(\delta\rho_x \pm \delta\rho_y)$. The Lagrangian density describing the low energy excitations is obtained as

$$\begin{aligned}\mathcal{L} \quad &= \sum_{p=\pm} \Big\{ 2i\rho_p \partial_\tau \varphi_p + \frac{1}{2} c_2 (\partial_x \varphi_p)^2 + \frac{1}{2} g_p \delta\rho_p^2 \\ &\quad c_2' \partial_x \varphi_+ \partial_x \varphi_- - m\cos(4\varphi_-) \Big\}, \end{aligned} \tag{4.13}$$

where $g_+ = 4(g_1 + g_2 - g_3)$, $g_- = 4(g_1 - g_2 + g_3)$, $c_2 = (K_x\rho_x^0 + K_y\rho_y^0)$, $c_2' = K_x\rho_x^0 - K_y\rho_y^0$ and $m = 2g_3\rho_x^0\rho_y^0$.

'Order' to 'disorder' phase transition of superfluid phases.— In the 'ordered' superfluid phase, Z_2 symmetry is spontaneously broken; while this symmetry is restored in the 'disordered' superfluid phase by fluctuations. From the definition of Z_2 symmetry, it is clear that the phase fluctuations, instead of density fluctuations, are crucial for this 'order' to 'disorder' phase transition. We thus integrate out the density fluctuations and get the effective theory for phase fluctuations as

$$\begin{aligned}\mathcal{L}[\varphi_+, \varphi_-] \quad &= \sum_p \frac{1}{2\pi\gamma_p} [\frac{1}{v_p} (\partial_\tau \varphi_p)^2 + v_p (\partial_x \varphi_p)^2] \\ &\quad + c_2' \partial_x \varphi_+ \partial_x \varphi_- - m\cos(4\varphi_-), \end{aligned} \tag{4.14}$$

with Luttinger parameters $\gamma_p = \frac{1}{2\pi}\sqrt{\frac{g_p}{c_2}}$ and sound velocities $v_p = \frac{1}{2}\sqrt{g_p c_2}$. The mixing term $c_2' = \partial_x\varphi_+\partial_x\varphi_-$ causes difficulties for analytic analysis because it breaks the Lorentz invariance. But it is negligible in the 'ordered' superfluid phase because the fluctuations of φ_- are gapped in this phase. The mixing term is neglected to gain qualitative understanding of the 'ordered' superfluid to 'disordered' superfluid phase transition. The theory for the phase difference φ_- fluctuations is

$$\begin{aligned}\mathcal{L}[\varphi_-] \quad &= \frac{1}{2\pi K_-} [\frac{1}{v_-} (\partial_\tau \varphi_-)^2 + v_- (\partial_x \varphi_-)^2] \\ &\quad - m\cos(4\varphi_-), \end{aligned} \tag{4.15}$$

which is Sine-Gordon theory. When m is greater than some critical $m_c(K_-)$, the Sine-Gordon theory is in a gapped phase and the φ_- field is locked at one minimum of $-m\cos(4\varphi_-)$, which corresponds to the 'ordered' superfluid phase. When $m < m_c(K_-)$, the $-m\cos(4\varphi_-)$ term

is irrelevant and the theory is in a gapless phase for which the fluctuation of φ_- is no longer locked. This phase corresponds to the 'disordered' superfluid phase.

In the 'ordered' superfluid phase, φ_- is gapped. The coupling between φ_+ and φ_- is negligible and this phase is characterized by an algebraic long range order $\langle \psi^*_\alpha(x,\tau)\psi_\beta(x',\tau')\rangle \sim f_{\alpha\beta}\left(\sqrt{(x-x')^2+v_+^2(\tau-\tau')^2}\right)^{-\gamma_+/2}$, with $f_{\alpha\beta}$ non-universal constants. The phase correlations of the original bosons are given by

$$\begin{aligned}
&\langle a_x^\dagger(j)a_x(j')\rangle \sim f_{xx}e^{iQ(j-j')}|j-j'|^{-\gamma_+/2}\\
&\langle a_y^\dagger(j)a_y(j')\rangle \sim f_{yy}|j-j'|^{-\gamma_+/2}\\
&\langle a_x^\dagger(j)a_y(j')\rangle \sim f_{xy}|j-j'|^{-\gamma_+/2}.
\end{aligned} \tag{4.16}$$

The key feature is that these algebraic correlations share the same power exponent.

In the 'disordered' superfluid phase, φ_- is gapless. To understand the main feature of this superfluid phase, we can safely neglect the g_3 terms. Through some algebra, the Lagrangian can be written in terms of φ_x and φ_y as

$$\begin{aligned}
\mathcal{L}[\varphi_x,\varphi_y] \quad &= \sum_{\alpha=x,y}\frac{1}{2\pi\gamma_\alpha}[\frac{1}{v_\alpha}(\partial_\tau\varphi_\alpha)^2+v_\alpha(\partial_x\varphi_\alpha)^2]\\
&+\lambda(\partial_\tau\varphi_x)(\partial_\tau\varphi_y),
\end{aligned} \tag{4.17}$$

with

$$\lambda = \frac{1}{\tilde{g}_+}-\frac{1}{\tilde{g}_-}, \tag{4.18}$$

$$\gamma_\alpha = \frac{1}{\pi\sqrt{K_\alpha\rho^0_\alpha(\tilde{g}_+^{-1}+\tilde{g}_-^{-1})}}, \tag{4.19}$$

$$v_\alpha = \sqrt{\frac{K_\alpha\rho^0_\alpha}{\tilde{g}_+^{-1}+\tilde{g}_-^{-1}}}, \tag{4.20}$$

where $\tilde{g}_\pm = 4(g_1 \pm g_2)$. Without considering the effect of vortex fluctuations, the Fourier transformed correlations are readily obtained as

$$\begin{aligned}
&\frac{1}{\beta L}\langle\varphi^*_\alpha(k,\omega)\varphi_\alpha(k,\omega)\rangle\\
&=\frac{\varsigma}{\omega^2\left[\tilde{g}_+^{-1}+\tilde{g}_-^{-1}\right]+K_\alpha k^2}+O((\frac{g_2}{g_1})^4),
\end{aligned} \tag{4.21}$$

with

$$\varsigma = 1 + \frac{[\tilde{g}_+^{-1} - \tilde{g}_-^{-1}]^2 \omega^4}{\left[(\tilde{g}_+^{-1} + \tilde{g}_-^{-1})\omega^2 + \frac{1}{2}c_2 k^2\right]^2 - \left[\frac{1}{2}c_2' k^2\right]^2}. \tag{4.22}$$

Here L is the system size and β is the inverse of temperature. ς has ω and k dependence. For arbitrary ω and k, ς satisfies $1 < \varsigma < 1 + \left(\frac{\tilde{g}_+^{-1} - \tilde{g}_-^{-1}}{\tilde{g}_+^{-1} + \tilde{g}_-^{-1}}\right)^2$. In our model, we have $1 < \varsigma < 13/9$. Thus the Luttinger parameters $\tilde{\gamma}_\alpha$ of the two components of the 'disordered' superfluid phase are given as $\tilde{\gamma}_\alpha = \sqrt{\varsigma}\gamma_\alpha$ (Eq. (4.21)), which satisfies $\gamma_\alpha < \tilde{\gamma}_\alpha < \sqrt{13}/3\gamma_\alpha$. Thus we conclude that the phase correlations that characterize this 'disordered' superfluid phase are estimated as $\langle \psi_\alpha^*(x,\tau)\psi_\beta(x,\tau')\rangle \sim f_\alpha \delta_{\alpha\beta}\left(\sqrt{(x-x')^2 + v_\alpha^2(\tau-\tau')^2}\right)^{-\tilde{\gamma}_\alpha/2}$. The phase correlations of the original bosons are within

$$\begin{aligned}
\frac{f_x}{|j-j'|^{\sqrt{13}/6\gamma_x}} &< e^{iQ(j-j')}\langle a_x^\dagger(j) a_x(j')\rangle < \frac{f_x}{|j-j'|^{\gamma_x/2}}, \\
\frac{f_y}{|j-j'|^{\sqrt{13}/6\gamma_y}} &< \langle a_y^\dagger(j) a_y(j')\rangle < \frac{f_y}{|j-j'|^{\gamma_y/2}},
\end{aligned} \tag{4.23}$$

where f_x and f_y are non-universal constants. $\langle a_y^\dagger(x) a_x(x')\rangle$ vanishes for 'disordered' superfluid phase. From the definition (Eq. (4.19)), $\gamma_x/\gamma_y = \sqrt{\frac{K_y\rho_y^0}{K_x\rho_x^0}} = \sqrt{|\frac{t_y\rho_y^0}{t_x\rho_x^0}|} \ll 1$, which is qualitatively in agreement with the numerical results shown in the last section. A detailed analysis considering the momentum-frequency dependent effect of α is left for future study. The phase correlation of p_y component decays much more rapidly than that of p_x component in the 'disordered' superfluid phase, which is very different from 'ordered' superfluid phase.

Localization transition of 'ordered' superfluid phase.— Since the fluctuation of φ_- is gapped in 'ordered' superfluid phase, the φ_- field can be trivially integrated over. In the representation of $\tilde{\theta}(x,\tau)$ defined as $\partial_x\tilde{\theta} = 2\pi\delta\rho_+(x,\tau)$, the theory for $\delta\rho_+$ and φ_+ can be rewritten as

$$L[\tilde{\theta}] = \frac{\gamma_+}{2\pi}\int dx d\tau \frac{1}{v_+}(\partial_\tau\tilde{\theta})^2 + v_+(\partial_x\tilde{\theta})^2. \tag{4.24}$$

To study the localization transition, we consider the effects of a lattice potential

$$\sum_{n>0} u_n \cos(2n\pi x)$$

with lattice constant $a = 1$. Near or at commensurate filling $\rho_x^0 + \rho_y^0 \approx \nu$ with ν an integer, the potential contributes to the theory for $\tilde{\theta}$ by

$$\Delta L = -\int dx d\tau u_\nu (\rho_x^0 + \rho_y^0) \cos\left(2\tilde{\theta} + 2\pi(\rho_x^0 + \rho_y^0 - \nu)x\right). \tag{4.25}$$

Thus the localization transition of the 'ordered' superfluid phase is just the same as the usual localization transition of one component of Bose gas in one dimension [52, 28]. For $\gamma_+ < \frac{1}{2}$, the lattice potential is irrelevant for both of commensurate filling and incommensurate filling and the 'ordered' superfluid is stable. For $\gamma_+ > \frac{1}{2}$ at commensurate filling, the Sine-Gordon term produced by the lattice potential is relevant and the 'ordered' superfluid phase undergoes a localization transition. For $\gamma_+ > \frac{1}{2}$ away from commensurate filling, the lattice potential does not produce a Sine-Gordon term and the 'ordered' superfluid phase is unstable but does not undergo a localization transition in the presence of the lattice potential [28].

Localization transition of 'disordered' superfluid phase.— In the 'disordered' superfluid phase fluctuation of φ_- is gapless, and the leading effect of the $-m\cos(4\varphi_-)$ term is to renormalize the Luttinger parameter K_-. To understand the localization transition of 'disordered' superfluid qualitatively, we simply ignore the $-m\cos(4\varphi_-)$ term. We observe that the difference between c_2 and c_2' is negligible for $|t_y| \ll |t_x|$, and the Lagrangian in Eq. 4.13 simplifies,

$$\mathcal{L} = \sum_{p=\pm}\left[2i\rho_p\partial_\tau\varphi_p + \frac{1}{2}g_p\delta\rho_p^2\right] + \frac{1}{2}c_2\left[\sum_p \partial_x\varphi_p\right]^2. \tag{4.26}$$

Since an external lattice potential only couples to $\delta\rho_+$ and does not couple to $\delta\rho_-$. We can integrate out $\delta\rho_-$, φ_- and φ_+ iteratively. Unexpectedly the resulting theory of $\delta\rho_+$ represented by $\tilde{\theta}$ has a nice form as

$$\begin{aligned} L[\tilde{\theta}] &= \frac{\gamma}{2\pi}\int dx d\tau \frac{1}{v}(\partial_\tau\tilde{\theta})^2 + v(\partial_x\tilde{\theta})^2 \\ &\quad -u(\rho_x^0 + \rho_y^0)\cos\left(2\tilde{\theta} + 2\pi(\rho_x^0 + \rho_y^0 - \nu)x\right), \end{aligned} \tag{4.27}$$

where the Luttinger parameter is given by $\gamma = \frac{1}{\pi}\sqrt{\frac{g_1}{c_2}}$ and the sound velocity is $v = \sqrt{2g_1c_2}$. From the Lagrangian, it is transparent that the localization transition of the 'disordered' superfluid phase is also the same as the localization transition of one component superfluid

phase [52, 28]. Here, we want to emphasize that $L[\tilde{\theta}]$ is independent of g_2 and g_3 in the 'disordered' superfluid phase. It is independent of g_3 because the fluctuation of φ_- is gapless. The physical consequence of this effect is that the mixing term $g_3\psi_x^*\psi_x^*\psi_y\psi_y$ is unimportant when $|t_y| \ll |t_x|$. The fact that $L[\tilde{\theta}]$ is independent of g_2 is nontrivial. From Eq. 4.13, g_2 is the density density interaction between the p_x and p_y components. This indicates the density of the p_y component vanishes near the localization transition of the 'disordered' superfluid.

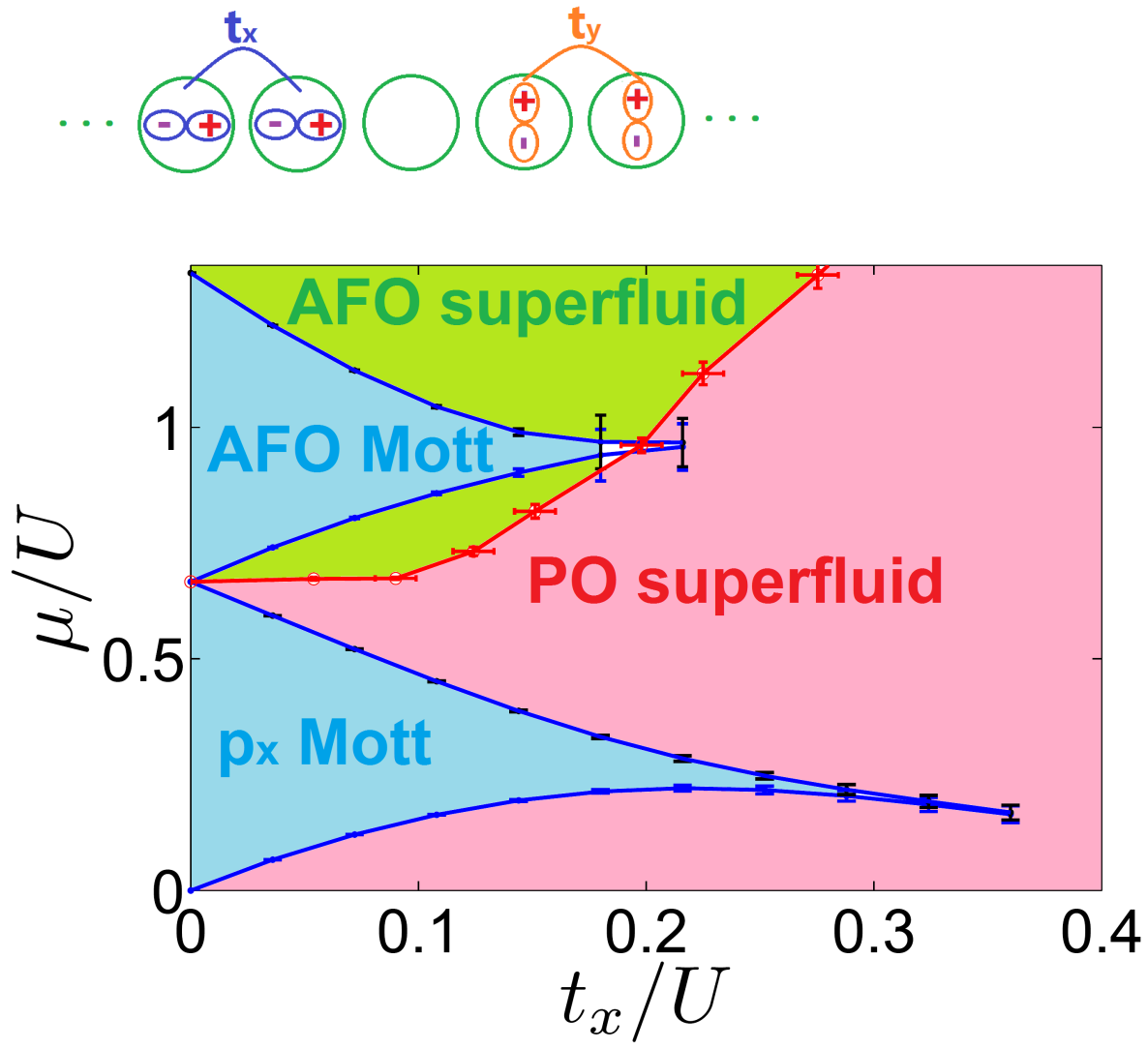

Figure 9: Phase diagram of a one dimensional lattice Bose gas with p_x and p_y orbital degrees of freedom. The upper panel shows the sketch of experimental setup we proposed. The green circles are used to denote the requirement of the approximate local isotropy of the lattice potential at each site. The lowest Mott lobe (with filling $\nu = 1$) is dominated by p_x bosons. The Mott state (with $\nu > 1$) has an AFO order (see text). We do not claim another phase for the tiny tip of the second Mott lobe beyond the red line because of numerical errors. The error bars near that tiny tip are large because the bond dimension of MPS we use is not large enough to capture the quantum state. The phase transition from the AFO SF phase (green shaded regime) to the PO SF (red shaded regime) destroys the AFO order. For sufficiently large hopping t_x or for low filling, the Bose gas has a crossover from PO SF to a p_x SF phase, which will not be discussed in this work.

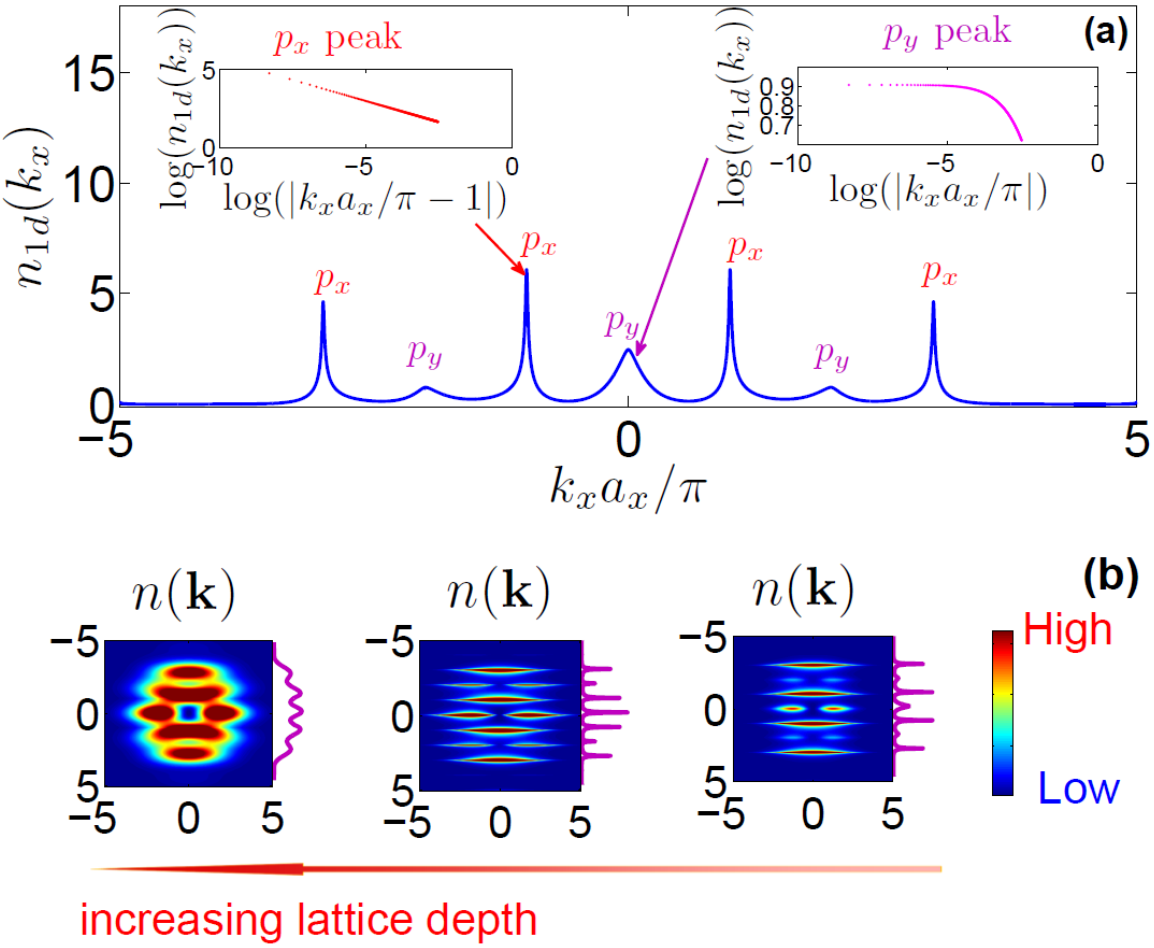

Figure 10: Momentum distributions $n(\mathbf{k})$. (a) shows the 1D momentum distribution in a geometrically 2D experimental setting (see paragraph "*Experimental proposal*"), $n_{1d}(k_x) = \int dk_y n(\mathbf{k})$ for PO SF phase. p_x peaks at $k_x a_x = (2j+1)\pi$ (j is some integer) are sharp, and p_y peaks at $k_x a_x = 2j\pi$ are broad. The insets show that the double logarithmic plot of $n_{1d}(k_x)$ near the sharp (broad) peaks is linear (non-linear). (b) shows the sketch of 2D momentum distributions ($n(\mathbf{k})$) in different phases (PO SF, AFO SF and AFO Mott from right to left). In three subgraphs the horizontal (vertical) axis is $k_y a_y/\pi$ ($k_x a_x/\pi$). The purple wiggles along each subgraph shows $n_{1d}(k_x)$. In the AFO SF phase, the p_y peaks which are broad in PO SF, are replaced by sharp peaks. In the AFO Mott phase, there are no sharp peaks.

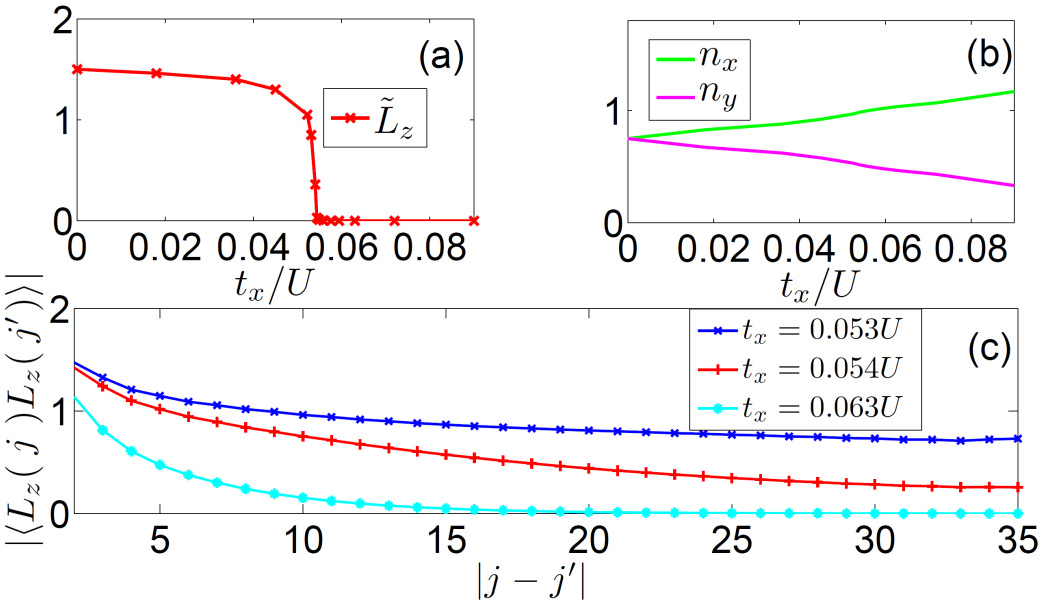

Figure 11: Properties of the AFO to PO phase transitions with total filling $\nu = 1.5$. (a) shows the Z_2 order parameter $\tilde{L}_z$. Our results indicate a continuous phase transition of the AFO order. (b) shows the filling of p_x and p_y bosons. The p_y component does not vanish across the phase transition. (c) shows correlation of the angular momentum on different sites near the phase transition. The correlation length diverges near the phase transition.

5.0 SP-COUPLED LADDER AND EXOTIC PHASES

Synthetic quantum matter exploiting the orbital degrees of freedom, such as the recent double-well optical lattices loaded with s and p orbital ultracold atoms, opens an avenue towards exploiting symmetries beyond natural crystals. Observations of exotic superfluidity were reported for bosons. We study interacting fermions on a two-leg ladder of orbitals with unequal parity, derived from the experimentally realized double-well lattices by dimension reduction. The staggered phases of sp-orbital quantum tunneling mimic the one dimensional spin-orbital coupling. At half filling, we find a topological insulator phase and study its Mott transition. Away from half filling, various types of superconducting and density waves are discussed.

Novel lattice geometries have been known to give rise to interesting many-body phenomena including topological states of quantum matter. In the context of ultracold quantum gases, optical lattices engineered with interfering laser beams can realize specific configurations of potentials of single or multiple periods not found in nature. For instance, double-well superlattices [56, 57] have matured into a powerful tool for manipulating orbital degrees of freedom [58, 59, 60, 14, 61, 16, 62, 63]. Controls of atoms in the s- and p-orbitals of the checkerboard [14] and hexagonal [16] optical lattices have also been demonstrated, and correlations between these orbitals tend to give exotic quantum states [14, 16, 64, 65, 44]. The spatial symmetry of the orbital wave function dictates the complex hopping amplitudes between nearby sites. Under certain circumstances, as for the uneven double wells, the orbital hopping pattern is sufficient for producing topologically nontrivial band structures [66]. Motivated by these developments, we consider a lattice of uneven double-wells where fermionic atoms are loaded up to the s- and p-orbital levels of the shallow and deep wells respectively, as shown in Fig. 12. This route of achieving topological band insulators and superfluids

is distinct from previous proposals that require rotation of the gas [67, 68], artificial gauge fields [69], spin-orbital coupling [70, 71, 72, 73], or p-wave triplet pairing [74].

5.1 ONE DIMENSIONAL ORBITAL LADDER

The one-dimensional ladder system is illustrated in Fig. 12**b** and 12**c**. This corresponds to the quasi-one dimensional limit of a standard double-well optical lattice, with the optical potential given by

$$V(x,y) = V_x \sin^2(kx) + V_1 \sin^2(ky) + V_2 \sin^2(2ky + \frac{\phi}{2}).$$

This optical lattice has a double well structure in the y-direction. For $V_{1,2} \gg V_x$, there is a large tunneling barrier between double wells in the y-direction, so in low energy physics the two dimensional system decouples into an array of dynamically isolated two-leg ladders of A and B sub-wells (Fig. 12), with each ladder extending in the x-direction. The relative well depth of the two legs is controlled by the phase ϕ and further by the ratio V_2/V_1. We will focus on a situation, similar to the setup in the experiment [14], where the s-orbital of leg A has roughly the same energy as the p_x-orbital of leg B (other p-orbitals have much higher energy). For example, one can choose $V_1 = 40E_R$, $V_2 = 20E_R$, $V_x = 4.0E_R$ and $\phi = 0.9\pi$ in experiments, where E_R is the recoil energy $\hbar^2k^2/2m$, with m the mass of atom and k the wave number of the laser. Such a setup will give the A (B) wells a depth $2.7E_R$ ($8.1E_R$). The tunneling rates of the various orbitals illustrated in FIG. 12(**c**) are given as $t_s = 0.053E_R$, $t_p = 0.40E_R$ and $t_{sp} = 0.064E_R$ in the tight binding approximation. The lattice constant $a = \pi/k$ is set as the length unit. We now consider a single species of fermions occupying these orbitals, with the low-lying s-orbital of leg B completely filled. Alternatively fermions can be directly loaded into the p_x-orbital of leg B, leaving the low-lying s empty, by techniques developed in recent experiments [59, 14, 63]. With these techniques, long-lived meta-stable states of atoms in high orbitals with life time on the order of several hundred milliseconds are demonstrated achievable [14].

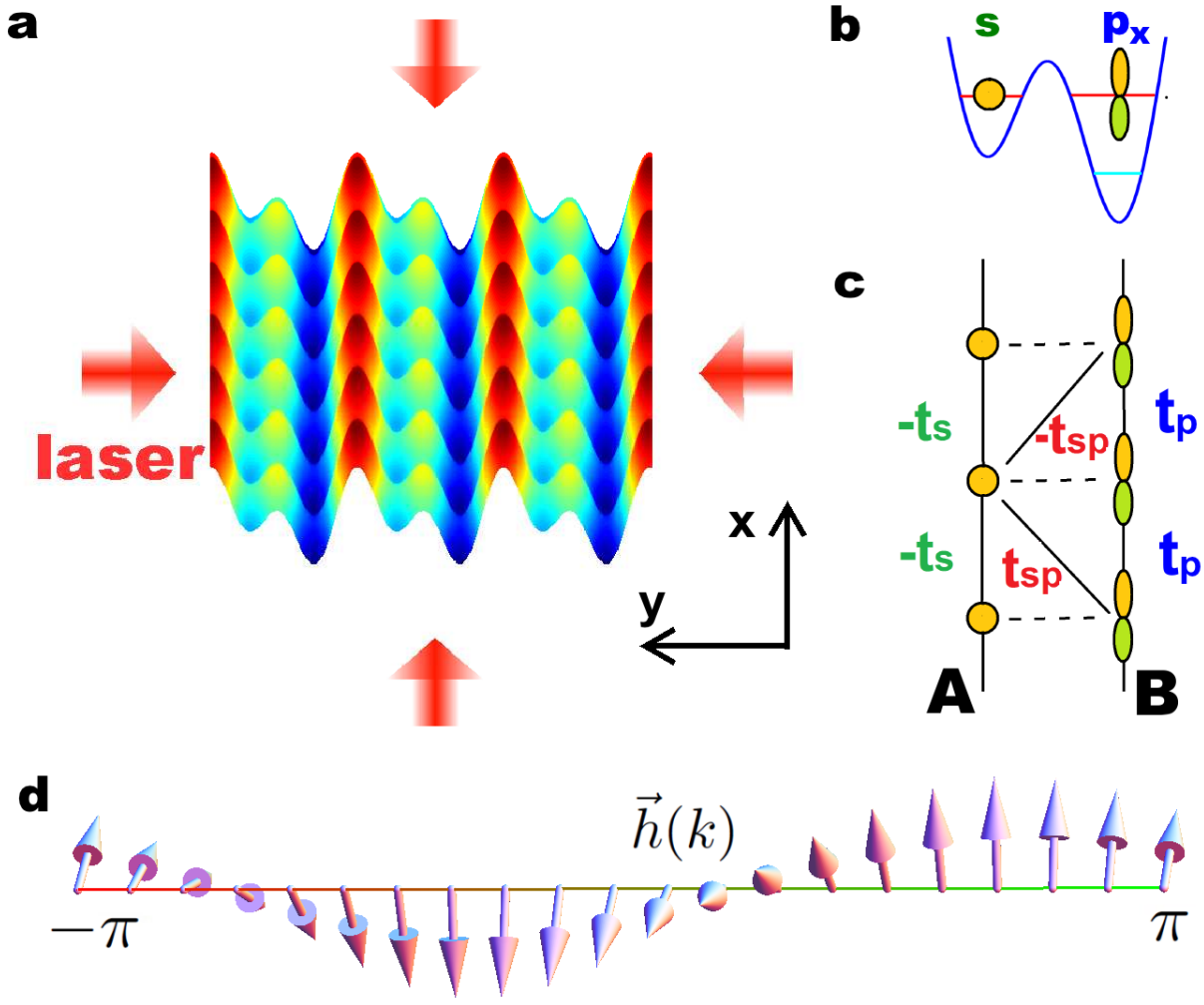

Figure 12: The uneven *sp*-orbital ladder system made from a two-dimensional double-well optical lattice through dimension reduction. **a**, An optical lattice of uneven sub-wells (light and dark blue), with parameters $V_x/V_1 = 0.3$, $V_2/V_1 = 1$ and $\phi = 0.6\pi$, develops high barriers (red ridges) in the y direction, slicing the lattice into dynamically decoupled uneven two-leg ladders. **b** and **c**, Schematic side and top views, respectively, of the ladder illustrate tunneling (t's) of fermions prepared in the degenerate s and p_x levels. **d**, Topological winding of Hamiltonian across the Brillouin zone.

The Hamiltonian of the *sp*-orbital ladder is then given by

$$H_0 = \sum_j C_j^\dagger \begin{bmatrix} -t_s & -t_{sp} \\ t_{sp} & t_p \end{bmatrix} C_{j+1} + h.c. - \sum_j \mu C_j^\dagger C_j, \tag{5.1}$$

where $C_j^\dagger = \left[a_s^\dagger(j), a_{p_x}^\dagger(j)\right]$, with $a_s^\dagger(j)$ and $a_{p_x}^\dagger(j)$ being fermion creation operators for the s- and p_x-orbitals on the A and B leg respectively. The relative sign of the hopping amplitudes is fixed by parity symmetry of the s and p_x orbital wave functions. As depicted in Fig. 12**c**, the hopping pattern plays a central role in producing a topological phase. With a proper global gauge choice, t_s, t_p and t_{sp} are all positive. The rung index j runs from 0 to $L-1$ with L the system size. At half filling (one particle per unit cell), for which the chemical potential $\mu = 0$, the Hamiltonian is particle-hole symmetric under transformation $C_j \to (-1)^j C_j^\dagger$. Topologically non-trivial band structure of this *sp*-orbital ladder, which shall be shown analytically next, may be heuristically speculated from the following comparison: the staggered quantum tunneling $t_{sp}\sum_j \left[C_j^\dagger(-i\sigma_y)C_{j+1} + h.c.\right]$ resembles spin-orbit interaction [75, 70, 71, 72, 73] when the s and p-orbital states are mapped to pseudo-spin-$\frac{1}{2}$ states. Such a staggered tunneling can also naturally arise in the checkerboard optical lattice already engineered in the experiment [14] by increasing the laser strength in one direction to reach the quasi-1D limit. The physics of the *sp*-orbital ladder is also connected to the more familiar frustrated ladder with magnetic flux [76], but the *sp*-orbital ladder appears much easier to realize experimentally.

5.2 TOPOLOGICAL INSULATOR PHASE AT HALF-FILLING

In the momentum space the Hamiltonian takes a simple and suggestive form,

$$\mathcal{H}(k) = h_0(k)\mathbb{I} + \vec{h}(k)\cdot\vec{\sigma}, \tag{5.2}$$

where $h_0(k) = (t_p - t_s)\cos(k)$, $h_x = 0$, $h_y(k) = 2t_{sp}\sin(k)$ and $h_z(k) = -(t_p + t_s)\cos(k)$. Here, $\mathbb{I}$ is the unit matrix, σ_x, σ_y and σ_z are Pauli matrices in the two-dimensional orbital space. The energy spectrum consists of two branches,

$$E_\pm(k) = h_0(k) \pm \sqrt{h_y^2(k) + h_z^2(k)}, \tag{5.3}$$

with a band gap $E_g = \min(2t_p + 2t_s, 4t_{sp})$, which closes at either $t_{sp} = 0$ or $t_s + t_p = 0$. An interesting limit that highlights the nontrivial band structure of our model is that when $t_p = t_s = t_{sp}$, the two bands are both completely flat. To visualize the topological properties of the band structure, one notices that as k is varied from $-\pi$ through 0 to $+\pi$, crossing the entire Brillouin zone, the direction of the $\vec{h}(k)$ vector winds an angle of 2π (Fig. 12**d**). The corresponding Berry phase is half of the angle, $\gamma = \pi$. The orbital ladder Hamiltonian H_0 belongs to the symmetry group $G_{++}^{-+}(U, T, C)$ in the notation of Ref. [77], since it has both particle-hole and time-reversal symmetry, in addition to the usual charge U(1) symmetry. Therefore, at half filling, it is a topological insulator characterized by an integer topological invariant, in this case the winding number 1, according to the general classification scheme of topological insulators and superconductors [77, 78].

5.2.1 Topological index

The topological nature of the *sp*-orbital ladder can be understood in terms of the winding number of the Hamiltonian in the momentum space. Given a Hamiltonian

$$\mathcal{H}(k) = h_0(k)\mathbb{I} + \vec{h}(k) \cdot \vec{\sigma}, \tag{5.4}$$

with $h_x = 0$, the winding number is defined as

$$W = \oint \frac{dk}{4\pi} \epsilon_{\nu\nu'} \hat{h}_\nu^{-1}(k) \partial_k \hat{h}_{\nu'}, \tag{5.5}$$

where $\hat{h} = \frac{\vec{h}}{|\vec{h}|}$ and $\epsilon_{yz} = -\epsilon_{zy} = 1$. This winding number is 1 for the *sp*-orbital ladder in the topological insulator phase (Fig. 12**d**).

The Hamiltonian in equation (5.4) can be written as $\mathcal{H}(k) = U(\mathbb{I} + \sigma_z)U^\dagger$, where $U = \exp(i\sigma_x\theta(k)/2)$, with $\theta(k)$ defined by $\begin{bmatrix} \cos(\theta) \\ \sin(\theta) \end{bmatrix} = \begin{bmatrix} \hat{h}_z(k) \\ \hat{h}_y(k) \end{bmatrix}$. The eigenvector of the lower

branch is given as $u(k) = e^{-i\theta(k)/2} U \begin{bmatrix} 0 \\ 1 \end{bmatrix}$. The Berry phase is given by

$$\begin{aligned} \gamma &= \oint dk i u^\dagger \partial_k u \\ &= i \oint dk \left[e^{-i\sigma_x \theta/2} e^{i\theta/2} \partial_k \left(e^{i\sigma_x \theta/2} e^{-i\theta/2} \right) \right]_{22} \\ &= \frac{1}{2} \oint dk \partial_k \theta = \frac{1}{4} \oint dk \frac{\partial_k \sin(\theta)}{\cos(\theta)} - \frac{\partial_k \cos(\theta)}{\sin(\theta)} \\ &= -W\pi. \end{aligned} \tag{5.6}$$

With the eigenvector $u(k)$ multiplied by a phase factor $e^{i\phi(k)}$ in which $\oint dk \partial_k \phi(k) = 2n\pi$, the Berry phase changes $2n\pi$. This means the Berry phase $\gamma = W\pi \mod 2\pi$. The winding number W being even and odd defines two classes of topological states in one dimension.

5.2.2 The gapped interpolation.

An interpolation between $\mathcal{H}(k)$ and $\mathcal{H}'(k)$ is defined as $h(k,\varphi) = \mathcal{H}(k) + \frac{\Delta_y}{2}[1 - \cos(\varphi)]\sigma_y + \Delta_x \sin(\varphi)\sigma_x = d_0(k) + \vec{d}(k,\varphi)\cdot\vec{\sigma}$, with $h(k,0) = \mathcal{H}(k)$ and $h(k,\pi) = \mathcal{H}'(k)$. The eigenvalues of this interpolation exhibit a finite gap for any (k,φ), given a sufficiently large Δ_x. The Chern number C_1 defined by $C_1 = \frac{1}{4\pi}\int dk d\varphi \hat{d} \cdot \frac{\partial \hat{d}}{\partial k} \times \frac{\partial \hat{d}}{\partial \varphi}$ is 1 for $\Delta_y > \Delta_y^c$, and is 0 for $0 < \Delta_y < \Delta_y^c$. Since the Chern parity $(-1)^{C_1}$ is well defined for gapped interpolations with fixing $h(k,0)$ and $h(k,\pi)$, C_1 being odd tells $\mathcal{H}(k)$ is topologically distinguishable from $\mathcal{H}'(k)$ [79].

5.2.3 Edge states

The nontrivial topology of the ladder system also manifests in existence of edge states. It is easiest to show the edge states in the flat band limit, $t_s = t_p = t_{sp} \equiv t$, by introducing auxiliary operators, $\phi_\pm(j) = [a_{p_x}(j) \pm a_s(j)]/\sqrt{2}$. Then the Hamiltonian only contains coupling between ϕ_+ and ϕ_- of nearest neighbors, but not among the ϕ_+ (or ϕ_-) modes themselves,

$$H_0 \to 2t \sum_j \phi_-^\dagger(j)\phi_+(j+1) + h.c. \tag{5.7}$$

Immediately, one sees that the operators $\phi_+(0)$ and $\phi_-(L-1)$ at the left and right end are each dynamically isolated from the bulk, and do not couple to the rest of the system (Fig. 13**a**). These loners describe the two edge states at zero energy. They are the bonding and anti-bonding modes of s- and p-orbitals, i.e., shared by the two rungs of the ladder.

For general parameters away from the flat band limit, the wave functions of the edge states are found not to confine strictly at $j = 0$ or $L-1$, but instead decay exponentially into the bulk with a characteristic length scale $\xi = 2/\log(|(\sqrt{t_s t_p} + t_{sp})/(\sqrt{t_s t_p} - t_{sp})|)$. We construct the exact wave functions of edge states, by rewriting H_0 in the following form

$$H_0 = \sum_j \Phi_j^\dagger \begin{bmatrix} t_1 & t_2 \\ t_3 & 0 \end{bmatrix} \Phi_{j+1} + h.c., \tag{5.8}$$

with

$$\Phi_j = \begin{bmatrix} \phi_+(j) \\ \phi_-(j) \end{bmatrix} = \frac{1}{\sqrt{t_s+t_p}} \begin{bmatrix} \sqrt{t_s} & \sqrt{t_p} \\ -\sqrt{t_p} & \sqrt{t_s} \end{bmatrix} C_j, \tag{5.9}$$

and $t_1 = (t_p - t_s)$, $t_2 = \sqrt{t_s t_p} - t_{sp}$ and $t_3 = \sqrt{t_s t_p} + t_{sp}$. The wave functions $w_{l/r,\nu}(j)$ of the edge states are introduced by $b_{l/r} = \sum_{j\,\nu=s,p} w_{l/r,\nu}(j) a_\nu(j) = \sum_{j\,\alpha=\pm} \tilde{w}_{l/r,\alpha}(j)\phi_\alpha(j)$, where $b_{l/r}$ is the fermion operator of the left/right edge state. The wave function of the left edge state b_l is given as

$$\tilde{w}_{l,+}(j) = \begin{cases} \exp(-j/\xi), & \text{if } j \text{ is even;} \\ 0, & \text{otherwise,} \end{cases}$$
$$\tilde{w}_{l,-}(j) = \begin{cases} -\frac{t_1}{t_2+t_3}\exp(-j/\xi), & \text{if } j \text{ is even;} \\ 0, & \text{otherwise,} \end{cases} \tag{5.10}$$

with the decay width $\xi = \frac{2}{\log(|t_3/t_2|)}$. The wave function of the right edge state can be constructed by performing parity transformation of the left edge state. As long as t_2 vanishes, the width $\xi \to 0$ and the edge states are completely confined on the ends of the ladder. With finite t_2 the edge states deconfine and decays exponentially. The critical point is $t_2/t_3 = 1$ ($t_{sp} = 0$), for which $\xi \to \infty$. At this point the bulk gap closes (Eq. (5.3)). The analysis presented here is confirmed by numerical calculations, as shown in Fig. 13**b** and 13**c**.. For the lattice strength given above, the decay width is estimated to be $2 \sim 3$ times of the lattice constant. Only for $t_{sp} = \sqrt{t_s t_p}$ which is potentially reachable in experiments, $\xi \to 0$, the edge states are completely confined at the edges. For $t_{sp} = 0$, the bulk gap closes and $\xi \to \infty$.

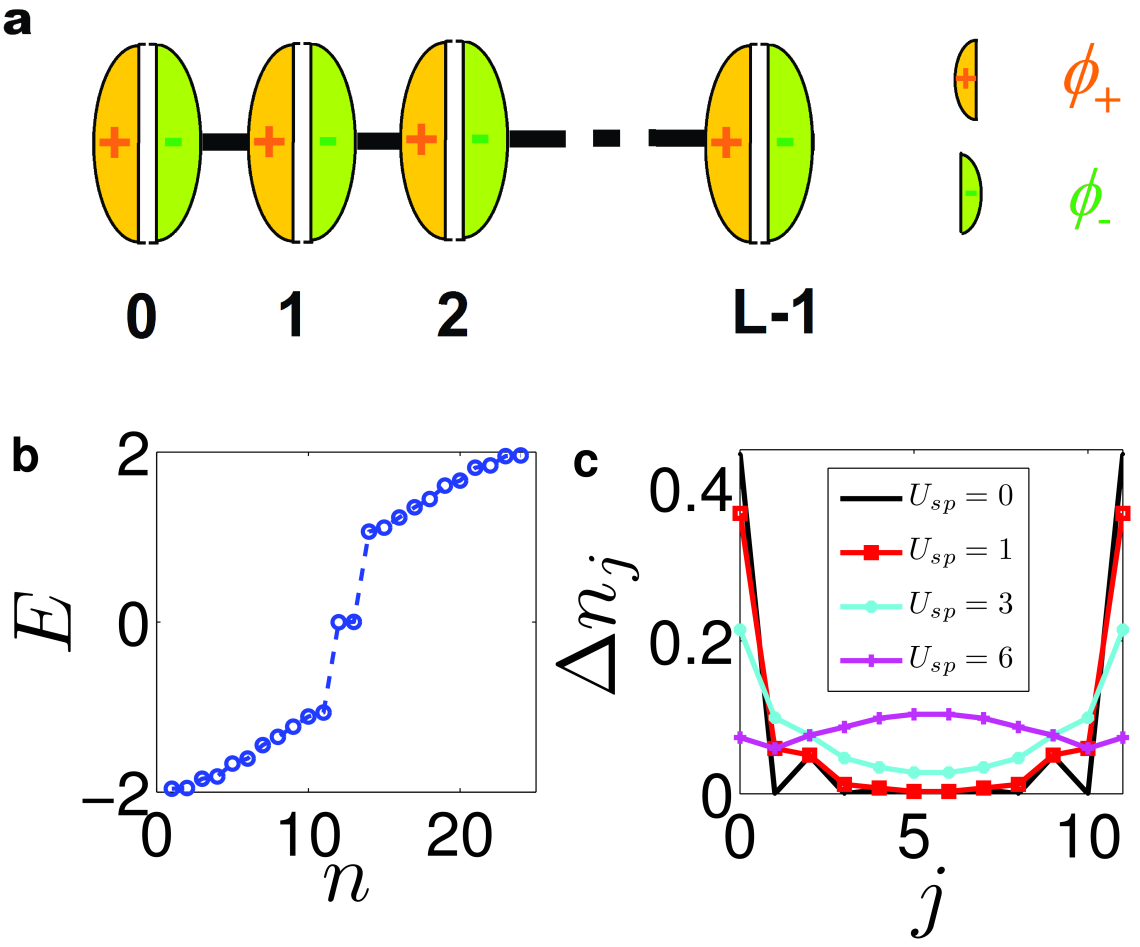

Figure 13: Bulk and edge eigenstates of the *sp*-orbital ladder. **a**. A pictorial representation of the simplified Hamiltonian in the flat band limit $t_s = t_p = t_{sp}$ showing the emergence of isolated edge modes. The definition of the $\phi_\pm$ operator is given in the main text. **b**. The eigen energies of a ladder with finite length $L = 12$ showing two degenerate zero energy states inside the gap. Here n index the different energies. **c**. The probability distribution of the in-gap states (Eq. (5.36)) for varying strengths of inter-orbital interaction U_{sp}. The in-gap states are shown localized on the edges and survive against finite interaction. In **b** and **c**, we choose $t_s = t_p = 2t_{sp}$ (taken as the energy unit).

5.2.4 Fractional charge and topological anti-correlations

For a finite ladder of length L with open boundary condition and populated by L fermions (half filling), $L-1$ fermions will occupy the valence band (bulk states) and one fermion will occupy the edge states (Fig. 13). Since the two edge states are degenerate, the ground state has a double degeneracy. The edge state is a fractionalized object carrying half charge (cold atoms are charge neutral, here charge refers to the number of atoms). This becomes apparent if we break the particle-hole symmetry by going infinitesimally away from half filling, e.g., tuning chemical potential $\mu = 0^+$. Then, the valence band and the two edge states will be occupied. With a charge density distribution on top of the half filled background defined as $\rho(j) = C_j^\dagger C_j - 1$, one finds $\sum_{0\le j<d}\langle\rho(j)\rangle|_{\mu=0^+} = \sum_{L-d-1<j'<L}\langle\rho(j')\rangle|_{\mu=0^+} = \frac{1}{2}$, where d satisfies $\xi \ll d \ll L$ (e.g., take $d = 5\xi$). A characteristic feature of the topological insulator (with the number of atoms fixed) is the topological anti-correlation of the charge at the boundaries,

$$\lim_{L\to\infty}\sum_{j,j'}\langle\rho(j)\rho(j')\rangle = -\frac{1}{4}.$$

In the sharp confinement limit, $\xi \to 0$, the edge states are well localized at the two ends of the ladder. The topological anti-correlation simplifies as $\langle\rho(0)\rho(L-1)\rangle = -\frac{1}{4}$, and the half charge is also well localized, i.e., $\langle\rho(0)\rangle_{\mu=0^+} = \langle\rho(L-1)\rangle_{\mu=0^+} = \frac{1}{2}$. Since the edge states are well isolated from the bulk states by an energy gap, they are stable against local Gaussian fluctuations. The coupling between the two edge states vanishes in the thermodynamic limit ($L \to \infty$), because the hybridization induced gap scales as $\exp(-\alpha L)$ as $L \to \infty$ [80].

5.3 ONE DIMENSIONAL REDUCED CHERN-SIMONS FIELD THEORY: DESCRIPTION OF THE FRACTIONAL CHARGE

To calculate the charge modulation induced by a domain wall connecting a topological insulator and a trivial insulator, we couple the ladder system to an auxiliary charge $U(1)$ gauge field (A_t, A_x) and construct a low energy effective field theory, which is $1+1$ dimensional reduced Chern-Simons Field theory [79]. A η dependent model Hamiltonian describing the

domain wall is introduced

$$
\begin{aligned}
H_\eta &= H_0 + \frac{\Delta_y}{2}\sum_j \left[1-\cos(\eta)\right] C_j^\dagger \sigma_y C_j + \Delta_x \sin(\eta) C_j^\dagger \sigma_x C_j \qquad (5.11)\\
&= \sum_k \tilde{C}_k^\dagger \mathcal{H}_\eta(k) \tilde{C}_k. \qquad (5.12)
\end{aligned}
$$

Here the σ_x term is introduced to guarantee a finite energy gap (Δ_ϵ) of H_η. The Fourier transformed Hamiltonian $\mathcal{H}_\eta$ is related to the Hamiltonian in Eq. 5.4 by $\mathcal{H}_\eta(k) = \mathcal{H}(k) + \frac{\Delta_y}{2}[1-\cos(\eta)]\sigma_y + \Delta_x \sin(\eta)\sigma_x$. We split the η field into two parts as $\eta = \eta_0 + \delta\eta(j,\tau)$. The field η_0 satisfies the boundary condition— $\eta_0(-\infty,\tau) = 0$, $\eta_0(\infty,\tau) = \pi$. For example it can be set as $\eta_0(j,\tau) = \arctan\left(\frac{j}{l_{dw}}\right) + \frac{\pi}{2}$, where l_{dw} is the characteristic width of the domain wall. To proceed we assume l_{dw} is much larger than the microscopic length scale ($\sim \frac{1}{\Delta_\epsilon^{1/z}}$) of the fermion system. The field $\delta\eta(j,\tau)$ satisfies a periodic boundary condition. In the following derivation we will treat η_0 as a quasi-static field since it varies slowly in space. (One can think that we are deriving a local effective field theory for a subsystem in which the variation of η_0 is negligible.)

With the model Hamiltonian H_η coupled to the gauge field, its Lagrangian is given by

$$
\begin{aligned}
&L[C^\dagger, C] = \int_0^\beta d\tau \mathcal{L}(\tau)\\
&\mathcal{L} = \sum_j \Big\{ C_j^\dagger D_\tau C_j + C_j^\dagger \mathcal{T}_{j\,j+1} C_{j+1} + C_{j+1}^\dagger \mathcal{T}_{j+1\,j} C_j\\
&+ \frac{\Delta_y}{2}\left[1-\cos(\eta)\right] C_j^\dagger \sigma_y C_j + \Delta_x \sin(\eta) C_j^\dagger \sigma_x C_j \Big\}, \qquad (5.13)
\end{aligned}
$$

with

$$
\begin{aligned}
D_\tau &= \partial_\tau + iA_\tau(j,\tau),\\
\mathcal{T}_{j\,j+1} &= e^{iA_x(j+1/2,\tau)} T_{j\,j+1},\\
T_{j\,j+1} &= \begin{bmatrix} -t_s & -t_{sp} \\ t_{sp} & t_p \end{bmatrix},\\
\mathcal{T}_{j\,j+1} &= \mathcal{T}_{j+1\,j}^\dagger. \qquad (5.14)
\end{aligned}
$$

It is readily verified that the Lagrangian has a $U(1)$ gauge symmetry defined by

$$\begin{aligned}
&A_\tau \to A_\tau + \partial_\tau \vartheta(j,\tau) \\
&A_x(j+1/2,\tau) \to A_x(j+1/2,\tau) + [\vartheta(j+1,\tau) - \vartheta(j,\tau)] \\
&C(j,\tau) \to C(j,\tau) e^{-i\vartheta(j,\tau)}.
\end{aligned} \tag{5.15}$$

In the continuum limit, A_x transforms as $A_x(x,\tau) \to A_x(x,\tau) + \partial_x \vartheta(x,\tau)$. In the following we shall write k as k_x, η_0 as k_y and $\delta\eta$ as A_y just to make the equations more compact. Then the Hamiltonian $\mathcal{H}_{\eta_0}(k)$ will be automatically written as $\mathcal{H}(k_x, k_y)$.

In the momentum-frequency ($K \equiv (k_x, i\omega)$) space the Lagrangian reads

$$\begin{aligned}
L &= \sum_{KK'} \tilde{C}^\dagger(K) \mathcal{D}_{KK'} \tilde{C}(K'), \\
\mathcal{D} &= \mathcal{D}^{(0)} + \delta\mathcal{D}, \\
\mathcal{D}^{(0)}_{KK'} &= [-i\omega + \mathcal{H}(k_x,k_y)]\, \delta_{KK'} \\
\delta\mathcal{D}_{KK'} &= \sum_\nu A_\nu(K-K') \Gamma_\nu(\frac{k_x + k'_x}{2}),
\end{aligned} \tag{5.16}$$

where $\Gamma_\tau = i\mathbb{I}$, $\Gamma_{\alpha=x,y} = \frac{\partial \mathcal{H}(k_x,k_y)}{\partial k_\alpha}$ and the index $\nu = \tau, x, y$. For convenience, we further introduce $G(K) = [-i\omega + \mathcal{H}(k_x,k_y)]^{-1}$

The effective action of the gauge field A_ν is defined as

$$S_{\text{eff}}[A_\nu] = -\ln \int D[C^\dagger, C] \exp\left(-L[C^\dagger, C; A_\nu]\right), \tag{5.17}$$

which can be calculated order by order as follows.

$$\begin{aligned}
S_{\text{eff}}[A_\nu] &= -\ln\det[\mathcal{D}] = -\text{Tr}\ln\mathcal{D} = -\text{Tr}\ln\left[\mathcal{D}^{(0)} + \delta\mathcal{D}\right] \\
&= -\text{Tr}\ln\mathcal{D}^{(0)} - \text{Tr}\left[\mathcal{D}^{(0)\,-1}\delta\mathcal{D}\right] + \frac{1}{2}\text{Tr}\left[\mathcal{D}^{(0)\,-1}\delta\mathcal{D}\right]^2 + \ldots.
\end{aligned} \tag{5.18}$$

Since we are calculating the charge/current induced by the domain wall configuration—η_0 field, we only keep the quadratic terms and thus the effective action is given by

$$\begin{aligned}
S_{\text{eff}} &= \frac{1}{2}\text{Tr}\left[\mathcal{D}^{(0)\,-1}\delta\mathcal{D}\right]^2 \\
&= \frac{1}{2}\sum_{\mu\nu Q} A_\mu(Q) A_\nu(-Q) \text{Tr}\sum_K G(K+Q/2)\Gamma_\mu(K) G(K-Q/2)\Gamma_\nu(K).
\end{aligned} \tag{5.19}$$

Although the theory is complicated, it can be simplified because we are only interested in a low energy theory. The generic form of S_{eff} at low energy is

$$S_{\text{eff}} = \beta L \sum_K A_\mu(Q) A_\nu(-Q) \left(q\mathcal{K}^{\mu\nu} + iq_0\mathcal{W}^{\mu\nu}\right), \tag{5.20}$$

with $Q = (q, iq_0)$. The massive terms are prohibited due to gauge invariance. By comparing the above equations we get

$$\mathcal{W}^{\mu\nu} = \frac{1}{2\beta L} \lim_{Q\to 0} \frac{d}{d(iq_0)} \text{Tr} \sum_K G(K + Q/2)\Gamma_\mu(K)G(K - Q/2)\Gamma_\nu(K), \tag{5.21}$$

$$\mathcal{K}^{\mu\nu} = \frac{1}{2\beta L} \lim_{Q\to 0} \frac{d}{dq} \text{Tr} \sum_K G(K + Q/2)\Gamma_\mu(K)G(K - Q/2)\Gamma_\nu(K). \tag{5.22}$$

Then we have

$$\mathcal{W}^{\mu\nu} = \frac{1}{4\beta L} \text{Tr} \sum_K \left[\partial_{i\omega} G(K)\right] \Gamma_\mu(K)G(K)\Gamma_\nu(K) - \mu \leftrightarrow \nu, \tag{5.23}$$

$$\mathcal{K}^{\mu\nu} = \frac{1}{4\beta L} \text{Tr} \sum_K \left[\partial_k G(K)\right] \Gamma_\mu(K)G(K)\Gamma_\nu(K) - \mu \leftrightarrow \nu. \tag{5.24}$$

It is clear that $\mathcal{W}$ and $\mathcal{K}$ are anti-symmetric. From Ref. [79], $\mathcal{W}^{xy} = \frac{i}{2} \oint \frac{dk_x}{2\pi} \Omega_{k_x k_y}$ where $\Omega_{k_x k_y}$ is the Berry curvature of the Hamiltonian $\mathcal{H}(k_x, k_y)$. Other terms of $\mathcal{W}$ coupling the temporal component—$\mathcal{W}^{\tau\nu}$—vanish because $G(K)$ and $\partial_{i\omega} G(K)$ commute. The commuting relation can be verified by choosing the eigen-basis of $\mathcal{H}(k_x, k_y)$. Now we have fully established the frequency part of the effective action, which is

$$\beta L \sum_K A_\mu(K) A_\nu(K) i\omega \mathcal{W}^{\mu\nu} = 2\beta L \sum_K W^{xy} A_x(-K)(-i\omega) A_y(K) \tag{5.25}$$

In the real space (continuum limit) this term reads $2\int dxd\tau \mathcal{W}^{yx}(A_y\partial_\tau A_x)$. From gauge invariance, it is readily proved that $-i\mathcal{K}^{\tau y} = \mathcal{W}^{xy}$. Thus the effective action is given by

$$S_{\text{eff}}[A_\mu] = 2\mathcal{W}^{yx} \int dxd\tau (A_y\partial_\tau A_x - A_y\partial_x A_\tau). \tag{5.26}$$

The real time action reads

$$\tilde{S}_{\text{eff}}[A_\mu] = 2i\mathcal{W}^{xy} \int dxdt (A_y\partial_t A_x - A_y\partial_x A_t). \tag{5.27}$$

The coefficient $\mathcal{W}^{xy}$ is related to the Berry phase $\gamma(\eta)$ of the Hamiltonian $\mathcal{H}_\eta(k)$ by $\mathcal{W}^{xy} = \frac{i}{4\pi}\partial_\eta\gamma(\eta)$. With A_y and k_y replaced by $\delta\eta$ and η_0, we have

$$\tilde{S}_{\text{eff}}[A_\mu] = \int dxdt(A_x\partial_t\eta - A_t\partial_x\eta)\frac{1}{2\pi}\partial_\eta\gamma(\eta). \tag{5.28}$$

Here, we have used $\partial_\nu\eta = \partial_\nu(\eta_0 + \delta\eta) = \partial_\nu\delta\eta$ for the reason that η_0 is treated as a static field in the above derivation. The effective action can actually be written down directly from the famous $2+1$ dimensional Chern-Simons field theory by a dimension reduction procedure [79]. The linear response of charge/current is given by $j_\nu = \frac{\delta S_{\text{eff}}}{\delta A_\nu}$. The charge carried by the domain wall is given by $Q = \int \frac{\tilde{S}_{\text{eff}}}{\delta A_t} = -\frac{1}{2\pi}\int dx\partial_x\eta\partial_\eta\gamma(\eta) = -\int \frac{d\eta}{2\pi}\partial_\eta\gamma(\eta)$. The charge Q is $1/2$ with $\Delta_x > 0$. The microscopic details of the domain wall can change Q by 1, so we conclude the charge carried by the domain wall is $Q = \frac{1}{2} \mod 1$. There is an additional one half charge at the boundary for an open system.

5.4 PHASE TRANSITIONS TO TRIVIAL BAND INSULATORS

5.4.1 Time reversal symmetry breaking and transition to the trivial insulator phase

An interesting topological phase transition to a trivial insulator can be tuned to occur when rotating the atoms on individual sites, for example, by applying the technique demonstrated in Ref. [81]. By rotating individual lattice sites the induced bare coupling term is $\Omega\sum_j \hat{L}_z(j)$ where the angular momentum operator $\hat{L}_z = -i(a^\dagger_{p_y}a_{p_x} - a^\dagger_{p_x}a_{p_y})$. This term couples the p_x to p_y-orbitals of the B-leg. One can tune the rotating frequency to match Ω with the transverse tunneling t_{sy} from the p_y-orbital of the B-leg to the nearby s-orbital on the A-leg. Despite the large energy band gap (ϵ_y) which separates the p_y-orbitals from the degenerate s and p_x orbitals (bear in mind that the s and p_x orbitals are from different legs of the ladder), the low energy effective Hamiltonian receives a standard 2nd-order effect from virtual processes, in which a particle jumps from a p_x-orbital to the on-site p_y-orbital and then to the nearby s-orbital. The correction is given by

$$\Delta H = \Delta_y C^\dagger_j \sigma_y C_j,$$

with $\Delta_y = \frac{\Omega^2}{\epsilon_y}$, which is an imaginary transverse tunneling between nearby s- and p_x-orbitals. This term preserves particle-hole symmetry but breaks both parity and time-reversal symmetries. The total Hamiltonian in the momentum space now reads $\mathcal{H}'(k) = \mathcal{H}(k) + \Delta_y \sigma_y$. This Hamiltonian belongs to the symmetry group $G_+(U, C)$ and allows a Z_2 classification of its topological properties [77]. Even though time-reversal symmetry is absent, particle-hole symmetry still ensures that Berry phase γ is quantized, with $\gamma \mod 2\pi = 0$ or π defining the trivial and topological insulator, respectively [79]. For our model $\mathcal{H}'$, the topological insulating phase with $\gamma = \pi$ is realized as long as $\Delta_y < \Delta_y^c = 2t_{sp}$. In another word, the Berry phase quantization is robust against the time-reversal symmetry breaking term Δ_y, and this topological phase is protected by particle-hole symmetry. For Δ_y greater than Δ_y^c, Berry phase vanishes and the system becomes a trivial band insulator. At the critical point the band gap closes. Apart from the Berry phase, the topological distinction between $\mathcal{H}'(k)$ and $\mathcal{H}(k)$ can also be seen from the gapped interpolation [79]. Besides probing the half charges on the boundaries, another signature for the critical point of the topological phase transition is the local density fluctuation, $\delta\rho = \frac{1}{L}\sum_j \sqrt{\langle \rho(j)\rho(j)\rangle}$. $\delta\rho$ is $1/\sqrt{2}$ when $\Delta_y = 0$, independent of other parameters t_s, t_p and t_{sp}, and decreases monotonically with increasing Δ_y. The peaks of $d\delta\rho^2/d\Delta_y$ reveal the critical points (Fig. 14**b**) and provide a reliable tool of detecting the topological phase transition in experiments.

It is feasible to prepare the ladder with phase separation: e.g., a topological insulator on the left half but a trivial insulator on the right half. This can be achieved by rotating the lattice sites on half of the ladder only. The system is now described by

$$H_\eta = H + \frac{\Delta_y}{2}\sum_j \left[1 - \cos\eta(j)\right] C_j^\dagger \sigma_y C_j \tag{5.29}$$

with a field configuration $\eta(j)$ which satisfies the boundary conditions $\eta(j = -\infty) = 0$ and $\eta(j = +\infty) = \pi$, and $\Delta_y > \Delta_y^c$. The charge distribution induced by the domain wall (the phase boundary) is calculated both numerically and from effective field theory shown in Appendix. Both approaches cross-verify that the domain wall carries half charge (Fig. 14**a**). The half charge can be detected [82] by the single site imaging technique in experiments [83, 84].

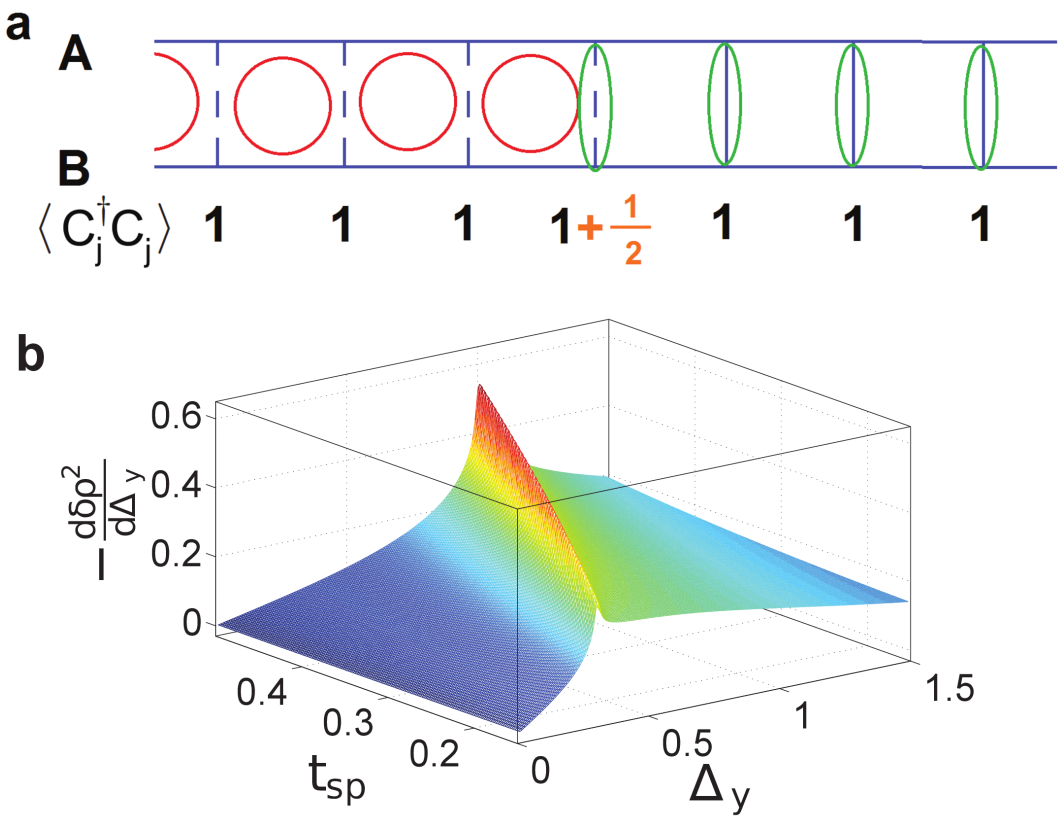

Figure 14: Phase transition between the topological and the trivial band insulator. **a**. A domain wall between a topological insulator ($t_s = t_p = t_{sp}$, $\Delta_y = 0$, left) and a trivial insulator ($t_s = t_p = t_{sp} = 0$, right). The circle represents the delocalized fermion shared by two neighboring rungs as depicted in Fig. 13**a**, whereas the ellipse represents localized fermion without hopping. The additional charge $\frac{1}{2}$ in the middle is the fractional charge carried on the domain wall. **b**. The derivative of density fluctuation, $-\frac{d\delta\rho^2}{d\Delta_y}$. It develops sharp peaks, measurable in experiments, along the line of topological critical points.

5.4.2 Local density fluctuation as probe of topological phase transitions from non-trivial to trivial insulators

In this section we derive an analytic formula for the density fluctuation, which can be measured in cold atom experiments. The density fluctuation in cold atom experiments measures $\delta\rho \equiv \frac{1}{L}\sum_j \left\langle \left(C_j^\dagger C_j - 1\right)^2 \right\rangle$.

First two flat-band limits—(1) ($\Delta_y = 0$, $t_s = t_p = t_{sp} \neq 0$) and (2) ($\Delta_y \neq 0$, $t_s = t_p = t_{sp} = 0$) are explored. The two limits give different Berry phases ($\gamma = \pi$ for Limit (1) and $\gamma = 0$ for Limit (2)). Limits (1) and (2) give non-trivial and trivial insulators respectively. For limit (1) fermions live on the bonds (one fermion per bond). The ground state can be written as

$$|G\rangle = \prod_j \frac{1}{\sqrt{2}} \left(\phi_-^\dagger(j) - \phi_+^\dagger(j+1)\right)|0\rangle, \tag{5.30}$$

with $|0\rangle$ the vacuum state with no particles. $\langle (C_j^\dagger C_j)^2 \rangle$ is given as follows

$$\begin{aligned}
\langle (C_j^\dagger C_j)^2 \rangle &= \sum_{\alpha=\pm,\alpha'=\pm} \langle \phi_\alpha^\dagger(j)\phi_\alpha(j)\phi_{\alpha'}^\dagger(j)\phi_{\alpha'}(j)\rangle \\
&= \sum_{\alpha,\alpha'} \left\{ \delta_{\alpha\alpha'}\langle \phi_\alpha^\dagger(j)\phi_{\alpha'}(j)\rangle - \delta_{\alpha,-\alpha'}\langle \phi_\alpha^\dagger(j)\phi_{\alpha'}^\dagger(j)\phi_\alpha(j)\phi_{\alpha'}(j)\rangle \right\} \\
&= \sum_{\alpha} \left\{ \langle \phi_\alpha^\dagger(j)\phi_\alpha(j)\rangle - \langle \phi_\alpha^\dagger(j)\phi_{-\alpha}^\dagger(j)\phi_\alpha(j)\phi_{-\alpha}(j)\rangle \right\} \\
&= 1 + 2 \times \left(\frac{1}{\sqrt{2}}\right)^4 = \frac{3}{2}
\end{aligned} \tag{5.31}$$

Then we have $\delta\rho = \frac{1}{\sqrt{2}}$. For Limit (2) there is no hopping between different unit cells and fermions localize on each unit cell. Fermions cannot tunnel between different unit cells, so the local density fluctuation vanishes, i.e., $\delta\rho = 0$.

For the generic case, the periodic boundary condition is adopted and the calculation is performed in the momentum space. In momentum space, the Fourier transformed operators are defined as $\tilde{\alpha}(k) = \frac{1}{\sqrt{L}}\sum_j \alpha_j e^{-ikj}$. The density fluctuation, which is a bulk property, does not depend on the boundary condition in the thermodynamic limit. The fermion operators of the eigen-modes (labeled by k) are introduced by $\left[\tilde{b}_\uparrow(k), \tilde{b}_\downarrow(k)\right]^T = U^\dagger \tilde{C}_k$. $\uparrow$ / $\downarrow$ here means the upper/lower band. The unitary matrix U is defined in Sec. 5.2.1. The ground

state of the fermionic ladder at half filling is $|G\rangle = \prod_k \tilde{b}^\dagger_\downarrow(k)|0\rangle$. The calculation of $\langle (C^\dagger_j C_j)^2\rangle$ is as follows

$$
\begin{aligned}
& \langle (C^\dagger_j C_j)^2\rangle \\
= \quad & \frac{1}{L^2}\sum_{\nu=s/p,\nu'=s/p}\sum_{k_1k_2k_3k_4} e^{i(k_2+k_4-k_3-k_1)j}\langle \tilde{a}^\dagger_\nu(k_1)\tilde{a}_\nu(k_2)\tilde{a}^\dagger_{\nu'}(k_3)\tilde{a}_{\nu'}(k_4)\rangle \\
= \quad & \frac{1}{L^2}\sum_{\nu,\nu'}\sum_{kk'}\Big\{\langle \tilde{a}^\dagger_\nu(k)\tilde{a}_\nu(k)\rangle\langle \tilde{a}^\dagger_{\nu'}(k')\tilde{a}_{\nu'}(k')\rangle + \langle \tilde{a}^\dagger_\nu(k)\tilde{a}_{\nu'}(k)\rangle\langle \tilde{a}_\nu(k')\tilde{a}^\dagger_{\nu'}(k')\rangle\Big\} \\
= \quad & \frac{1}{L^2}\sum_{kk'}\Big\{\langle \tilde{b}^\dagger_\downarrow(k)\tilde{b}_\downarrow(k)\tilde{b}^\dagger_\downarrow(k')\tilde{b}_\downarrow(k')\rangle \\
& + \sum_{\nu\nu',s_1s_2s_3s_4}\langle \tilde{b}^\dagger_{s_1}(k)\tilde{b}_{s_2}(k')\tilde{b}^\dagger_{s_3}(k')\tilde{b}_{s_4}(k)\rangle [U(k)]^*_{\nu s_1}[U(k')]_{\nu s_2}[U(k')]^*_{\nu' s_3}[U(k)]_{\nu' s_4}\Big\} \\
= \quad & \frac{1}{L^2}\sum_{kk'}\Big\{1+\langle \tilde{b}^\dagger_\downarrow(k)\tilde{b}_\uparrow(k')\tilde{b}^\dagger_\uparrow(k')\tilde{b}_\downarrow(k)\rangle [U^\dagger(k)]_{\downarrow\nu}[U(k')]_{\nu\uparrow}[U^\dagger(k')]_{\uparrow\nu'}[U(k)]_{\nu'\downarrow}\Big\} \\
= \quad & 1+\frac{1}{L^2}\sum_{kk'}|[U^\dagger(k)U(k')]_{\downarrow\uparrow}|^2. \qquad (5.32)
\end{aligned}
$$

The term $\frac{1}{L^2}\sum_{kk'}|[U^\dagger(k)U(k')]_{\downarrow\uparrow}|^2$ simplifies as

$$
\begin{aligned}
& \frac{1}{L^2}\sum_{kk'}\left|[U^\dagger(k)U(k')]_{\downarrow\uparrow}\right|^2 = \frac{1}{L^2}\sum_{kk'}\left|\left[e^{-i\sigma_x\theta(k)/2}e^{i\sigma_x\theta(k')/2}\right]_{\downarrow\uparrow}\right|^2 = \frac{1}{L^2}\sum_{kk'}\sin^2\left(\frac{\theta(k)-\theta(k')}{2}\right) \\
= \quad & \frac{1}{2}\left[1-\left(\oint\frac{dk}{2\pi}\cos(\theta(k))\right)^2-\left(\oint\frac{dk}{2\pi}\sin(\theta(k))\right)^2\right]. \qquad (5.33)
\end{aligned}
$$

Due to the particle-hole symmetry $h_z(k) = -h_z(\pi - k)$ and that $h(k) = h(\pi - k)$, and we thus have $\cos(\theta(k)) = -\cos(\theta(\pi - k))$, so that $\oint dk\cos(\theta(k)) = 0$. Then the density fluctuation of a particle-hole symmetric insulator is given by

$$
\delta\rho^2 = \frac{1}{2}\left[1-\left(\oint\frac{dk}{2\pi}\sin(\theta(k))\right)^2\right]. \qquad (5.34)
$$

In the absence of the the imaginary transverse tunneling ($\Delta_y = 0$), time-reversal symmetry is also respected. Here we have $\sin(\theta(k)) = -\sin(\theta(-k))$ because $h_y(k) = -h_y(-k)$. Apparently $\oint dk\sin(\theta(k)) = 0$, so we conclude $\delta\rho^2 = \frac{1}{2}$ for $\Delta_y = 0$, regardless of t_s, t_p and t_{sp}.

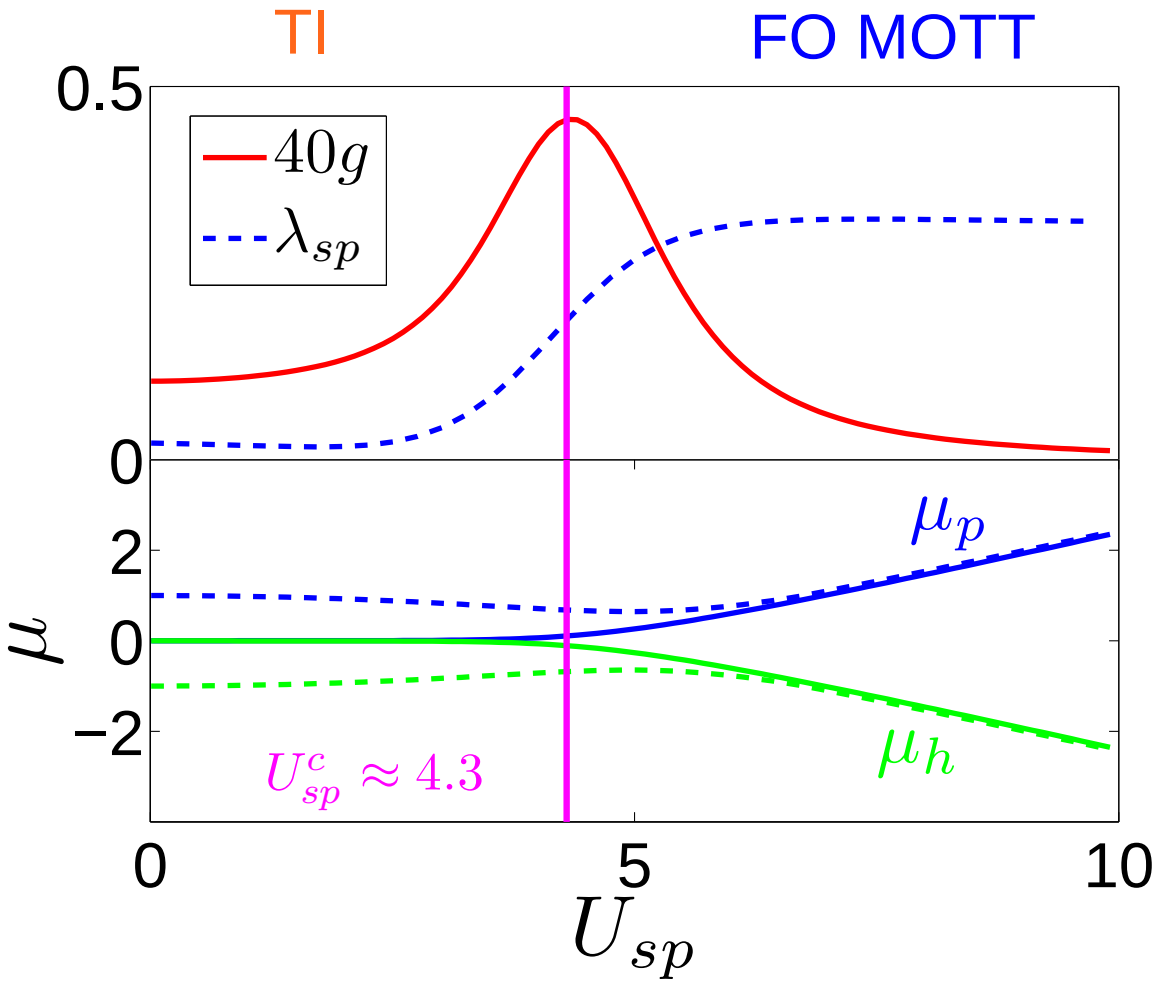

Figure 15: Transition from a topological insulator (TI) phase into a Mott insulator with ferro-orbital (FO) order with increasing interaction. Top panel shows the fidelity metric g and the ferro-orbital order parameter λ_{sp}. Bottom panel shows the particle/hole chemical potential (μ_p/μ_h). The finite charge gap $\mu_p - \mu_h$ in the bulk calculated with periodic boundary condition (dashed lines) comparing with the vanishing gap with open boundary condition (solid lines) indicates in-gap states on the edge. The length L is 12, and $t_s = t_p = 2t_{sp}$ (taken as the energy unit) in this plot.

5.5 MOTT TRANSITIONS

We further examine the stability of the topological phase and its quantum phase transitions in the presence of interaction using exact diagonalization. For single-species fermions on the *sp*-orbital ladder, the leading interaction term is the on-site repulsion between different orbitals,

$$H_{\text{int}} = \sum_j U_{sp} \left[n_s(j) - \frac{1}{2} \right] \left[n_p(j) - \frac{1}{2} \right]. \tag{5.35}$$

To characterize the stability of the topological phase against the inter-orbital interaction H_{int} (see Eq. (5.35)), we use the exact diagonalization method to calculate the fidelity metric $g \equiv 2\left[1 - |\langle \psi_L^0(U_{sp}) | \psi_L^0(U_{sp} + \delta U_{sp}) \rangle|\right] / L(\delta U_{sp})^2$, where $|\psi_N^0(U_{sp})\rangle$ is the ground state wave function of the Hamiltonian $H = H_0 + H_{\text{int}}$ for a finite chain of length L with $N = L$ fermions. A peak in the fidelity metric indicates a quantum phase transition [85]. In presence of interaction, the edge states survive as in-gap states (zero energy single particle/hole excitations) [85]. The energy of single particle (hole) excitation is defined as μ_p (μ_h) by $\mu_p = E_{L+1} - E_L$ ($\mu_h = E_L - E_{L-1}$), where E_N is the ground state energy of the ladder loaded with N fermions. The spatial distribution of the in-gap states is defined as the density profile (Δn_j) of a hole created out of the ground state, which is

$$\Delta n_j = \langle \psi_L^0 | \rho(j) | \psi_L^0 \rangle - \langle \psi_{L-1}^0 | \rho(j) | \psi_{L-1}^0 \rangle, \tag{5.36}$$

where $|\psi_N^0\rangle$ is the ground state with N fermions. The density profile Δn_j is found to be localized on the edges when $U_{sp} \ll U_{sp}^c$, and to delocalize when approaching the critical point and finally disappear (Fig. 13**c**). The Mott state appearing at the strong coupling regime has a ferro-orbital order $\langle \hat{O}_{sp}(j) \rangle$, with $\hat{O}_{sp}(j) = C_j^\dagger \sigma_x C_j$ (Fig. 15). In our numerical calculation of finite system size, the correlation matrix $[\mathcal{C}]_{j_1 j_2} = \langle \hat{O}_{sp}(j_1) \hat{O}_{sp}(j_2) \rangle$ is calculated and the strength of the ferro-orbital order λ_{sp} is defined as the maximum eigenvalue of $[\mathcal{C}]/L$, extrapolated to the thermodynamic limit.

The orbital physics of this Mott insulator can be described by an effective Hamiltonian with the double occupancy projected out. Then the two states, $a_s^\dagger(j)|\Omega\rangle$ and $(-1)^j a_p^\dagger(j)|\Omega\rangle$,

are mapped to two pseudo-spin $\frac{1}{2}$ states. The resulting effective Hamiltonian (for $t_s = t_p \equiv t_0$) is the well-known XXZ Hamiltonian given as

$$H_{\text{eff}} = \sum_{<ij>} \{J_{yz} (\mathbf{S}_y(i)\mathbf{S}_y(j) + \mathbf{S}_z(i)\mathbf{S}_z(j)) + J_x \mathbf{S}_x(i)\mathbf{S}_x(j)\}, \tag{5.37}$$

with $J_x = 2\frac{t_0^2+t_{sp}^2}{U_{sp}}$ and $J_{yz} = 2\frac{t_0^2-t_{sp}^2}{U_{sp}}$. The XXZ Hamiltonian predicts a gapped Mott insulator for the sp-orbital ladder with a ferro-orbital order $\langle C_j^\dagger \sigma_x C_j \rangle$, which spontaneously breaks the particle-hole symmetry. The ferro-orbital order gets weaker as t_s gets smaller. A rich phase diagram of orbital ordering is expected and will be investigated in the future.

5.6 COUPLED LADDERS AND FLAT BANDS IN TWO DIMENSIONS

Remarkably, the zero-energy edge states of the sp orbital ladder survive even when the system is extended to two dimensions with finite inter-ladder coupling (e.g., by reducing $V_{1,2}$ relative to V_x in the setup of Fig. 12**a**). The zero modes of individual ladder morph into a flat band with double degeneracy (Fig. 17). The lack of dispersion in the y direction is related to the inter-ladder hopping pattern, which does not directly couple the edge states but only s- and p-orbitals on different rungs (Fig. 16). The unexpected flat band in 2D is an exact consequence of the p-orbital parity and hence is protected by symmetry. The flat band makes the edge states in this 2D optical lattice distinct from that of quantum Hall effect previously proposed with lattice rotation [68, 86], artificial gauge field [87] or optical flux [88]. Such a flat band is reminiscent of that at the zigzag edge of graphene, but with the difference that the present flat band is protected by the parity of the orbital wavefunctions. The diverging density of states associated with the flat band provides a fertile ground for interaction-driven many body instabilities. Future work will tell whether strongly correlated topological states exist in such two-dimensional interacting systems.

The flat dispersion can be rigorously proved using an unitary transformation and arguments based on the quantization of Berry phase. Due to the experimental setup the leading inter-ladder coupling is the coupling between the B (A) chain and the A (B) chain of the

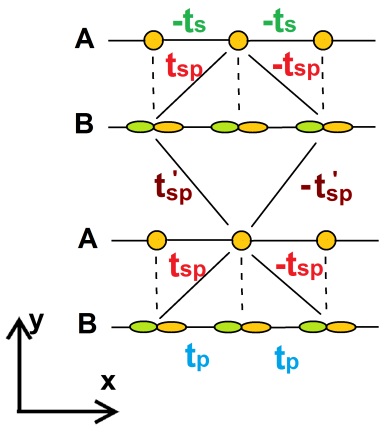

Figure 16: Schematic plot of the coupled ladders. The leading inter-ladder coupling is t'_{sp}. The absence of coupling between nearest s and p orbitals is due to parity.

nearest ladder (FIG. 16). The tight binding Hamiltonian describing such a coupled two dimensional system is given as

$$H_{2D} = \sum_{\mathbf{R}} \left\{ C^{\dagger}_{\mathbf{R}} T C_{\mathbf{R}+\hat{x}} + C^{\dagger}_{\mathbf{R}} T' C_{\mathbf{R}+\hat{x}+\hat{y}} - C^{\dagger}_{\mathbf{R}} T' C_{\mathbf{R}+\hat{y}-\hat{x}} + h.c. \right\}, \tag{5.38}$$

where $\mathbf{R}$ labels the positions of lattice sites and $\hat{x}$ ($\hat{y}$) is the primitive vector in the x- (y-) direction. The intra-ladder coupling matrix T is given as $\begin{bmatrix} -t_s & -t_{sp} \\ t_{sp} & t_p \end{bmatrix}$, and the inter-ladder coupling matrix T' is given as $\begin{bmatrix} 0 & 0 \\ t'_{sp} & 0 \end{bmatrix}$, with t'_{sp} the inter-ladder coupling strength. In the momentum space the Hamiltonian reads $H_{2D} = \sum_{\mathbf{k}} \tilde{C}^{\dagger}(\mathbf{k}) \mathcal{H}_{2D}(\mathbf{k}) \tilde{C}(\mathbf{k})$, with

$$\mathcal{H}_{2D}(\mathbf{k}) = \begin{bmatrix} -2t_s \cos k_x & -2i(t_{sp} + t'_{sp} e^{-ik_y}) \sin k_x \\ 2i(t_{sp} + t'_{sp} e^{ik_y}) \sin k_x & 2t_p \cos k_x \end{bmatrix}. \tag{5.39}$$

The Hamiltonian $\mathcal{H}_{2D}(\mathbf{k})$ can be rewritten as $\mathcal{H}_{2D}(\mathbf{k}) = U^{\dagger}(k_y) \tilde{\mathcal{H}}_{2D}(k_x, k_y) U(k_y)$ with

$$\tilde{\mathcal{H}}_{2D}(k_x, k_y) = \begin{bmatrix} -2t_s \cos k_x & -2i\tilde{t}_{sp} \sin k_x \\ 2i\tilde{t}_{sp} \sin k_x & 2t_p \cos k_x \end{bmatrix} \tag{5.40}$$

and $U(k_y) = e^{i\sigma_z \varsigma(k_y)/2}$, where $\tilde{t}_{sp} = |t_{sp} + t'_{sp} e^{-ik_y}|$, and $\varsigma(k_y) = \arg(t_{sp} + t'_{sp} e^{-ik_y})$. With k_y fixed, $\mathcal{H}_{2D}(k_x, k_y)$ can be treated as a one-dimensional Hamiltonian, the form of which is exactly the same as that describing a single sp-orbital ladder (realized in the limit of $t'_{sp} = 0$). Thus as a one-dimensional Hamiltonian, $\mathcal{H}_{2D}(k_x, k_y)$ for a given k_y defines a Berry phase π. We thus conclude that the one-dimensional topological insulator survives even with finite inter-ladder couplings.

The existence of edge states in the presence of inter-ladder coupling is verified by directly calculating the energy spectra of the 2D system on a cylinder geometry (an open cylinder in the x-direction). From the energy spectra shown in Fig. 17 it is clear that the edge states are stable against inter-ladder couplings.

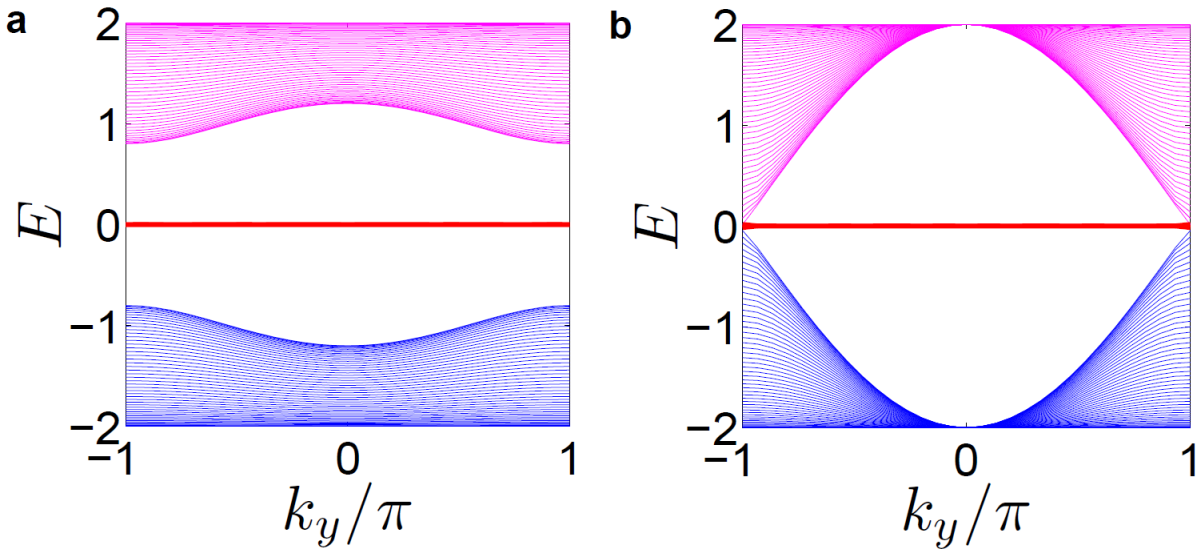

Figure 17: The energy spectra of the two dimensional system of coupled ladders with $t_s = t_p = 2t_{sp}$ (taken as the energy unit here), and length $L = 200$. An open (periodic) boundary condition is applied in the x (y) direction. **a** and **b** show the spectra with the small and large inter-ladder coupling, $t'_{sp} = t_{sp}/5$ and $t'_{sp} = t_{sp}$, respectively. A flat band (red line) at zero energy with double degeneracy generically appear for $0 < t'_{sp} < t_{sp}$.

5.7 DISCUSSION

5.7.1 Comparison with the SSH model.

The mathematical description of the *sp*-orbital ladder H_0 is similar to the celebrated Su-Schrieffer-Heeger (SSH) model [89]. While the two systems belong to the same symmetry class $G_{++}^{-+}(U,T,C)$ of 1D topological insulators [77], the orbital ladder contains new physics beyond the SSH model. Firstly, the edges states of the *sp*-orbital ladder have quite different spatial structures. For example, the sharp confinement of the edge states only requires $t_{sp} = \sqrt{t_s t_p}$, rather than the energy spectrum being dispersionless. In contrast, sharp confinement coincides with the flat band limit in the SSH model, when one of its hoppings vanishes. Moreover, the edge modes form flat bands in the presence of inter-ladder coupling. The original SSH model does not have such a nice property. Secondly and more importantly, tunneling in the orbital ladder can form π flux loops and allow time-reversal symmetry breaking, as shown in $\mathcal{H}'$ discussed above. This gives rise to an interesting Z_2 topological insulating state [77]. In contrast, breaking time-reversal symmetry within the SSH model of spinless fermions is impossible because the tunneling is strictly one-dimensional and thus cannot form flux loops.

5.7.2 Connection to Majorana fermions

In the flat band limit $t_s = t_p = t_{sp} = t$ (or equivalently $t_1 = t_2 = 0$) we can introduce particle-hole mixed operators $\phi_{\uparrow/\downarrow}(j) = [a_p(j) \pm a_s^\dagger(j)]/\sqrt{2}$. The *sp*-orbital ladder maps to two decoupled Kitaev's p-wave superconducting chains [74],

$$H_0 \to t \sum_{j\sigma} \left\{ \phi_\sigma^\dagger(j)\phi_\sigma(j+1) + P_\sigma \phi_\sigma^\dagger(j)\phi_\sigma^\dagger(j+1) + h.c. \right\}, \tag{5.41}$$

with $P_{\uparrow/\downarrow} = \pm$.

It is instructive to rewrite the fermion operators $\phi_\pm$ defined in Sec. 5.2.3 in terms of Majorana fermion operators as $\phi_\pm = \frac{1}{2}(\psi_{1\pm} - i\psi_{2\mp})$, with $\psi_{\ell p} = \psi_{\ell p}^\dagger$, and $\{\psi_{\ell p}, \psi_{\ell' p'}\} =$

$2\delta_{pp'}\delta_{\ell\ell'}$. The resulting Hamiltonian in Eq. (5.8) reads

$$H_0 = \frac{i}{2}\sum_j [\psi_{1+}(j), \psi_{2-}(j), \psi_{1-}(j), \psi_{2+}(j)] \begin{bmatrix} 0 & -t_1 & 0 & -t_2 \\ t_1 & 0 & t_2 & 0 \\ 0 & -t_3 & 0 & 0 \\ t_3 & 0 & 0 & 0 \end{bmatrix} \begin{bmatrix} \psi_{1+}(j+1) \\ \psi_{2-}(j+1) \\ \psi_{1-}(j+1) \\ \psi_{2+}(j+1) \end{bmatrix}. \quad (5.42)$$

In the flat band limit, the Hamiltonian maps to two decoupled Majorana Fermi chains [74],

$$H_0 \to i\tfrac{t_3}{2}\textstyle\sum_j [\psi_{2+}(j)\psi_{1+}(j+1) - \psi_{1-}(j)\psi_{2-}(j+1)]\,. \quad (5.43)$$

The unpaired Majorana fermion operators are $\psi_{1+}(0)$, $\psi_{2-}(0)$, $\psi_{2+}(L-1)$ and $\psi_{1-}(L-1)$. These Majorana fermion operators give a many-body ground state manifold of Z_4 degeneracy for $\mu = 0$ in the grand canonical ensemble [74]. Since $[\phi_+^\dagger(0)\phi_+(0), H] = 0$, $[\phi_-^\dagger(L-1)\phi_-(L-1), H] = 0$ and $[\phi_+^\dagger(0)\phi_+(0), \phi_-^\dagger(L-1)\phi_-(L-1)] = 0$, one can label the degenerate ground states by operators $\phi_+^\dagger(0)\phi_+(0)$ and $\phi_-^\dagger(L-1)\phi_-(L-1)$ in such a way as follows,

$$|G_0\rangle\text{: } \phi_+^\dagger(0)\phi_+(0)|G_0\rangle = 0 \text{ and } \phi_-^\dagger(L-1)\phi_-(L-1)|G_0\rangle = 0, \quad (5.44)$$

$$|G_+\rangle = \phi_+^\dagger(0)|G_0\rangle, \quad (5.45)$$

$$|G_-\rangle = \phi_-^\dagger(L-1)|G_0\rangle, \quad (5.46)$$

$$|G_{+-}\rangle = \phi_+^\dagger(0)\phi_-^\dagger(L-1)|G_0\rangle. \quad (5.47)$$

(The states $|G_+\rangle$ and $|G_-\rangle$ have the same number of fermions, providing the Z_2 degeneracy at half filling in the canonical ensemble.) In the Z_4 degenerate ground state manifold the operators $\phi_+(0)$ and $\phi_-(L-1)$ read as

$$\phi_+(0) = |G_0\rangle\langle G_+| + |G_-\rangle\langle G_{+-}| \quad (5.48)$$

$$\phi_-(L-1) = |G_0\rangle\langle G_-| - |G_+\rangle\langle G_{+-}|. \quad (5.49)$$

To demonstrate the deconfined Dirac fermion excitations explicitly in this ground state manifold, we can label the states by $d_1^\dagger d_1$ and $d_2^\dagger d_2$, where d_1 and d_2 are fractionalized

Dirac fermion operators $d_1 = (\psi_{1+}(0) - i\psi_{2+}(L-1))/2$ and $d_2 = (\psi_{2-}(0) - i\psi_{1-}(L-1))/2$, respectively. The relabeled states are defined by

$$|\tilde{G}_0\rangle\text{: } d_1^\dagger d_1|\tilde{G}_0\rangle = 0 \text{ and } d_2^\dagger d_2|\tilde{G}_0\rangle = 0, \tag{5.50}$$

$$|\tilde{G}_1\rangle = d_1^\dagger|\tilde{G}_0\rangle, \tag{5.51}$$

$$|\tilde{G}_2\rangle = d_2^\dagger|\tilde{G}_0\rangle, \tag{5.52}$$

$$|\tilde{G}_{12}\rangle = d_1^\dagger d_2^\dagger|\tilde{G}_0\rangle. \tag{5.53}$$

These states embedding fractionalized Dirac fermions are actually given by $|\tilde{G}_0\rangle = (|G_+\rangle - |G_-\rangle)/\sqrt{2}$, $|\tilde{G}_1\rangle = (|G_0\rangle - |G_{+-}\rangle)/\sqrt{2}$, $|\tilde{G}_2\rangle = -(|G_0\rangle + |G_{+-}\rangle)/\sqrt{2}$ and $|\tilde{G}_{12}\rangle = -(|G_+\rangle + |G_-\rangle)/\sqrt{2}$. A transition from $|\tilde{G}_0\rangle$ to $|\tilde{G}_1\rangle$ creates one fractionalized Dirac fermion excitation.

In general, e.g., away from flat band limit, the unpaired Majorana fermion operators ψ are defined by $[\psi, H_0] = 0$. The four unpaired Majorana fermion operators are $\psi_1 = b_l + b_l^\dagger$, $\psi_2 = i(b_l - b_l^\dagger)$, $\psi_3 = b_r + b_r^\dagger$ and $\psi_4 = i(b_r - b_r^\dagger)$, where the Dirac fermion operators b_l and b_r are defined in Sec. 5.2.3.

Topologically protected Majorana fermions with Majorana number -1 [74, 90, 91] can be realized on the orbital ladder using schemes similar to those proposed in Ref. [70, 72, 73, 71], e.g., by inducing weak pairing of the form $\sum_j \Delta a_s(j)a_p(j) + h.c.$. The staggered quantum tunneling t_{sp} mimics the spin-orbit coupling. For the sp-orbital ladder with $2t_s < |\mu| < 2t_p$, we find that the Majorana number is -1 and the resulting Majorana zero modes are topologically protected. The topologically protected Majorana state is a promising candidate for topological quantum computing [92, 93].

6.0 LUTTINGER LIQUID PHASES OF SP-ORBITAL LADDER

To complete the study of the *sp*-orbital ladder proposed in the last chapter, we study Luttinger liquid phases away from half-filling [19]. These phases can be realized with dipolar molecules or atoms loaded into a ladder, dipole moments being aligned by an external field. The two orbital components have distinct hoppings. The tunneling between them is equivalent to a partial Rashba spin-orbital coupling when the orbital space (s, p) is identified as spanned by pseudo-spin 1/2 states. A rich phase diagram, including incommensurate orbital density wave, pair density wave and other exotic superconducting phases, is obtained with bosonization analysis. In particular, superconductivity is found in the repulsive regime.

Orbital degrees of freedom [13] play a fundamental role in understanding the unconventional properties in solid state materials [94]. Recent experiments in optical lattices have demonstrated that orbitals can also be used to construct quantum emulators of exotic models beyond natural crystals. Orbital lattices are attracting growing interests due to their unique and fascinating properties resulting from the spatial nature of the degenerate states. For example, the bosonic $p_x + ip_y$ superfluid [31, 1, 32, 33, 18] state has been prepared on a bipartite square lattice [14], and later the other complex superfluid with s and p orbitals correlated was observed on a hexagonal lattice [16].

Previous studies of multicomponent cold gases mainly focused on hyperfine states of alkali atoms [5, 57]. In a cold gas of atoms with two approximately degenerate hyperfine states, the realized pseudo-spin SU(2) symmetry makes it possible to emulate the Fermi Hubbard model in optical lattices [95, 25, 96]. To engineer spin-orbital couplings and the resulting topological phases, one has to induce Raman transitions between the hyperfine states to break the pseudo-spin symmetry [97, 98, 99]. In contrast, due to the spatial nature of the orbital degrees of freedom, the symmetry in orbital gases, such as that in $p_x + ip_y$ superfluid [14],

can be controlled by simply changing the lattice geometry as shown in Ref. [14, 16, 63, 100], where unprecedented tunability of double-wells has been demonstrated. With a certain lattice geometry, a spin-orbital like coupling can naturally appear in an orbital gas with s and p-orbitals without Raman transitions [27]. Theoretical studies of orbital physics largely focusing on two or three dimensions suggest exotic orbital phases [31, 1, 32, 101, 102, 33, 42, 12, 103, 104, 43, 66, 105] beyond the scope of spin physics.

In this chapter, we study a one dimensional orbital ladder with s and p orbitals coupled [64, 27]. We shall derive such an effective model for dipolar molecules or atoms [106, 107, 108, 109, 110] loaded in a double-well optical lattice. The tunneling rates (or effective mass) of each orbital component are highly tunable by changing the lattice strength. Couplings between s and p orbitals mimic spin-orbital couplings [27]. This orbital system suggests the possibility of exploring the equivalent of the exciting spin-orbital coupled physics in dipolar gases yet without requiring the use of synthetic gauge fields, and hence it provides an interesting and simple alternative route. A rich phase diagram, including incommensurate orbital density wave (ODW), pair density wave (PDW) [111, 76, 112, 113], and other exotic superconducting phases, is found with bosonization analysis. The PDW phase realized here is a superconducting phase, that features an oscillating Cooper pair field with a period of π. The incommensurate ODW phase has an oscillating particle-hole pair, which tends to break the time-reversal symmetry. An exotic superconducting phase on the repulsive side is also discovered.

6.1 MODEL

Consider a cold ensemble of polar molecules or atoms, e.g., ^{40}K^{87}Rb [106, 108, 109], OH [114], ^{23}Na^{40}K [110], or Dy [107], whose dipole moments are controlled by an external field as demonstrated in experiments. Long-lived polar molecules have been realized in optical lattices [109]. Let the ensemble trapped by a ladder-like optical lattice of the type studied in [27]. As shown in the schematic picture in [27], the lattice consists of two chains of potentials of unequal depth. We consider a single species of fermionic atoms/molecules occupying

the s and p orbitals of the shallow and deep chains respectively, with other low-lying orbitals completely filled. Alternatively, fermions can be directly loaded into the high orbitals, by techniques developed in recent experiments [14, 63]. Meta-stable states in high orbitals with long life time up to several hundred milliseconds are demonstrated achievable [14]. To suppress chemical reactions of polar molecules, the latter approach is preferable. The single particle Hamiltonian of the sp-orbital ladder is then given by [27]

$$H_0 = \sum_j C_j^\dagger \begin{bmatrix} -t_s & -t_{sp} \\ t_{sp} & t_p \end{bmatrix} C_{j+1} + h.c. \tag{6.1}$$

where $C_j^\dagger = [a_s^\dagger(j), a_p^\dagger(j)]$, and $a_s^\dagger$ ($a_p^\dagger$) is the creation operator for the s-orbital (p-orbital). The lattice constant is set as the length unit. In the proposed optical lattice setup [27], the ratios t_s/t_p and t_{sp}/t_p are small (typically around 0.1).

The band structure is readily obtained by Fourier transform $C_j = \int \frac{dk}{2\pi} \tilde{C}(k) e^{ikj}$. The Hamiltonian in the momentum space reads as $H_0 = \int \frac{dk}{2\pi} \tilde{C}^\dagger(k) \tilde{\mathcal{H}}(k) \tilde{C}(k)$, with $\tilde{\mathcal{H}}(k) = h_0(k)\sigma_0 + \vec{h}(k) \cdot \vec{\sigma}$, where $h_0(k) = (t_p - t_s)\cos(k)$, $h_x(k) = 0$, $h_y(k) = 2t_{sp}\sin(k)$ and $h_z(k) = -(t_p + t_s)\cos(k)$. Here σ_0 is the identity matrix and $\sigma_{x,y,z}$ are Pauli matrices. The two bands are given by $E_\pm(k) = h_0(k) \pm \sqrt{h_y^2(k) + h_z^2(k)}$, which are shown in FIG. 18. The Hamiltonian is rewritten as $H_0 = \int \frac{dk}{2\pi} \sum_{\wp=\pm} E_\wp(k) \phi_\wp^\dagger(k) \phi_\wp(k)$. We define an angle variable θ by $\cos(\theta(k)) = h_z/|\vec{h}|$ and $\sin(\theta(k)) = h_y/|\vec{h}|$ to save writing. Here, we only consider lower than half filling, i.e., less than one particle per unit cell. The lower band is thus partially filled and the upper band is empty. Since we are interested in the low-energy physics, the spectrum E_- is linearized around the Fermi momenta $\pm k_{F\nu}$. Here, $\nu = A$ or B, and $\pm k_{FA}$ are inner Fermi points and $\pm k_{FB}$ are outer Fermi points (FIG. 18). The resulting Fermi velocities are $v_{F\nu} = |\frac{\partial E_-(k)}{\partial k}|_{k=k_{F\nu}}$. The operators capturing the low energy fluctuations are defined with right (Ψ) and left ($\overline{\Psi}$) moving modes $\Psi_A(k) = \phi_-(k_{FA} + k)$, $\overline{\Psi}_A(k) = \phi_-(-k_{FA} + k)$, $\Psi_B(k) = \phi_-(-k_{FB} + k)$ and $\overline{\Psi}_B(k) = \phi_-(k_{FB} + k)$. The field operators are introduced by $\psi_\nu(x) = \int \frac{dk}{2\pi} \Psi_\nu(k) e^{ikx}$ and $\bar{\psi}_\nu(x) = \int \frac{dk}{2\pi} \overline{\Psi}_\nu(k) e^{ikx}$. These field operators are related to lattice operators by

$$\begin{aligned} C(j) &\rightarrow \lambda^A \psi_A(x) e^{ik_{FA}x} + \lambda^{A*} \bar{\psi}_A(x) e^{-ik_{FA}x} \\ &+ \lambda^B \psi_B(x) e^{-ik_{FB}x} + \lambda^{B*} \bar{\psi}_B(x) e^{ik_{FB}x}, \end{aligned} \tag{6.2}$$

where

$$\lambda^{\nu} = \begin{bmatrix} i\sin(\theta_{\nu}/2) \\ \cos(\theta_{\nu}/2) \end{bmatrix},$$

with $\theta_A = \theta(k_{FA})$ and $\theta_B = \theta(-k_{FB})$. The substitution in Eq. (6.2) and the energy linearization are valid for weakly interacting fermions at low temperature.

With polar molecules or atoms loaded on the *sp*-ladder, we include all momentum-independent interactions (momentum-dependent part is irrelevant in the Renormalization group flow [38]) allowed by symmetry. The long-range tail of dipolar interaction could modify the correlations in gapped phases, but its effect in gapless phases is negligible [115, 19]. The Hamiltonian density of the interactions is given by

$$\begin{aligned} \mathcal{H}_{\text{int}} &= \sum_{\nu\nu'} \frac{1}{2} g_4^{\nu\nu'} \left[J_{\nu} J_{\nu'} + \bar{J}_{\nu} \bar{J}_{\nu'} \right] + g_2^{\nu\nu'} J_{\nu} \bar{J}_{\nu'} \\ &\quad + g_3 \left\{ \bar{\psi}_A^* \bar{\psi}_B \psi_A^* \psi_B + \bar{\psi}_B^* \bar{\psi}_A \psi_B^* \psi_A \right\}, \end{aligned} \tag{6.3}$$

where $J_{\nu} =: \psi_{\nu}^* \psi_{\nu} :$ and $\bar{J}_{\nu} =: \bar{\psi}_{\nu}^* \bar{\psi}_{\nu} :$. For the symmetric case $t_s = t_p$, an Umklapp process

$$\mathcal{H}_{um} = g_u \left\{ \bar{\psi}_A^* \psi_A \psi_B^* \bar{\psi}_B + \bar{\psi}_B^* \psi_B \psi_A^* \bar{\psi}_A \right\} \tag{6.4}$$

becomes allowed for the reason that $k_{FA} + k_{FB} = \pi$. Since dipolar interactions between polar molecules or atoms decay as $1/r^3$, the leading interaction in the proposed double-well lattice setup [27] is

$$H_{\text{int}} = U \sum_j \left[a_s^{\dagger}(j) a_s(j) - \frac{1}{2} \right] \left[a_p^{\dagger}(j) a_p(j) - \frac{1}{2} \right].$$

The strength of U is tunable by changing the dipole moment. In the weak interacting limit, the g-ology couplings are related to U by $g_4^{\nu\nu} = U$, $g_4^{AB} = g_4^{BA} = U \sin^2\left(\frac{\theta_A - \theta_B}{2}\right)$, $g_2^{\nu\nu} = U \sin^2(\theta_{\nu})$, ${g_2}^{AB} = {g_2}^{BA} = U$,

$$g_3 = U \sin(\theta_A) \sin(\theta_B),$$

and

$$g_u = U \cos(\theta_A) \cos(\theta_B),$$

at tree level [38]. Considering strong interactions or the finite ranged tail of dipolar interactions, the g-ology couplings will be renormalized due to neglected irrelevant couplings. By

manipulating the direction of dipole moments with an external field, the interaction can be either repulsive or attractive [106, 108, 109, 110].

We follow the notation convention of Ref. [116], where the bosonization identity takes the form

$$\begin{aligned}\psi_\nu &= \frac{1}{\sqrt{2\pi}}\eta_\nu e^{-i\sqrt{\pi}(\varphi_\nu+\vartheta_\nu)} \\ \bar{\psi}_\nu &= \frac{1}{\sqrt{2\pi}}\bar{\eta}_\nu e^{i\sqrt{\pi}(\varphi_\nu-\vartheta_\nu)},\end{aligned} \tag{6.5}$$

where η_ν is the Klein factor and ϑ_ν is the dual field of boson field φ_ν. The charge and orbital boson fields are further introduced here by $[\varphi_c, \varphi_o] = [\varphi_A, \varphi_B]T$, with the matrix T given by

$$T = \frac{1}{\sqrt{2}}\begin{bmatrix} 1 & -1 \\ 1 & 1 \end{bmatrix}.$$

and their duals fields are $[\vartheta_c, \vartheta_o] = [\vartheta_A, \vartheta_B]T$. The Bosonized Hamiltonian density reads

$$\begin{aligned}\mathcal{H} &= \mathcal{H}_c + \mathcal{H}_o + \mathcal{H}_{\rm mix}, \\ \mathcal{H}_c &= \frac{u_c}{2}\left[K_c\Pi_c^2 + \frac{1}{K_c}(\partial_x\varphi_c)^2\right], \\ \mathcal{H}_o &= \frac{u_o}{2}\left[K_o\Pi_o^2 + \frac{1}{K_o}(\partial_x\varphi_o)^2\right] \\ &\quad + \frac{1}{2\pi^2}\left[g_3\cos(\sqrt{8\pi}\vartheta_o) + g_u\cos(\sqrt{8\pi}\varphi_o)\right], \\ \mathcal{H}_{\rm mix} &= u_m\left[K_m\Pi_c\Pi_o + \frac{1}{K_m}(\partial_x\varphi_c)(\partial_x\varphi_o)\right],\end{aligned} \tag{6.6}$$

with $u_{\alpha=c/o} = \sqrt{(v_+ + \tilde{g}_4^{\alpha\alpha}/2\pi)^2 - (\tilde{g}_2^{\alpha\alpha}/2\pi)^2}$,

$$K_\alpha = \sqrt{\frac{2\pi v_+ + \tilde{g}_4^{\alpha\alpha} - \tilde{g}_2^{\alpha\alpha}}{2\pi v_+ + \tilde{g}_4^{\alpha\alpha} + \tilde{g}_2^{\alpha\alpha}}},$$

$$u_m = \sqrt{(v_- + \tilde{g}_4^{co}/2\pi)^2 - (\tilde{g}_2^{co}/2\pi)^2},$$

and

$$K_m = \sqrt{\frac{2\pi v_- + \tilde{g}_4^{co} - \tilde{g}_2^{co}}{2\pi v_- + \tilde{g}_4^{co} + \tilde{g}_2^{co}}},$$

where

$$v_+ = (v_{FA} + v_{FB})/2,$$

$$v_- = (-v_{FA} + v_{FB})/2$$

and the transformed coupling matrices $\tilde{g}_4$ and $\tilde{g}_2$ are given by $[\tilde{g}] = T^{-1}[g]T$. The mixing term $\mathcal{H}_{\text{mix}}$ vanishes for the symmetric case with $t_s = t_p$.

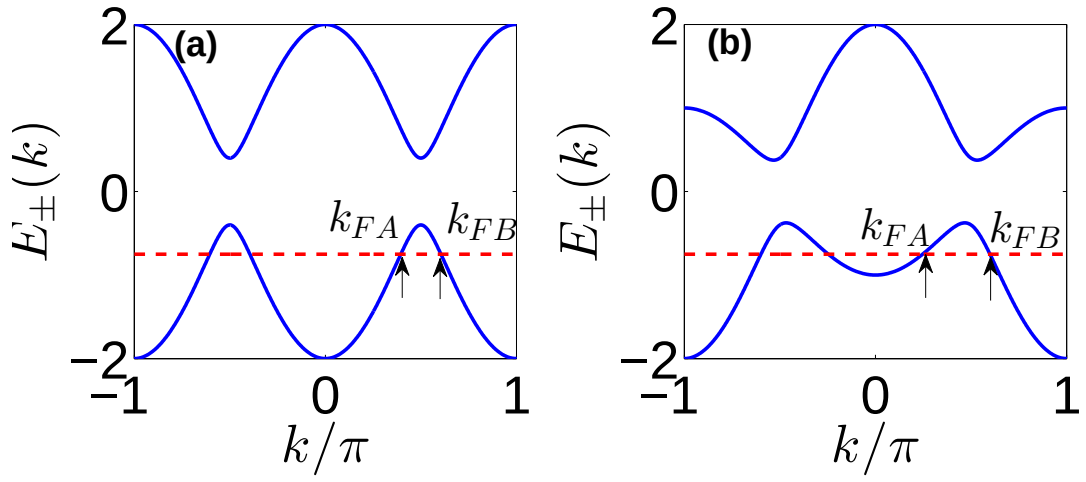

Figure 18: Sketch of the band structure of the *sp*-orbital ladder. Red dashed lines indicates the level of chemical potentials, showing four fermi points. (a), the symmetric case with $t_s = t_p$. (b), the asymmetric case with $t_s < t_p$.

6.2 QUANTUM PHASES AND TRANSITIONS OF THE SYMMETRIC CASE

For the symmetric case with $t_s = t_p$ (FIG. 18), the Hamiltonian has an accidental Z_2 symmetry, $C_j \to (-1)^j \sigma_x C_j$ and Fermi momenta are related by $k_{FA} = \pi - k_{FB} \equiv k_F$. This Z_2 symmetry implies that $v_{FA} = v_{FB}$, ${g_4}^{AA} = {g_4}^{BB}$ and ${g_2}^{AA} = {g_2}^{BB}$. We find that the transformed coupling matrices $\tilde{g}_2$ and $\tilde{g}_4$ are diagonal and that the orbital-charge mixing term $\mathcal{H}_{\text{mix}}$ vanishes. In other words, the Z_2 symmetry guarantees orbital-charge separation. The charge part H_c is quadratic and the orbital part H_o is a Sine-Gordon model [54].

With attraction, we have $K_o < 1$, $g_u > 0$, and the Sine-Gordon term g_u is relevant (flows to $+\infty$) in the renormalization group (RG) flow [54]. This corresponds to an orbital gapped

phase with $\cos(\sqrt{8\pi}\varphi_o)$ locked at -1. In this phase, quantum fluctuations of φ_o become massive, and the divergent susceptibilities are the following: charge density wave (CDW) and PDW [111, 76, 113] given by the operators:

$$\begin{aligned} O_{\mathrm{CDW}}(x) &= \psi_A^* \bar{\psi}_A e^{-2ik_{FA}x} - \psi_B^* \bar{\psi}_B e^{2ik_{FB}x} \\ &\propto e^{-2ik_F x} e^{i\sqrt{2\pi}\varphi_c} \sin(\sqrt{2\pi}\varphi_o) \\ O_{\mathrm{PDW}}(x) &= \psi_A \bar{\psi}_B e^{i(k_{FA}+k_{FB})x} + \psi_B \bar{\psi}_A e^{-i(k_{FA}+k_{FB})x} \\ &\propto (-1)^x e^{-i\sqrt{2\pi}\vartheta_c} \sin(\sqrt{2\pi}\varphi_o) \end{aligned}$$

Due to orbital-charge separation, the CDW and PDW correlation functions are readily given by

$$\langle O_{\mathrm{CDW}}(x) O^\dagger_{\mathrm{CDW}}(0)\rangle \propto e^{-2ik_F x} x^{-K_c}, \tag{6.7}$$

$$\langle O_{\mathrm{PDW}}(x) O^\dagger_{\mathrm{PDW}}(0)\rangle \propto (-1)^x x^{-1/K_c}. \tag{6.8}$$

Since $K_c > 1$ for attraction, the algebraic PDW order is dominant. In this phase, the superconducting pairing $\mathcal{O}_{\mathrm{SC}} = a_s(j)a_p(j)$ oscillates in space with a period of π.

With repulsion, we have $K_o > 1$, and thus g_3 is relevant [54]. This gives an orbital gapped phase with $\cos(\sqrt{8\pi}\vartheta_o)$ locked at 1, because $g_3 < 0$. The fluctuations of ϑ_o are massive, and the divergent susceptibilities are ODW and superconducting SC^+ given by the operators:

$$\begin{aligned} O_{\mathrm{ODW}}(x) &= e^{-i(k_{FA}-k_{FB})x}(\psi_A^* \bar{\psi}_B - \psi_B^* \bar{\psi}_A) \\ &\propto e^{-i(k_{FA}-k_{FB})x} e^{i\sqrt{2\pi}\varphi_c} \cos(\sqrt{2\pi}\vartheta_o) \\ O_{\mathrm{SC}^+}(x) &= \psi_A \bar{\psi}_A + \psi_B \bar{\psi}_B \\ &\propto e^{-i\sqrt{2\pi}\vartheta_c} \cos(\sqrt{2\pi}\vartheta_o) \end{aligned}$$

Since $K_c < 1$ for repulsion, the dominant algebraic order here is ODW, for which the correlation function is given by

$$\langle O_{\mathrm{ODW}}(x) O^\dagger_{\mathrm{ODW}}(0)\rangle \propto e^{-i(k_{FA}-k_{FB})x} x^{-K_c}. \tag{6.9}$$

In the ODW phase, the particle-hole pairing in terms of lattice operators reads $\mathcal{O}_{\mathrm{ODW}}(j) = C_j^\dagger \sigma_y C_j$. This ODW order is incommensurate with an oscillation period $2\pi/(k_{FA} - k_{FB})$

in real space. If we go beyond the one-dimensional limit and consider small transverse tunnelings [27], a true long-range ODW order $\langle O_{\mathrm{ODW}}(x)\rangle \propto e^{i(k_{FA}-k_{FB})x}$ is expected. Such an order breaks time-reversal symmetry.

The ODW and PDW phases predicted by Bosonization analysis are further verified in numerical simulations with matrix products state, in which open boundary condition is adopted. The superconducting correlation

$$C_{\mathrm{SC}}(j'-j) = \langle a_p^\dagger(j) a_s^\dagger(j) a_s(j') a_p(j')\rangle$$

and the orbital density wave correlation

$$C_{\mathrm{ODW}}(j'-j) = \langle C_j^\dagger \sigma_y C_j C_{j'}^\dagger \sigma_y C_{j'}\rangle$$

are calculated. In our calculation, the two points j and j' are 10 sites away from the boundaries to minimize the boundary effects. The convergence of these correlations is checked in numerical simulations. FIG. 19 shows the Fourier transform of these correlations, defined by $\mathcal{C}(k) = \sum_{j\neq 0} C(j) e^{-ikj}$, which approaches to its thermodynamic limit with increasing system size (FIG. 19). The sharp peaks of $\mathcal{C}_{\mathrm{SC}}(k)$ at momenta $\pm\pi$ on the attractive side tell the quantum state has a PDW order shown in Eq. 6.8. On the repulsive side sharp dips of $\mathcal{C}_{\mathrm{ODW}}(k)$ at finite momenta verify the incommensurate ODW order shown in Eq. 6.9. With numerical calculations, we also find the existence of PDW phase in the strongly attractive regime if $t_s \neq t_p$. The phase transition from ODW to PDW is second order.

6.3 QUANTUM PHASES AND TRANSITIONS OF THE ASYMMETRIC CASE

For the asymmetric case—$t_s < t_p$ (FIG. 18), the Fermi velocity $v_{FB} > v_{FA}$ and the orbital-charge separation no longer holds. Thus, the orbital and charge degrees of freedom cannot be treated separately. The other difference with the symmetric case is that the Umklapp process g_u does not exist. Since the effects of g_4 couplings are just to renormalize the Fermi

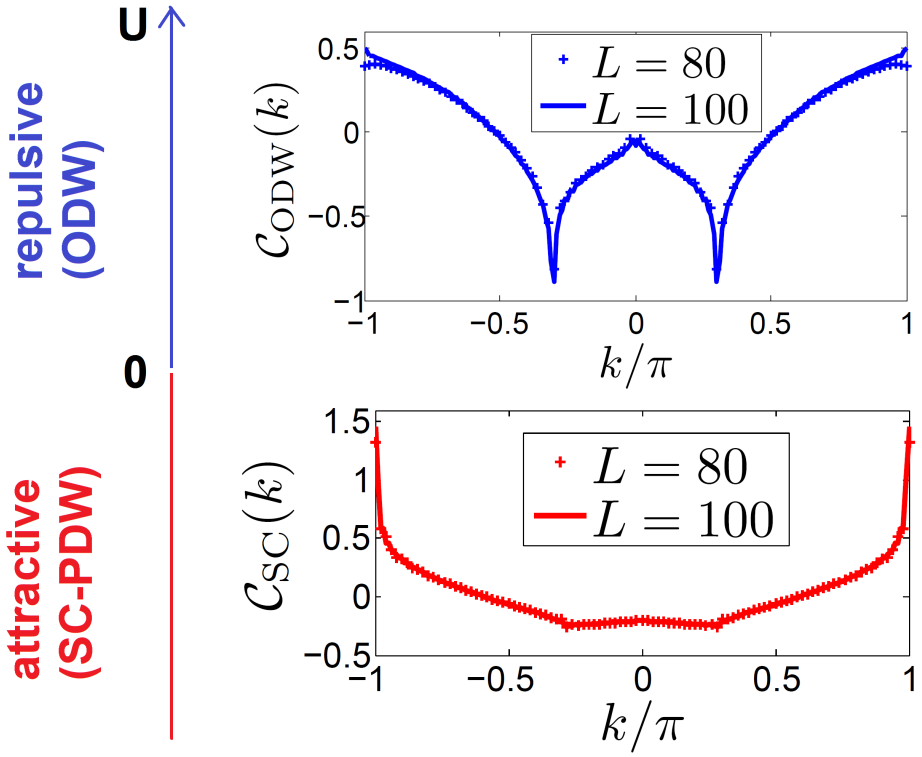

Figure 19: The phase diagram of the symmetric *sp*-orbital ladder with $t_s = t_p = 2t_{sp}$. $\mathcal{C}_{\rm ODW}(k)$ and $\mathcal{C}_{\rm SC}(k)$ show the Fourier transform of the orbital density wave and superconducting correlations, respectively. Numerical results with matrix product state methods [2] are calculated for the system at two different sizes $L = 80$ and 100 at filling $\frac{1}{L}\sum_j \langle a_s^\dagger(j)a_s(j) + a_p^\dagger(j)a_p(j)\rangle = 0.7$. In the upper (lower) graph, the interaction $U = 3t_s$ ($U = -3t_s$).

velocities [117, 118, 119, 120]. For simplicity, we do not consider such effects and set $g_4^{\nu\nu'} = 0$ here. The one-loop RG equations are given by [120],

$$\begin{aligned} \frac{dg_2^{\nu\nu'}}{dl} &= \frac{g_3^2}{2\pi}\left[\frac{\delta_{\bar{\nu}\nu'}}{v_+} - \frac{\delta_{\nu\nu'}}{v_{F\bar{\nu}}}\right], \\ \frac{dg_3}{dl} &= \frac{g_3}{2\pi}\sum_{\nu}\left[\frac{g_2^{\nu\bar{\nu}}}{v_+} - \frac{g_2^{\nu\nu}}{v_{F\nu}}\right], \end{aligned} \tag{6.10}$$

where l is the flow parameter ($l \to \infty$) and $\bar{\nu} = A$ (B) for $\nu = B$ (A). The RG flow of the Sine-Gordon term g_3 is obtained as

$$\begin{aligned} & \sqrt{|C|}/g_3(l) \\ = \; & F\left[-\mathrm{sgn}(g_3 Y)\sqrt{\frac{2|C|D}{\pi v_+}}l + F^{-1}[\frac{\sqrt{|C|}}{g_3(0)}]\right], \end{aligned} \tag{6.11}$$

with

$$C = \frac{2v_{FA}v_{FB}v_+^2}{v_{FA}v_{FB}+v_+^2}\left[\frac{{g_2}^{AB}}{v_+} - \frac{{g_2}^{AA}}{2v_{FA}} - \frac{{g_2}^{BB}}{2v_{FB}}\right]^2 - g_3^2, \tag{6.12}$$

$$D = \frac{v_{FA}v_{FB}+v_+^2}{\pi v_{FA}v_{FB}v_+}, \tag{6.13}$$

and

$$Y = \frac{{g_2}^{AB}}{v_+} - \frac{{g_2}^{AA}}{2v_{FA}} - \frac{{g_2}^{BB}}{2v_{FB}}. \tag{6.14}$$

The function F is the hyperbolic function "sinh" (the trigonometric function "sin") if $C > 0$ ($C < 0$). When $Y > 0$, g_3 always flows to ∞ and the system is in some gapped phase. When $Y < 0$, g_3 flows to ∞ only if $C < 0$. g_3 is irrelevant only if $C > 0$ and $Y < 0$. In the weak interacting regime, we have

$$Y/U = \frac{1}{v_+} - \frac{\sin^2(\theta_A)}{2v_{FA}} - \frac{\sin^2(\theta_B)}{2v_{FB}}. \tag{6.15}$$

We will consider the regime $Y/U > 0$ (this condition holds when t_{sp} is weak compared with $t_s + t_p$) in the following.

With repulsion ($U > 0$, $Y > 0$), g_3 is relevant and flows to $-\infty$ in RG flow. Then the dual orbital field ϑ_o is locked with $\cos(\sqrt{8\pi}\vartheta_o) = 1$ and its fluctuations ϑ_o are massive. The

key effect of orbital-charge mixing can be seen from its modification of the dynamics of the conjugate fields, given as

$$\Pi_{\theta_o} = \frac{K_o}{u_o}\partial_t\vartheta_o + \frac{K_o u_m}{K_m u_o}\partial_x\varphi_o, \tag{6.16}$$

$$\Pi_{\varphi_c} = \frac{1}{u_c K_c}\partial_t\varphi_c + \frac{K_m u_m}{K_c u_c}\partial_x\vartheta_o, \tag{6.17}$$

where Π_ϖ is the conjugate field of ϖ. The Lagrangian is constructed by

$$\mathcal{L}(x,t) = \Pi_{\vartheta_o}\partial_t\vartheta_o + \Pi_{\varphi_c}\partial_t\varphi_c - \mathcal{H}.$$

With massive fluctuations of ϑ_o integrated out, the Lagrangian of the charge field φ_c is given by

$$\mathcal{L}_c = \frac{1}{2\gamma}\left[\frac{1}{u}(\partial_t\varphi_c)^2 - u(\partial_x\varphi_c)^2\right] + O\left((\partial\varphi_c)^4\right), \tag{6.18}$$

with the renormalized Luttinger parameter and sound velocity given by

$$\gamma = \frac{K_c}{\sqrt{1-\frac{K_c K_o}{K_m^2}\frac{u_m^2}{u_c u_o}}}, \tag{6.19}$$

$$u = \sqrt{u_c^2 - u_m^2\frac{u_c K_c K_o}{u_o K_m^2}}. \tag{6.20}$$

To zeroth order in the interaction U, the renormalized Luttinger parameter is

$$\gamma = \left[1-\left(\frac{v_-}{v_+}\right)^2\right]^{-1/2}. \tag{6.21}$$

Our result reproduces the perturbative result [120] when the orbital-charge mixing term is small. The diverging susceptibilities are ODW and SC^+, and the corresponding correlation functions are given as

$$\langle O_{\mathrm{SC}^+}(x)O^\dagger_{\mathrm{SC}^+}(0)\rangle \propto x^{-1/\gamma}, \tag{6.22}$$

$$\langle O_{\mathrm{ODW}}(x)O^\dagger_{\mathrm{ODW}}(0)\rangle \propto e^{-i(k_{FA}-k_{FB})x}x^{-\gamma}. \tag{6.23}$$

With sufficiently weak repulsion $\gamma > 1$, the dominant order is SC^+, of which the pairing in terms of lattice operators is $\mathcal{O}_{\mathrm{SC}} = a_s(j)a_p(j)$. We emphasize here that this pairing does not oscillate in real space. Such a superconducting phase arises in the repulsive regime due to the

orbital-charge mixing and the pinning effect of the dual orbital field ϑ_o. The Sine-Gordon term g_3 causing this pinning effect is finite only when the coupling of sp-orbitals t_{sp} is finite, and g_3 is monotonically increasing when t_{sp} is increased. Thus the transition temperature of this repulsive superconducting phase can be increased by tuning t_{sp}, which makes this exotic superconducting phase potentially realizable in experiments. With stronger repulsion, the renormalized Luttinger parameter γ decreases. Eventually with repulsion larger than some critical strength, we have $\gamma < 1$, and the repulsive superconducting phase gives way to the ODW phase.

With attractive interaction, the condition $Y/U > 0$ gives $Y < 0$. Thus g_3 is relevant and flows to $+\infty$ when $C < 0$. The Sine-Gordon term $\cos(\sqrt{8\pi}\vartheta_o)$ is locked at -1, and the dominant order is superconducting SC^-, given by

$$\begin{aligned} O_{\mathrm{SC}^-} &= \psi_A\bar{\psi}_A - \psi_B\bar{\psi}_B \\ &\propto e^{-i\sqrt{2\pi}\vartheta_c}\sin(\sqrt{2\pi}\vartheta_o). \end{aligned} \tag{6.24}$$

In numerical simulations we find the SC^- phase competing with PDW in the strongly attractive regime. When g_3 is irrelevant ($C > 0$, $Y < 0$), the orbital ladder is in a two component Luttinger liquid phase exhibiting two gapless normal modes and each mode is a mixture of orbital and charge.

In experiments, radio-frequency spectroscopy can be used to probe spectra functions [121, 122], which exhibit the signatures of pairings of the predicted phases. In orbital density wave phases, where there are diverging correlations $\langle C_j^\dagger\sigma_y C_j C_{j'}^\dagger\sigma_y C_{j'}\rangle$, the quench dynamics of occupation numbers of s and p orbitals is a probe of such orders [123].

7.0 FINITE TEMPERATURE MELTING OF SUPERCONDUCTING STRIPES

The role of topological excitations of striped superconducting states has been intensively studied [40, 124, 125, 126, 127] since at finite temperature the proliferation of those defects can lead to possible exotic phases, such as the charge 4 superfluid [127, 128]. A typical striped superconducting state is the Fulde-Ferrell-Larkin-Ovchinnikov (FFLO) [129, 130] state which is believed to exist in heavy-fermion superconductor $CeCoIn_5$ [131, 132] and has been recently proposed to occur in the system involving p-orbital bands [64, 104]. Since the FFLO order is more likely to occur in the quasi-one-dimensional (1D) system [133], cold atom systems with two imbalanced species of atoms confined in a lattice array of 1D tubes formed by coherent laser beams [24] seems more promising to display the direct evidence. Since the inter-tube coupling can be tuned relatively with ease in cold atom systems by controlling the intensity of trapping lasers, it is suitable to study the dimensional crossover phenomena [134, 135, 136, 137].

Numerous exotic phases have been predicted from effective field theories [125], but the phase diagram of these exotic phases is not established for cold atom experiments yet. In cold atom experiments, the microscopic parameters (like interaction strength) are tunable and measurable, and this motivates our detailed study of the Kosterlitz-Thouless (KT) transitions of the Larkin-Ovchinnikov (LO) phase starting from a microscopic model. In this work we study a quasi-1D two-dimensional (2D) spinful fermionic system composed of coupled 1D tubes as illustrated in Fig. 20a where at zero temperature the LO order is the ground state. We determine the KT temperature of LO phase (the FFLO regime in Fig. 20b [133]) as a function of inter-tube coupling $t_\perp$ from a microscopic model. We found that over a wide range of parameters the fractional defect dominates the phase transition

and transition temperature is linear in $t_\perp$ for small $t_\perp$ (Fig. 21a). At zero temperature the transition from LO to normal phase, driven by the disappearance of the Fermi surface nesting upon increasing $t_\perp$, is of first order (Fig. 21b). Our method is efficient and can be used to determine the Goldstone excitations of any stripe order involving charge or spin degrees of freedom.

7.1 FREE ENERGY OF SUPERCONDUCTING STATES

The microscopic model we use is a one band model with attractive contact interaction in a quasi-1D system [133]. The Hamiltonian is

$$H = \sum_{\vec{k},\sigma_1\sigma_2} \xi_{\sigma_1\sigma_2}(\vec{k}) c^\dagger_{\sigma_1}(\vec{k}) c_{\sigma_2}(\vec{k}) + U \sum_{\vec{R}} \psi^\dagger_\uparrow(\vec{R})\psi^\dagger_\downarrow(\vec{R})\psi_\downarrow(\vec{R})\psi_\uparrow(\vec{R}), \tag{7.1}$$

where $\psi_\sigma(\vec{R})$ is a fermionic annihilation operator on site $\vec{R}$, and $c_\sigma(k)$ is its Fourier transformation

$$\psi_\sigma(\vec{R}) = \frac{1}{\sqrt{N_s}} \sum_{\vec{k}} c_\sigma(\vec{k}) e^{i\vec{k}\cdot\vec{R}},$$

with N_s the total number of lattice sites. Here we will derive a theory for general dispersion $\xi_{\sigma_1\sigma_2}(\vec{k})$, including spin-orbital coupling, spin imbalance, etc. The superconducting gap we consider here is

$$\Delta(\vec{R}) = U\langle\psi_\downarrow(\vec{R})\psi_\uparrow(\vec{R})\rangle. \tag{7.2}$$

With a mean field approximation, the Hamiltonian can be written as

$$\begin{aligned} H &\approx H_M \\ &= \sum_{\vec{k},\sigma_1\sigma_2} \xi_{\sigma_1\sigma_2}(\vec{k}) c^\dagger_{\sigma_1}(\vec{k}) c_{\sigma_2}(\vec{k}) + \sum_{\vec{R}} \left[\psi^\dagger_\uparrow(\vec{R})\psi^\dagger_\downarrow(\vec{R})\Delta(\vec{R}) + \Delta^*(\vec{R})\psi_\downarrow(\vec{R})\psi_\uparrow(\vec{R}) - \frac{|\Delta|^2}{U}\right] \\ &= \sum_{\vec{k},\sigma_1\sigma_2} \xi_{\sigma_1\sigma_2}(\vec{k}) c^\dagger_{\sigma_1}(\vec{k}) c_{\sigma_2}(\vec{k}) - N_s \sum_{\vec{k}} \frac{|\Delta(\vec{k})|^2}{U} \\ &+ \sum_{\vec{k}_1,\vec{k}_2} \left[c^\dagger_\uparrow(\vec{k}_1) c^\dagger_\downarrow(\vec{k}_2)\tilde{\Delta}(\vec{k}_1+\vec{k}_2) + c_\downarrow(\vec{k}_1) c_\uparrow(\vec{k}_2)\tilde{\Delta}^*(\vec{k}_1+\vec{k}_2)\right], \end{aligned} \tag{7.3}$$

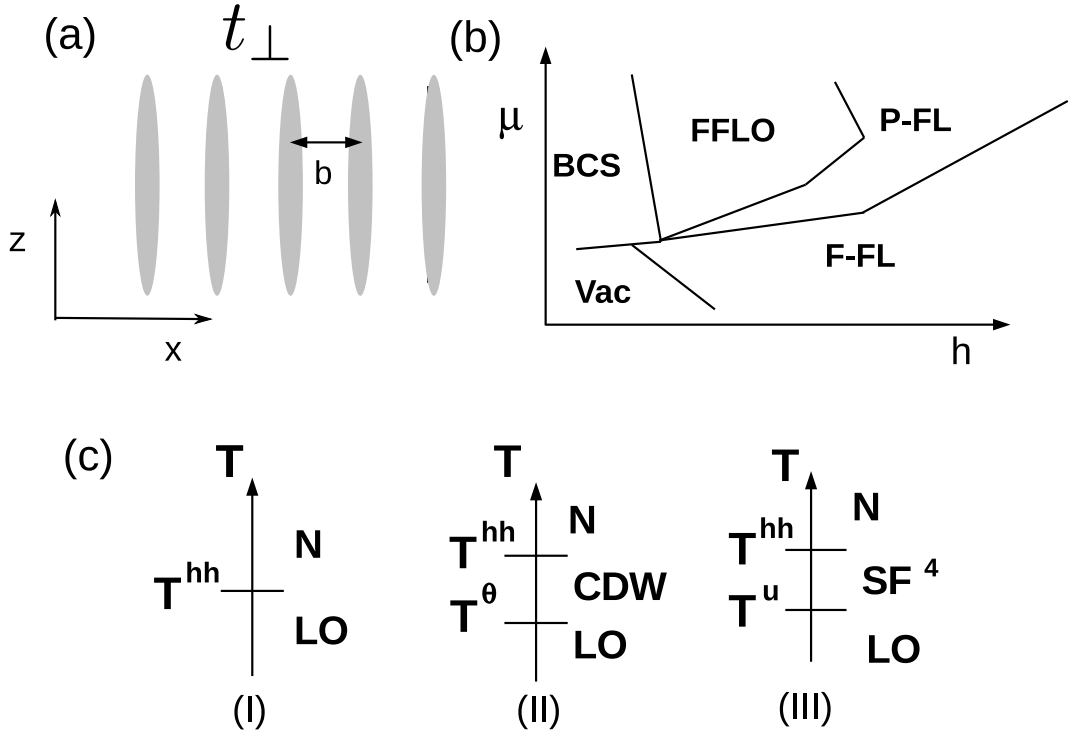

Figure 20: (a) Configuration of the system: arrays of 1D tubes with inter-tube distance b and inter-tube tunneling $t_\perp$. (b) A schematic plot of quasi-1D phase diagram as a function of μ and h. Vac: vacuum state (no particle); P-FL: partially polarized Fermi liquid; F-FL: fully polarized Fermi liquid. Our study here focuses on the FFLO regime. (c) Possible phases as a function of temperature. N:normal Fermi liquid; CDW: charge density wave; SF^4: charge 4 superfluid.

where $\tilde{\Delta}(\vec{k})$ is the Fourier transformation of $\Delta(\vec{R})$, given by

$$\Delta(\vec{R}) = \sum_{\vec{k}} \tilde{\Delta}(\vec{k}) e^{i\vec{k}\cdot\vec{R}}.$$

Introducing $\Psi(\vec{k}) = [c_\uparrow(\vec{k}), c_\downarrow(\vec{k}), c_\uparrow^\dagger(\vec{k}), c_\downarrow^\dagger(\vec{k})]^T$, the mean field Hamiltonian can written as

$$H_M = \frac{1}{2}\sum_{\vec{k}_1,\vec{k}_2} \Psi^\dagger(\vec{k}_1)\mathcal{H}_{\rm BdG}(\vec{k}_1,\vec{k}_2)\Psi(\vec{k}_2) + \frac{1}{2}\sum_{\vec{k}}\Big[\xi_{\uparrow\uparrow}(\vec{k}) + \xi_{\downarrow\downarrow}(\vec{k})\Big] - N_s\sum_{\vec{k}}\frac{|\Delta(\vec{k})|^2}{U}, \quad (7.4)$$

where the Bogoliubov-de Genne (BdG) Hamiltonian matrix $\mathcal{H}_{\rm BdG}$ is given by

$$\mathcal{H}_{\rm BdG}(\vec{k}_1,\vec{k}_2) = \begin{bmatrix} \delta_{\vec{k}_1\vec{k}_2}\xi_{\uparrow\uparrow}(\vec{k}_1) & \delta_{\vec{k}_1\vec{k}_2}\xi_{\uparrow\downarrow}(\vec{k}_1) & 0 & \tilde{\Delta}(\vec{k}_1+\vec{k}_2) \\ \delta_{\vec{k}_1\vec{k}_2}\xi_{\downarrow\uparrow}(\vec{k}_1) & \delta_{\vec{k}_1\vec{k}_2}\xi_{\downarrow\downarrow}(\vec{k}_1) & -\tilde{\Delta}(\vec{k}_1+\vec{k}_2) & 0 \\ 0 & -\tilde{\Delta}^*(\vec{k}_1+\vec{k}_2) & -\delta_{\vec{k}_1\vec{k}_2}\xi_{\uparrow\uparrow}(\vec{k}_1) & -\delta_{\vec{k}_1\vec{k}_2}\xi_{\downarrow\uparrow}(\vec{k}_1) \\ \tilde{\Delta}^*(\vec{k}_1+\vec{k}_2) & 0 & -\delta_{\vec{k}_1\vec{k}_2}\xi_{\uparrow\downarrow}(\vec{k}_1) & -\delta_{\vec{k}_1\vec{k}_2}\xi_{\downarrow\downarrow}(\vec{k}_1) \end{bmatrix}. \quad (7.5)$$

A key property of the BdG matrix is that

$$O\mathcal{H}_{\rm BdG}(\vec{k}_1,\vec{k}_2)O^{-1} = -\mathcal{H}^*_{\rm BdG}(\vec{k}_1,\vec{k}_2), \quad (7.6)$$

with

$$O = \begin{bmatrix} 0 & 0 & 1 & 0 \\ 0 & 0 & 0 & 1 \\ 1 & 0 & 0 & 0 \\ 0 & 1 & 0 & 0 \end{bmatrix}.$$

From this property it is apparent that eigenvalues of $\mathcal{H}_{\rm BdG}$ must show in $\pm$ pairs, i.e., if ϵ is its eigenvalue, so is $-\epsilon$. The eigenvalues (e_n) and eigenvectors $\lambda_j^{(n)}(\vec{k})$ of the BdG matrix are given by $\sum_{j',\vec{k}'}\mathcal{H}_{{\rm BdG}jj'}(\vec{k},\vec{k}')\lambda_{j'}^{(n)}(\vec{k}') = e_n\lambda_j^{(n)}(\vec{k})$. In the eigen basis, the mean field Hamiltonian reads as

$$H_M = \frac{1}{2}\sum_n e_n\Phi_n^\dagger\Phi_n + \frac{1}{2}\sum_{\vec{k}}\Big[\xi_{\uparrow\uparrow}(\vec{k}) + \xi_{\downarrow\downarrow}(\vec{k})\Big] - N_s\sum_{\vec{k}}\frac{|\Delta(\vec{k})|^2}{U}, \quad (7.7)$$

where $\Phi_n = \sum_{j,\vec{k}}\lambda_j^{(n)*}(\vec{k})\Psi_j(\vec{k})$. From the property in Eq. ((7.6)), it can be proved that the mean field Hamiltonian can be rewritten as

$$H_M = \sum_{e_n>0}\left[e_n\Phi_n^\dagger\Phi_n - \frac{1}{2}e_n\right] + \frac{1}{2}\sum_{\vec{k}}\Big[\xi_{\uparrow\uparrow}(\vec{k}) + \xi_{\downarrow\downarrow}(\vec{k})\Big] - N_s\sum_{\vec{k}}\frac{|\Delta(\vec{k})|^2}{U}. \quad (7.8)$$

The free energy defined by this mean field Hamiltonian is

$$\begin{aligned} F[\Delta] &= -T\sum_{e_n>0}\log\left[1+\exp(-e_n/T)\right]-\frac{1}{2}\sum_{e_n>0}e_n+\frac{1}{2}\sum_{\vec{k}}\left[\xi_{\uparrow\uparrow}(\vec{k})+\xi_{\downarrow\downarrow}(\vec{k})\right] \\ &- N_s\sum_{\vec{k}}\frac{|\Delta(\vec{k})|^2}{U}. \end{aligned} \tag{7.9}$$

Since the eigenvalues show in $\pm$ pairs, the free energy can be rewritten as

$$\begin{aligned} F[\Delta] &= -\frac{T}{2}\sum_{n}\log\left[1+\exp(-e_n/T)\right]+\frac{1}{2}\sum_{\vec{k}}\left[\xi_{\uparrow\uparrow}(\vec{k})+\xi_{\downarrow\downarrow}(\vec{k})\right] \\ &- N_s\sum_{\vec{k}}\frac{|\Delta(\vec{k})|^2}{U}. \end{aligned} \tag{7.10}$$

7.2 FLUCTUATIONS OF THE LO PHASE IN A COUPLED ARRAY OF TUBES

The Hamiltonian describing the LO phase in the coupled array of tubes (FIG. 20) is given by

$$H_M=\sum_{\vec{k},\sigma}E_\sigma(\vec{k})c^\dagger_\sigma(\vec{k})c_\sigma(\vec{k})+g_{1D}\sum_x\int dz\psi^\dagger_\uparrow(x,z)\psi^\dagger_\downarrow(x,z)\psi_\downarrow(x,z)\psi_\uparrow(x,z). \tag{7.11}$$

Here x labels different tubes and z is the one dimensional coordinate for each tube (FIG. 20). The dispersion of the system is given by

$$E_\sigma(\vec{k})=\frac{\hbar^2k_z^2}{2m}-2t_\perp\cos(k_x)-\mu+h(-)^\sigma,$$

where m is the mass of atoms loaded in the tubes, $t_\perp$ is the transverse tunneling, μ is the chemical potential and h is the effective Zeeman splitting. The general expression we have derived (Eq. (7.10)) applies on this particular system by replacing $N_s\sum_{\vec{k}}\frac{|\Delta(\vec{k})|^2}{U}$ by $L_zN_x\sum_{\vec{k}}\frac{|\Delta(\vec{k})|^2}{g_{1D}}$, with L_z the length of each tube and N_x number of tubes. We will use a one dimensional scattering length $a_{1D}=-\frac{2\hbar^2}{mg_{1D}}$ as the length unit, and the corresponding energy scale $\epsilon_B=\frac{\hbar^2}{ma_{1D}^2}$ as the energy unit. Taking $a_{1D}=100$nm, $m=6/(6\times10^{23})g$ (^{6}Li), as realizable in experiments [24], ϵ_B/k_B is approximately $1.5\times10^{-6}K$.

The order parameter for the LO phase is give by

$$\Delta(x,z) = g_{1D}\langle\psi_\downarrow(x,z)\psi_\uparrow(x,z)\rangle \sim \Delta_0 f(z), \tag{7.12}$$

where Δ_0 is the amplitude of the order parameter while $f(z)$ describes the stripe satisfying $f(z) = f(z+\frac{2\pi}{Q})$. The LO wave vector Q is set by mismatched fermi surfaces [129, 130, 133]. We first calculate the order parameter at zero temperature by the variational method where we assume a sinusoidal form $\Delta(x,z) = \Delta_0\cos(Qz)$, i.e., $f(z)$ in Eq. ((7.12)) is chosen to be $\cos Qz$.

Since the LO phase breaks both translational and $U(1)$ symmetries, it has two branches of Goldstone modes – the oscillation of the stripe, and the phase fluctuation of the amplitude [125, 126, 127]. Under these fluctuations, the order parameter becomes

$$\Delta(x,z) = \Delta_0 e^{i\theta(x,z)}\, f(z+u(x,z)) \tag{7.13}$$

where $u(x,z)$, $\theta(x,z)$ are generalized elastic fields [138] to describe the Goldstone modes. Physically u represents the small oscillation of the stripe LO order whereas θ the phase fluctuation of the amplitude. In the quasi-1D system, x and z directions are not equivalent. Therefore to the quadratic order the total free energy in terms of generalized elastic fields are described by two anisotropic XY models [139, 127]

$$\Delta F = \sum_x dz\left[\frac{A}{2}(Q\delta_x u)^2 + \frac{B}{2}(Qu_z)^2 + \frac{C}{2}(\delta_x\theta)^2 + \frac{D}{2}(\theta_z)^2\right] \tag{7.14}$$

where $\delta_x u = u(x+1,z) - u(x,z)$ and $\delta_x\theta = \theta(x+1,z) - \theta(x,z)$ describe fluctuations of u and θ on neighboring tubes. And u_z and θ_z are the continuous derivatives $\partial_z u$ and $\partial_z\theta$. In our notation, u and θ/Q have the dimension of length, their first derivatives are dimensionless, and coefficients A, B, C, D have the dimension of energy. For results presented here, we take $f(z) = \cos Qz$ which is $(e^{iQz} + e^{-iQz})/2$. In this case, these two Goldstone modes correspond to phase fluctuations of two Fulde-Ferrell (FF) order [129] $\Delta(x,z) = \Delta_0(e^{iQ(z+u^+)} + e^{-iQ(z+u^-)})/2$.

In 2D, each elastic field is associated with one topological defect. For u the defect is the (edge) dislocation satisfying $\oint\vec{\nabla}u\cdot d\vec{l} = Ln_d$; for θ the defect is the vortex satisfying $\oint\vec{\nabla}\theta\cdot d\vec{l} = 2\pi n_v$ with n_d, n_v integers. There is another topological defect referred to as a

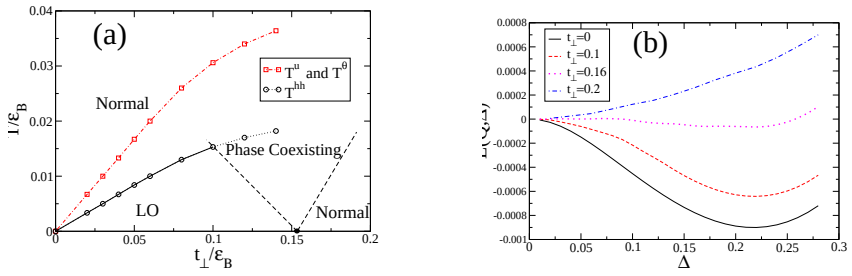

(a) (b)

Figure 21: (a) Phase diagram for $\mu = 2$, $h = 1.145$, $Q = 1.2$, $\Delta_0 = 0.22$. Curves with ligands are computed whereas two dashed lines embracing the phase coexisting region are schematic. The calculated transition temperature T^{hh} within the phase coexisting region is not well defined and its plot is switched to the dotted line with circles. (b) Energy as a function of gap amplitude Δ for $\mu = 2$, $h = 1.145$, $Q = 1.2$, $t_\perp = 0 - 0.2$. The energy minimum occurs at $\Delta = 0.22$ for $t_\perp < 0.15$.

half-vortex half-dislocation (HH) where $(n_d, n_v) = (\pm 1/2, \pm 1/2)$, which originates from the Z_2 symmetry of the order parameter [127, 126] – when circulating around an HH defect, each of the half vortex and the half dislocation introduces a minus sign leaving the order parameter unchanged. The proliferation of topological defects leads to Kosterlitz-Thouless (KT) transition. The KT transition temperature $T^u = \frac{\pi}{2}\sqrt{AB}$ for dislocations, $T^\theta = \frac{\pi}{2}\sqrt{CD}$ for vortices, and $T^{hh} = \frac{\pi}{8}(\sqrt{AB} + \sqrt{CD}) = (T^u + T^\theta)/4$ for HH [127]. The last temperature cannot be highest. When increasing the temperature, there are three distinct possibilities as illustrated in Fig. 20c: (I) T^{hh} is the lowest, (II) T^θ the lowest, and (III) T^u the lowest [127]. For (I) there is only one transition from LO to normal state at T^{hh}. For (II), the LO phase first becomes a charge density wave (CDW) state at T^θ and then normal at T^{hh}. For (III),the LO phase first becomes a charge 4 superfluid at T^u and then normal at T^{hh}.

7.3 CALCULATING STIFFNESS COEFFICIENTS FROM THE MICROSCOPIC MODEL

To obtain coefficients A, B, C, D in Eq. (7.14), we take the following approach. Take B as an example, we choose $u(x,z) = u_z z$, $\theta(x,z) = 0$, compute ΔF (Eq. (7.10)) for several u_z, and fit $\delta F(u_z) \equiv \Delta F(u_z)/(N_x L_z) = \frac{B}{2}(Qu_z)^2$. The same procedure apply to A, C, D. There is another approach to obtain these coefficients involving Green's function [140] which requires computing the inverse of a matrix and is very time-consuming. Our approach instead only involves the computation of eigenvalues [141] which allows us to include more k-points.

We use $\mu = 2$, $h = 1.145$, $t_\perp = 0.1$ as an example. Minimizing the energy functional with respect to Δ_0 and Q leads to $Q = 1.2$, $\Delta_0 = 0.22$. Fig. 22 shows $\delta F(\theta_z)$ for $\theta(x,z) = \theta_z z$ and $\delta F(\theta_x)$ for $\theta(x,z) = \theta_x x$ from which the quadratic fit leads to $C = 0.00168$ and $D = 0.23$. Fig. 23 shows $\delta F(Qu_z)$ for $u(x,z) = u_z z$ and $\delta F(Qu_x)$ for $\theta(x,z) = u_x x$ from which we can fit $A = 0.00168$ and $B = 0.234$. Note that $f(z)$ is taken to be $\cos Qz$ for the results presented here. However we emphasize that the coefficients A, B, C, D can be obtained for any given order parameters.

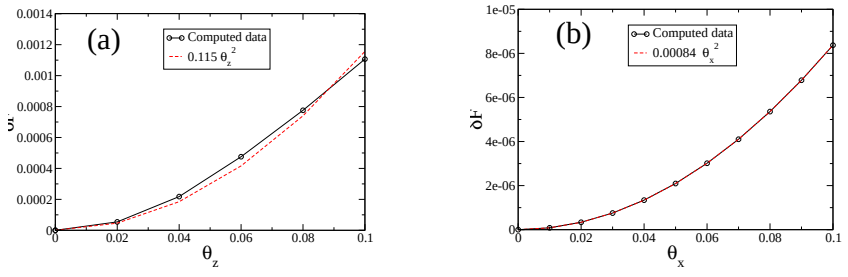

(a) (b)

Figure 22: Energy density as a function of θ_z and θ_x for $\mu = 2$, $h = 1.145$, $Q = 1.2$, $\Delta_0 = 0.22$. The energy cost is computed from Eq. 7.10

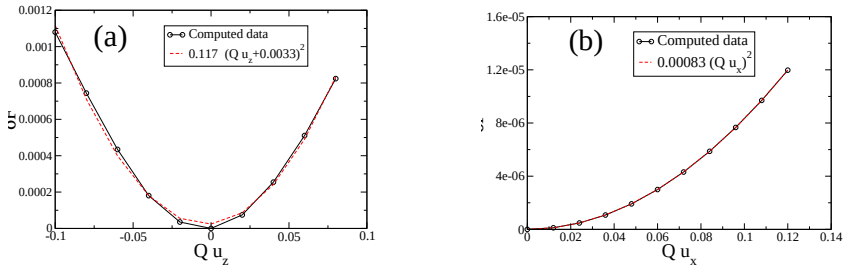

(a) (b)

Figure 23: Energy density as a function of u_z and u_x for $\mu = 2$, $h = 1.145$, $Q = 1.2$, $\Delta_0 = 0.22$. The energy cost is calculated from Eq. 7.10

7.4 PHASE TRANSITIONS OF LO STRIPES

We compute the coefficients for several $t_\perp$ and determine all three KT transition temperatures. Our main result is shown in Fig. 21a where the phase diagram as a function of T and $t_\perp$ is plotted for a representative set of parameters $\mu = 2$, $h = 1.145$, $Q = 1.2$, $\Delta_0 = 0.22$. When $t_\perp = 0$, there is no inter-tube coupling and no correlation along x leading to zero T^{KT}. As the system goes from pure 1D to quasi-1D, $T^{KT}(t_\perp) \propto t_\perp$. More specifically, we found the coefficients associated with z derivative, i.e. B and D, depend very weakly on $t_\perp$ whereas those with x derivative, i.e. A and C, depend quadratically on $t_\perp$. This explains the linear $t_\perp$ dependence of T^{KT} ($\propto \sqrt{AB}, \sqrt{CD}$). We found T^θ and T^u are very close because the "cosine" ansatz is very close to two *decoupled* FF order with opposite wave vector for small Δ_0 and it is the coupling between u^+ and u^- (the fluctuations of two FF orders) which lifts the degeneracy of u and θ fields. In this case the proliferation of half-vortex half-dislocation costs the least energy and the system only undergoes one transition from LO to normal at T^{hh} when raising the temperature, as shown in the case I of Fig. 20c. The transition temperature is of the order of 0.03 ϵ_B which is roughly 8×10^{-8}K for the system of ^{6}Li with $a_{1D} = 100$nm. One also notes that the obtained $T^{KT}(\sim 0.03)$ is an order of magnitude smaller than the mean field gap $\Delta_0(= 0.22)$, so the coefficients computed at $T = 0$ are almost

identical (less than 1% difference) to those computed at $T \sim T^{KT}$.

At $T = 0$, our simulation suggests the quantum phase transition from LO to normal phases upon increasing $t_\perp$ is of first order. Fig. 21b shows the energy as a function of Δ for $\mu = 2$, $h = 1.145$, $Q = 1.2$, $t_\perp \in (0, 0.2)$ where the minimum determines the value of Δ_0. We found that as $t_\perp$ increases Δ_0 stays around 0.22 and when $t_\perp > 0.16$ Δ_0 becomes zero. Around $t_\perp = 0.16$, the $E(\Delta)$ is essentially flat with several shallow minima. We note that the FFLO to normal transition as a function of temperature (fixed μ, and h) [131, 132] or h (fixed μ, T) [142] is also of first order. At finite temperature around the critical $t_\perp$, the system is in the phase coexisting region.

We have assumed a sinusoidal order parameter in the current calculation. However near BCS/LO transition (Fig. 20b) [143, 133], the order parameter behaves more domain-wall like [142, 144] than sinusoidal. Therefore the ansatz with sinusoidal order parameter does not capture all physics. Close to the BCS/LO transition, we expect that the stripe fluctuation should be stronger than the phase fluctuation ($A < C$, $B < D$) and a two-stage transition with charge 4 superfluid shown as the case III in Fig. 20c can happen. In a cold atom trap where the chemical potential is a position-dependent, the interface between phases shown in Fig. 20c is unavoidable and worth investigating.

7.5 CONCLUSION

To conclude, we have computed from a microscopic model the effective theories of Goldstone modes of the LO order for a quasi-1D fermionic system from which the Kosterlitz-Thouless transition temperatures are determined. The transition temperatures are found to depend linearly on the inter-tube coupling $t_\perp$. However, the method applied here neglects the quantum fluctuation along the 1D tubes which can modify this linear $t_\perp$ dependence, especially at $t_\perp \to 0$ [145]. As $t_\perp$ increases, the system goes to a phase coexisting regime sandwiched by the LO and normal phases. Our approach can generally determine the Goldstone excitations of any stripe order involving charge or spin from a microscopic model which should be useful for comparison between theories and experiments.

8.0 BOSE-EINSTEIN SUPERSOLID PHASE FOR MOMENTUM DEPENDENT INTERACTIONS

Since Penrose and Onsager's first discussion [146] on the potential existence of a "supersolid", namely a phase with co-existence of superfluid and crystalline order, both experimental [147] and theoretical [148, 149, 150, 151] attempts have been made for decades in the search of this novel phase. Recently reported observation of "supersolid" phase in He-4 systems [152, 153] revitalized this fundamental interest. Nevertheless, some subsequent experimental evidences as well as various proposed microscopic mechanisms [154] remain controversial.

Progress on the physics of cold atoms and molecules opens a new possibility to study the "supersolid" phase thanks to clean and controlled experimental systems. Engineering artificial interaction potentials using internal degrees of freedom of atoms and molecules [155, 156, 157] allows one to address a theoretical question, namely what interaction potentials can support the supersolid phase in continuous space. Recent experimental progress on dipolar quantum gases allows to explore new physics of quantum many body systems with non-local interactions [158, 159, 160, 161, 162]. It is well established that non-local interaction potentials stabilize the supersolid phase on lattice [163]. The possibility of finding a Bose-Einstein supersolid phase [164] was also put forward for several continuum model systems such as dipolar quantum gases [165, 166, 167, 168], atom-molecule mixture gases [169] and Rydberg atom gases [170, 157, 156]. Recently, Henkel *et al* [170] found that the Fourier transform of an isotropically repulsive van der Waals interaction potential with a "softened" core has a partial attraction in momentum space, which gives rise to a transition from a homogeneous Bose-Einstein condensate (BEC) to a supersolid phase due to roton instability. However, whether the supersolid phase they found is stable against fluctuations and how it should compare with the non-superfluid (normal) crystal phase has not been studied. Recent

work on dipolar gases [171] showed that the dipolar dominating interaction does not support a supersolid phase in the phase diagram between the uniform superfluid and the normal crystal phase, where this phase had been speculated to exist.

In our work [172], we show that interaction potentials, which display a minimum of negative value at a finite momentum, lead to a modulating superfluid order, namely a Bose-Einstein supersolid (BES) phase. We perform effective field theory analysis and variational calculation to determine not only the phase boundary between the uniform superfluid (USF) phase and BES, which has been previously analyzed by roton instability for dipolar [164, 165, 166, 167, 168] or van der Waals interaction [170], but also the phase boundary between BES and the normal (non-superfluid) insulating crystal (IC) phase. We shall begin with a heuristic argument to show how a stripe BES phase should arise from the competition between kinetic and interaction energy in the regime of roton instability. Next, we shall study as a concrete example the "softened" dipolar interaction recently proposed for Rydberg atomic gases [157]. A similar potential is also proposed in Ref. [170]. We will establish the ground state in the sense of variational principle and find a first order phase transition from the uniform superfluid phase to the triangular crystalline BES phase. Finally, we shall compare the energies of BES and IC phases of the same lattice configurations, and find a regime in which the triangular-lattice BES is stable and has lower energy than both USF and (normal) IC. The result is summarized in Fig. 24.

8.1 HAMILTONIAN AND ANALYSIS

To explore the physics of the BES phase, we start with the continuum Hamiltonian of two dimensional interacting bosons

$$\begin{aligned} H &= \int d^2\vec{r}\hat{\psi}^\dagger(\vec{r})\left[-\tfrac{\hbar^2}{2m}\nabla^2-\mu\right]\hat{\psi}(\vec{r}) \\ &+ \tfrac{1}{2}\int d^2\vec{r}_1 d^2\vec{r}_2\hat{\psi}^\dagger(\vec{r}_1)\hat{\psi}^\dagger(\vec{r}_2)V(\vec{r}_1-\vec{r}_2)\hat{\psi}(\vec{r}_2)\hat{\psi}(\vec{r}_1), \end{aligned} \tag{8.1}$$

where the first term of H corresponds to the kinetic energy, and the second the two-body interaction energy.

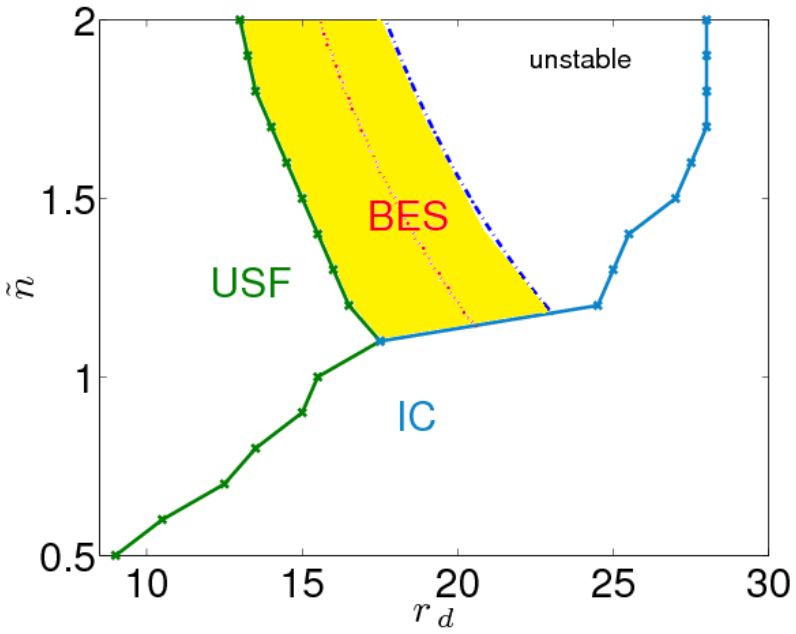

Figure 24: The phase diagram of bosons with step-like interaction. Uniform superfluid (USF), insulating crystal (IC), and Bose-Einstein supersolid (BES) phases are separated by 'solid lines' with "×" showing the data points from variational calculation. Analysis of the collective excitation spectrum shows the instability of USF at the 'red dotted line' and that of BES at the 'dark blue dash dotted line'. At low density, USF phase and IC phase exist; while at high density the new stable BES phase is found in the 'yellow shaded' regime. When $\tilde{n} \gtrsim 1$, the IC state is not stable (see text).

It is commonly accepted that the ground state for such a continuous bosonic system should be USF at the kinetic energy dominating regime. The USF phase is described by a coherent state $|\text{USF}\rangle = \exp(\int d^2x\sqrt{n}e^{i\phi_0}\hat{\psi}^\dagger(x))|\Omega\rangle$ where n is the mean particle density, ϕ_0 a constant phase, and $|\Omega\rangle$ the vacuum state with no particle. The energy of this state is given by $E_{\text{USF}} = \frac{N}{2}nU(\mathbf{k}=\mathbf{0})$, where N is the mean particle number and $U(\mathbf{k})$ is Fourier transform of the interaction potential. We first analyze the instability of the USF phase. This can be performed using an effective field theory approach [173, 174]. The real time action of this bosonic system is $S[\bar{\psi},\psi] = \int d^2x\,dt\left\{i\hbar\bar{\psi}\partial_t\psi - \mathscr{H}[\bar{\psi},\psi]\right\}$. Fluctuations on top of the uniform superfluid state are considered by writing the boson field $\psi(x,t) = [\rho_0+\delta\rho]^{1/2}e^{i\phi}$, assuming $\delta\rho$ and $|\nabla\phi|$ are small. The quasiparticle spectrum is readily derived after integrating out the $\delta\rho$ field: $\epsilon(\mathbf{k}) = \sqrt{\frac{\hbar^2\mathbf{k}^2}{2m}(\frac{\hbar^2\mathbf{k}^2}{2m}+2nU(\mathbf{k}))}$. For a potential that has a negative minimum at a finite momentum, this spectrum at that momentum drops, eventually hits zero and becomes imaginary when increasing the density n. This suggests that the assumed USF (coherent) state is unstable towards possible crystalline order.

To show the BES phase arises, we first give a heuristic argument by considering a simple stripe BES state $|\text{BES}\rangle = \exp\left(\sqrt{N}(\frac{\sqrt{2}}{2}b^\dagger_{\mathbf{Q}/2}+\frac{\sqrt{2}}{2}b^\dagger_{-\mathbf{Q}/2})\right)|\Omega\rangle$, where $\mathbf{Q}=[Q,0]$, and $\mathbf{Q}$ the minimum point of $U(\mathbf{k})$. The energy of this state is given by $E_{\text{sBES}} = N\left(\frac{\hbar^2Q^2}{8m}+\frac{1}{4}nU(\mathbf{Q})\right)+E_{\text{USF}}$. When the term $\frac{\hbar^2Q^2}{8m}+\frac{1}{4}nU(\mathbf{Q})$ is negative, namely the interaction energy dominates over the kinetic energy, the stripe BES state has lower energy than the USF state. (We also go beyond the mean field state and compare with the two component fragmented state $|f\rangle = \sum_{l=-N/2}^{l=N/2}\alpha_l\frac{(b^\dagger_{\mathbf{Q}/2})^{\frac{N}{2}+l}(b^\dagger_{-\mathbf{Q}/2})^{\frac{N}{2}-l}}{\sqrt{(\frac{N}{2}+l)!}\sqrt{(\frac{N}{2}-l)!}}|\Omega\rangle$, where $\{\alpha_l\}$ are variational parameters [175], and the coherent stripe BES state is found to have the lowest energy.) We thus conclude the BES state arises from the competition of kinetic energy and interaction energy.

To be concrete, we further apply the two-particle interaction of a step-like form $V(\vec{r}) = \frac{D}{r_0^3}$ if $r < r_0$; $V(r) = \frac{D}{r^3}$ otherwise. The form of this potential is an approximation to the interaction between polarized Rydberg atoms proposed in Ref. [157]. Two dimensionless parameters of this system are $\tilde{n} \equiv n \times r_0^2$ and $r_d \equiv \frac{2mDn^{1/2}}{\hbar^2}$. $\tilde{n}$ characterizes the relation between r_0 and the inter-particle distance, and r_d characterizes the strength of interaction. A phase transition from USF to IC has been found when varying r_d at the regime of $\tilde{n} \approx 0.9$ [171]. The IC (single particle per site) phase is described in a second quantization form

by $|\Psi_{\rm IC}\rangle = \prod_{\vec{R}_i} c^\dagger_{\vec{R}_i}|0\rangle$, where $\vec{R}_i$ is the direct lattice vector at site i, and the single particle wavefunction corresponding to $c^\dagger_{\vec{R}_i}$ is the Wannier function $\phi_{\vec{R}_i}(\vec{r})$.

The Fourier transform of this step-like interaction is shown in FIG. 2(a). It is straightforward to obtain the excitation spectrum, which is shown in FIG. 2(b). It can be seen that the spectrum displays instability. The origin of this effect is that the Fourier transform of the interaction, $U(\mathbf{k})$, has a negative minimum at a finite momentum. Now the question is to find the stable variational minimum in the coherent state space. With $|G\rangle = \exp(\int d^2\mathbf{x}\phi(\mathbf{x})\hat{\psi}^\dagger(\mathbf{x}))|\Omega\rangle$ (so that $\hat{\psi}(\mathbf{x})|G\rangle = \phi(\mathbf{x})|G\rangle$), the energy of this state is readily given by:

$$E = \int d\mathbf{r}\frac{\hbar^2}{2m}|\vec{\nabla}\phi|^2 + \tfrac{1}{2}\int d\mathbf{r}_1 d\mathbf{r}_2 V(\mathbf{r}_1-\mathbf{r}_2)|\phi(\mathbf{r}_1)|^2|\phi(\mathbf{r}_2)|^2\,, \tag{8.2}$$

where $V(\vec{r})$ is the interaction potential.

8.2 VARIATIONAL ANALYSIS

We first check whether the system favors an extended or localized state. This purpose is fulfilled by applying the Gaussian ansatz which means $\phi(\vec{r}) = \frac{\sqrt{N}}{\sqrt{\pi}\sigma}e^{-\frac{|\vec{r}|^2}{2\sigma^2}}$. The total energy of this system is given by $E_t = E_k + E_{dip}$, where the kinetic energy $E_k = N\frac{\hbar^2}{2m\sigma^2}$ and the interaction energy $E_{dip} = N^2\frac{1}{2\pi^2}\frac{D}{r_0^3}g(\frac{r_0}{\sigma})$. Here, $g(x)$ is approximately $\pi^2(1-e^{-2x^2})$. The energy per particle is $\frac{\hbar^2}{2m\sigma^2} + \frac{ND}{2\pi^2 r_0^3}g(\frac{r_0}{\sigma})$. In thermodynamic limit $N\to\infty$, interaction dominates and $E(\sigma) = \frac{ND}{2\pi^2 r_0^3}g(\frac{r_0}{\sigma})$. We found that as long as $\int d^2\vec{r}V(\vec{r}) > 0$, $\sigma\to\infty$ minimizes the energy, implying the system favors an extended state in space. Since for $r_d > 0$ $\int d^2\vec{r}V(\vec{r}) > 0$, we conclude that the system favors an extended state when r_d is positive.

Up to this point, we have learned that this system favors an extended state which is not necessarily a uniform superfluid. Having argued heuristically above that a momentum dependent interaction may favor a BES state, it is natural to compare the energy of a new, non-uniform coherent state which has discrete lattice symmetries. Thus, we can write the condensate wavefunction in such a form $\phi(\vec{r}) = \langle\psi(\vec{r})\rangle = \sqrt{n}\sum_{\mathbf{K}}\phi_{\mathbf{K}}e^{i\mathbf{K}\cdot\vec{r}}$ with $\mathbf{K} =$

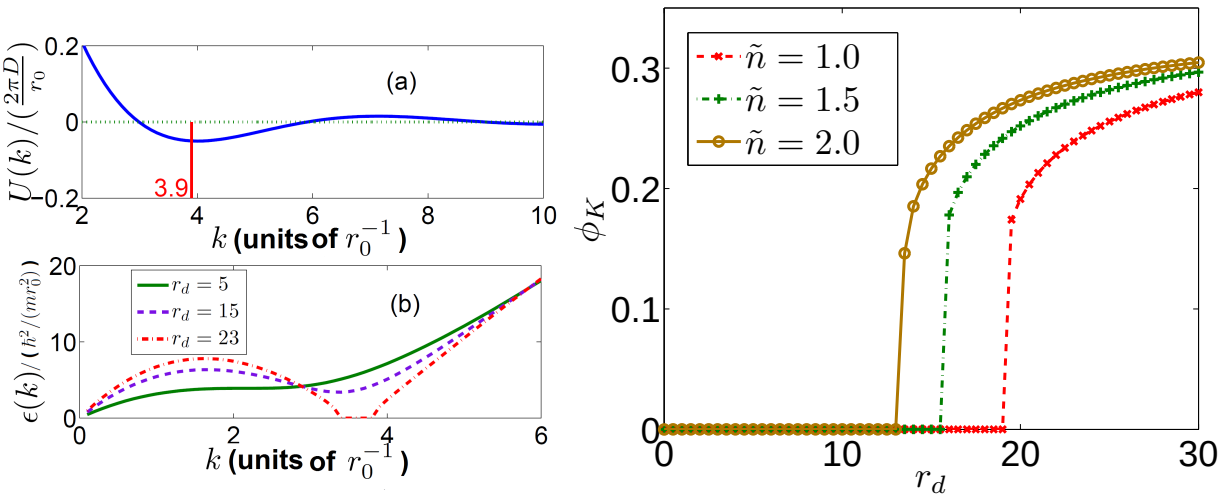

Figure 25: LEFT figure (a): Fourier transform of the step-like two-body interaction. LEFT figure (b): Shows the Bogoliubov quasiparticle spectrum for a USF state. The plot shows the real part of the spectrum with $\tilde{n} = 1$. The solid line corresponds $r_d = 5$, the dashed line to $r_d = 15$, and the dashed dotted line $r_d = 23$. RIGHT figure: Shows the phase transition from the USF to the triangular crystalline BES phase. $|\phi_{\mathbf{K}}|^2 \equiv \frac{1}{N}\langle b^\dagger_{\mathbf{K}} b_{\mathbf{K}}\rangle$ is the occupation fraction of the lowest finite momentum.

$p\mathbf{G}_1 + q\mathbf{G}_2$, where $\mathbf{G}_1$ and $\mathbf{G}_2$ are two primitive vectors spanning the two dimensional reciprocal lattice. The corresponding ground state is $|G\rangle = \exp\left(\sum_{\mathbf{K}} \sqrt{N}\phi_{\mathbf{K}} b^\dagger_{\mathbf{K}}\right)|\Omega\rangle$. The order parameter that characterizes the phase transition from USF to BES is an occupation fraction at some finite momentum K, $|\phi_{\mathbf{K}}|^2 = \frac{1}{N}\langle b^\dagger_{\mathbf{K}} b_{\mathbf{K}}\rangle$.

In this assumed ground state subspace, the energy per particle is given by

$$\begin{aligned} E &= \textstyle\sum_{\mathbf{K}} \frac{\hbar^2 K^2}{2m}\phi^*_{\mathbf{K}}\phi_{\mathbf{K}} \\ &\quad + \tfrac{n}{2}\textstyle\sum_{\mathbf{K}_1,\mathbf{K}_2,\mathbf{q}} U(\mathbf{q})\phi^*_{\mathbf{K}_1+\mathbf{q}}\phi^*_{\mathbf{K}_2-\mathbf{q}}\phi_{\mathbf{K}_2}\phi_{\mathbf{K}_1}\,. \end{aligned} \tag{8.3}$$

Now, the problem reduces to minimizing this energy functional with such a constraint $\sum_{\mathbf{K}} |\phi_{\mathbf{K}}|^2 = 1$, which is equivalent to the enforcement of conservation of the total particle number. By $\delta\left(E - \mu\sum_{\mathbf{K}}\phi^*_{\mathbf{K}}\phi_{\mathbf{K}}\right)/(\delta\phi^*_{\mathbf{K}}) = 0$, we obtain

$$\mu\phi_{\mathbf{K}} = \frac{\hbar^2 K^2}{2m}\phi_{\mathbf{K}} + n\sum_{\mathbf{K}',\mathbf{q}} V(\mathbf{q})\phi^*_{\mathbf{K}'+\mathbf{q}}\phi_{\mathbf{K}'}\phi_{\mathbf{K}+\mathbf{q}}\,, \tag{8.4}$$

where μ is the chemical potential.

We compute the energies for three different configurations — stripe, square and triangle lattices — and found that the triangular lattice is the most energetically favored. The optimal lattice constant a_{BES} is found to be slightly larger than $2\pi/Q_{\min}$ where $U(Q_{\min})$ corresponds to the negative minimum of the potential. For the particular step-like interaction, $Q_{\min}$ is related to r_0 by $Q_{\min} \approx \frac{3.9}{r_0} \sim \frac{\pi}{r_0}$. The transition between USF and BES is of first order as shown in FIG. 25.

8.3 VARIATIONALLY COMPARED WITH INSULATING CRYSTAL

The energy of the IC state is estimated to compare with the BES state. The IC state is described by $|\Psi_{\mathrm{IC}}\rangle = \prod_{\vec{R}_i} c^\dagger_{\vec{R}_i}|0\rangle$ where the single particle wavefunction corresponding to the creation operator $c^\dagger_{\vec{R}_i}$ is the Wannier function $\phi_{\vec{R}_i}(\vec{r})$. Here we consider the case where each localized wave function contains exactly one boson, forming a triangular lattice. The lattice constant a_c is thus determined by the density ($a_c = [2/(\sqrt{3}n)]^{1/2}$), which is different from

the lattice constant of BES, a_{BES}, determined by the minimum point of $U(\mathbf{k})$. The Wannier function is approximated by a localized Gaussian $\phi_{\vec{R}_i}(\vec{r}) \sim \frac{1}{\sqrt{\pi}\sigma} \exp(-\frac{(\vec{r}-\vec{R}_i)^2}{2\sigma^2})$ with σ/a_c ranging from 0 to 0.3 over which the overlap between neighboring Gaussian wavefunctions can be neglected [176] and the energy is obtained by $E_{\mathrm{IC}}(\sigma) = \langle \Psi_{\mathrm{IC}}|H|\Psi_{\mathrm{IC}}\rangle$. The calculation involves calculating an integral with Monte Carlo methods, which causes some noise of the phase boundary of the IC phase. When $\tilde{n} \gtrsim 1$, minimizing $E_{\mathrm{IC}}(\sigma)$ gives $\sigma/a_c \to 0.3$, indicating the IC state with the given lattice constant is unstable. We expect insulating crystals with more than one particle per site [177, 156] or insulating crystal-supersolid phase separation to exist in the 'unstable' regime.

In the phase diagram (FIG. 24), the BES is stable and is the most energy-favored in the 'yellow shaded' regime. The lower boundary is determined by comparing the energy of BES state and $E_{\mathrm{IC}}(\sigma = 0.3a_c)$ while the right boundary is computed from the instability of the BES spectrum. In the 'unstable' regime, the proposed BES state has lower energy than the IC state but is not stable against quantum fluctuations.

8.4 CONCLUSION

A bosonic system with two-body interaction potentials which display a negative minimum at a finite momentum is studied. We found a stable supersolid phase arising from BEC at finite momenta. The stability of this novel supersolid phase is checked against quantum fluctuations. A unique feature of the BES state is that it breaks both $U(1)$ and translational symmetry with a single order parameter, namely, the superfluid order parameter $\langle \psi(\vec{r})\rangle$ is not only finite but also spatially modulated. The physical interpretation is that particles are not localized in space but condensed to a single, common wavefunction which is modulated like a solid. This is conceptually different from one of widely considered supersolid pictures of He-4 [146, 153, 152] in which supersolidity is a mixture of two orderings: atoms form charge-density-wave order (a crystal structure) and in the same time vacancies or interstitials undergo usual (zero-momentum) BEC. For the conventional superfluid phase originated from zero-momentum BEC, there exists long range phase coherence but the phase correlation

function is homogeneous, not modulated, in space. In contrast, for the IC (insulating crystal) phase, particles are localized in space to each lattice site, so there is no long range phase coherence. Therefore, as prediction for cold gas experiments, a signature of the new BES phase is the modulated phase coherence. This new state also opens fundamental questions for future studies, for example, how the supercurrent is affected by the simultaneous presence of crystalline ordering, and topological configurations such as a vortex coupled to a crystal defect.

APPENDIX A

RENORMALIZATION GROUP FLOW OF THE SINE-GORDON MODEL

In this appendix, we will calculate the Renormalization group flow of the two-dimensional Sine-Gordon model by the Wilsonian momentum shell approach. The partition function defining the Sine-Gordon model is given by

$$Z = \int_{k<\Lambda} D\phi(k) \exp\left(- \int d^2\mathbf{x} \left[\frac{1}{2} (\vec{\nabla}\phi)^2 - g\cos(2\pi\sqrt{\beta}\phi) \right] \right), \tag{A.1}$$

where $k < \Lambda$ specifies the high-energy cut-off of this theory. We proceed by splitting the fast ($>$) and slow ($<$) modes as

$$\phi(\mathbf{x}) = \phi_>(\mathbf{x}) + \phi_<(\mathbf{x}), \tag{A.2}$$

with

$$\begin{aligned} \phi_>(\mathbf{x}) &= \int_{\frac{\Lambda}{s}<|\mathbf{k}|<\Lambda} \frac{d^2\mathbf{k}}{(2\pi)^2} \phi(\mathbf{k}) e^{i\mathbf{k}\cdot\mathbf{x}} \\ \phi_<(\mathbf{x}) &= \int_{|\mathbf{k}|<\frac{\Lambda}{s}} \frac{d^2\mathbf{k}}{(2\pi)^2} \phi(\mathbf{k}) e^{i\mathbf{k}\cdot\mathbf{x}}, \end{aligned} \tag{A.3}$$

where $s > 1$. The partition function can be rewritten as

$$Z = \int D\phi_< \exp\left\{ -\frac{1}{2} \int d^2\mathbf{x} (\vec{\nabla}\phi_<)^2 \right\} \times Z' \tag{A.4}$$

$$Z' = \int D\phi_> \exp\left\{ -\frac{1}{2} \int d^2\mathbf{x} (\vec{\nabla}\phi_>)^2 + g \int d^2\mathbf{x} \cos\left(2\pi\sqrt{\beta}(\phi_< + \phi_>) \right) \right\}. \tag{A.5}$$

With fast modes integrated out, the slow part receives corrections. To get the corrections we need to calculate $\log Z'$, which can be expressed in the following cumulant expansion

$$\begin{aligned}
\log Z' &= C_1 + \frac{1}{2}C_2 + O(g^3) && \text{(A.6)}\\
C_1 &= g\int d^2\mathbf{x}\left\langle \cos\left(2\pi\sqrt{\beta}(\phi_< + \phi_>)\right)\right\rangle_>^c && \text{(A.7)}\\
C_2 &= g^2\int d^2\mathbf{x}d^2\mathbf{y}\left\langle \cos\left(2\pi\sqrt{\beta}(\phi_<(\mathbf{x}) + \phi_>(\mathbf{x}))\right)\cos\left(2\pi\sqrt{\beta}(\phi_<(\mathbf{y}) + \phi_>(\mathbf{y}))\right)\right\rangle_>^c, && \text{(A.8)}
\end{aligned}$$

where the average $\langle\ldots\rangle_>$ is a Gaussian average

$$\langle\ldots\rangle_> = \frac{\int D\phi_> \ldots \exp\left\{-\frac{1}{2}\int d^2\mathbf{x}(\vec{\nabla}\phi_>)^2\right\}}{\int D\phi_> \exp\left\{-\frac{1}{2}\int d^2\mathbf{x}(\vec{\nabla}\phi_>)^2\right\}}.$$

The first order cumulant C_1 is obtained as

$$\begin{aligned}
C_1 &= \frac{1}{2}g\int d^2\mathbf{x}\langle e^{i2\pi\sqrt{\beta}(\phi_< + \phi_>)} + c.c.\rangle_>^c\\
&= ge^{-2\pi^2\beta G_>(0)}\int d^2\mathbf{x}\cos\left(2\pi\sqrt{\beta}\phi_<(\mathbf{x})\right), && \text{(A.9)}
\end{aligned}$$

where the propagator $G_>(\mathbf{x})$ is given by

$$\begin{aligned}
G_>(\mathbf{x}) &= \langle\phi_>(\mathbf{x})\phi_>(0)\rangle_> = \int_> \frac{d^2\mathbf{k}}{(2\pi)^2}\frac{e^{i\mathbf{k}\cdot\mathbf{x}}}{\mathbf{k}^2}\\
&= \int_{\Lambda/s}^{\Lambda}\frac{dp}{2\pi}\int_0^{2\pi}\frac{d\theta}{2\pi}\frac{e^{ip|\mathbf{x}|\cos(\theta)}}{p}\\
&= \frac{1-s^{-1}}{2\pi}J_0(\Lambda|\mathbf{x}|) && \text{(A.10)}
\end{aligned}$$

The second order cumulant C_2 is obtained as

$$\begin{aligned}
C_2 &= \frac{1}{4}g^2\int d^2\mathbf{x}d^2\mathbf{y}\langle\left[e^{i2\pi\sqrt{\beta}(\phi_<(\mathbf{x})+\phi_>(\mathbf{x}))} + c.c.\right]\left[e^{i2\pi\sqrt{\beta}(\phi_<(\mathbf{y})+\phi_>(\mathbf{y}))} + c.c.\right]\rangle_>^c\\
&= \frac{1}{2}g^2e^{-4\pi^2\beta G_>(0)}\int d^2\mathbf{x}d^2\mathbf{y}\left[e^{-4\pi^2\beta G_>(\mathbf{x}-\mathbf{y})} - 1\right]\\
&\quad\times\left[\cos\left(2\pi\sqrt{\beta}(\phi_<(\mathbf{x}) + \phi_<(\mathbf{y}))\right) + \cos\left(2\pi\sqrt{\beta}(\phi_<(\mathbf{x}) - \phi_<(\mathbf{y}))\right)\right]. && \text{(A.11)}
\end{aligned}$$

Since $G_>(\mathbf{x})$ is small for large distance, the integral $\int d^2\mathbf{x}d^2\mathbf{y}$ in C_2 is dominated by the short distance part with $|\mathbf{x}-\mathbf{y}|$ being small. We are thus allowed to do power expansions around $\mathbf{x}=\mathbf{y}$. In the coordinates ($\mathbf{R}=\frac{\mathbf{x}+\mathbf{y}}{2}, \mathbf{r}=\mathbf{x}-\mathbf{y}$), C_2 simplifies as

$$\begin{aligned} C_2 &\approx \frac{1}{2}g^2 e^{-4\pi^2\beta G_>(0)} \int d^2\mathbf{R}d^2\mathbf{r} \left[e^{-4\pi^2\beta G_>(\mathbf{r})}-1\right] \\ &\quad \times \left[\cos\left(4\pi\sqrt{\beta}\phi(\mathbf{R})\right) + 1 - 2\pi^2\beta(\mathbf{r}\cdot\vec{\nabla}_{\mathbf{R}}\phi_<(\mathbf{R}))^2\right]. \end{aligned} \tag{A.12}$$

The generated term $\cos\left(4\pi\sqrt{\beta}\phi\right)$ will be neglected for the reason that it is less relevant than $\cos\left(2\pi\sqrt{\beta}\phi\right)$. We thus have

$$\begin{aligned} C_2 &\to \frac{1}{2}g^2 e^{-4\pi^2\beta G_>(0)} \int d^2\mathbf{r}\left[e^{-4\pi^2\beta G_>(\mathbf{r})}-1\right]\int d^2\mathbf{R} \\ &- \pi^2 g^2\beta e^{-4\pi^2\beta G_>(0)} \int d^2\mathbf{r}\left[e^{-4\pi^2\beta G_>(\mathbf{r})}-1\right]\mathbf{r}^2 \times \int d^2\mathbf{R}\frac{1}{2}(\vec{\nabla}\phi_<)^2. \end{aligned} \tag{A.13}$$

We do not consider the renormalization group flow of free energy here, so we will neglect the constant terms in the cumulants.

Now Z' is given by

$$\begin{aligned} \log Z' &= g e^{-2\pi^2\beta G_>(0)} \int d^2\mathbf{x}\cos(2\pi\sqrt{\beta}\phi_<) \\ &+ \frac{1}{2}\pi^2 g^2\beta e^{-4\pi^2\beta G_>(0)} a_2 \int d^2\mathbf{R}[-\frac{1}{2}(\vec{\nabla}\phi_<)^2] + const, \end{aligned} \tag{A.14}$$

with

$$a_2 = \int d^2\mathbf{r}\left[e^{4\pi^2\beta G_>(\mathbf{r})}-1\right]\mathbf{r}^2.$$

The partition function Z is obtained as

$$\begin{aligned} Z \propto \int D\phi_<(\mathbf{R}) \exp \quad & \left[-\left(1+\frac{1}{2}\pi^2 g^2\beta a_2 e^{-4\pi^2\beta G_>(0)}\right)\int d^2\mathbf{R}\frac{1}{2}(\vec{\nabla}\phi_<)^2\right. \\ & \left. + g e^{-2\pi^2\beta G_>(0)}\int d^2\mathbf{R}\cos(2\pi\sqrt{\beta}\phi_<(\mathbf{R}))\right]. \end{aligned} \tag{A.15}$$

After the rescaling

$$\begin{aligned} \mathbf{x}' &= \mathbf{x}/s \\ \phi'(\mathbf{x}') &= \phi_<(\mathbf{x})\sqrt{1+\frac{1}{2}\pi^2 g^2\beta a_2 e^{-4\pi^2\beta G_>(0)}}, \end{aligned} \tag{A.16}$$

the renormalization group transformation is given by

$$g' = s^2 g e^{-2\pi^2 \beta G_>(0)} \tag{A.17}$$

$$\beta' = \frac{\beta}{1 + \frac{1}{2}\pi^2 g^2 \beta a_2 e^{-4\pi^2 G_>(0)}}. \tag{A.18}$$

With $s = e^{dl}$, the renormalization group flow is obtained as

$$\frac{dg}{dl} = g\left[2 - \pi\beta\right] \tag{A.19}$$

$$\frac{d\beta}{dl} = -2\pi^4 \beta^3 g^2 \alpha \Lambda^{-4}, \tag{A.20}$$

where $\alpha = \int_0^\infty x^3 J_0(x)$. It is clear that the renormalization group equations depend on the precise cutoff. Nonetheless the physical quantities are independent of the cutoff. A procedure of deriving renormalization group equations for an arbitrary cutoff can be found in Ref. [178].

APPENDIX B

XY MODEL AND ITS DUALITY TO SINE-GORDON MODEL

The partition function of the XY model on a square lattice is given by

$$Z = \prod_{\mathbf{R}} d\theta(\mathbf{R}) \exp\left\{-\beta \sum_{\mathbf{R}} [2 - \cos[\theta(\mathbf{R}) - \theta(\mathbf{R}+\hat{x})] - \cos[\theta(\mathbf{R}) - \theta(\mathbf{R}+\hat{y})]]\right\}. \quad \text{(B.1)}$$

Here $\mathbf{R}$ labels the lattice sites with primitive vectors $\hat{x}$ and $\hat{y}$. In this chapter we will a shorthand notation $\theta(\mathbf{R}+\hat{\mu}) - \theta(\mathbf{R}) \to \Delta_\mu\theta$, with $\hat{\mu} = \hat{x}$ or $\hat{y}$. Due to the difficulty of the cosine terms, this XY model cannot be analyzed elegantly. Instead we will show that the XY model is dual to the Sine-Gordon model at low temperature (β being large). For large β, we have the following Villain approximation [179]

$$\exp\{-\beta[1-\cos(\Delta\theta)]\} \approx (1/\sqrt{2\pi\beta}) \sum_{l=-\infty}^{+\infty} \exp[il\Delta\theta] \exp(-l^2/2\beta). \quad \text{(B.2)}$$

With this approximation, the partition function (Eq. (B.1)) can be rewritten as

$$Z \propto \prod_{\mathbf{R}'} d\theta(\mathbf{R}') \left(\prod_{\mathbf{R},\mu} \sum_{l_\mu(\mathbf{R})=-\infty}^{\infty} \exp(il_\mu\Delta_\mu\theta) \exp\left(-l_\mu^2(\mathbf{R})/2\beta\right) \right). \quad \text{(B.3)}$$

The introduced variables $l_\mu(\mathbf{R})$ is a two component integer-valued vector field. The integrals over $\theta(\mathbf{R})$ can be carried out and we get a resulting constraint

$$\Delta_\mu l_\mu(\mathbf{R}) = 0. \quad \text{(B.4)}$$

The constraint can be elegantly solved by the parametrization

$$l_\mu(\mathbf{R}) = \varepsilon_{\mu\nu}\Delta_\nu n(\mathbf{R}), \tag{B.5}$$

where n is an inter-valued scalar field, and $\varepsilon_{\mu\nu}$ is defined by $\varepsilon_{xx} = \varepsilon_{yy} = 0$ and $\varepsilon_{xy} = -\varepsilon_{yx} = 1$. Now, the partition function becomes

$$Z \propto \sum_{n(\mathbf{R})=-\infty}^{\infty} \exp\left\{-(1/2\beta)\sum_{\mathbf{R},\mu}[\Delta_\mu n(\mathbf{R})]^2\right\}. \tag{B.6}$$

With the Poisson summation formula

$$\sum_n g(n) = \sum_{m=-\infty}^{\infty}\int_{-\infty}^{\infty} d\phi g(\phi)e^{2\pi i m\phi},$$

we have

$$Z \propto \int\prod_{\mathbf{R}} d\phi(\mathbf{R}) \sum_{m(\mathbf{R})=-\infty}^{\infty} \exp\left\{-\frac{1}{2\beta}\sum_{\mathbf{R},\mu}(\Delta_\mu\phi)^2 + 2\pi i\sum_{\mathbf{R}} m(\mathbf{R})\phi(\mathbf{R})\right\} \tag{B.7}$$

Integration of fast modes of $\phi(\mathbf{R})$ generates a chemical potential term $\log y\sum_{\mathbf{R}} m^2(\mathbf{R})$, which should be incorporated in the partition function. Thus we have

$$Z \Rightarrow \int\prod_{\mathbf{R}} d\phi(\mathbf{R}) \sum_{m(\mathbf{R})=-\infty}^{\infty} \exp\left\{-\frac{1}{2\beta}\sum_{\mathbf{R},\mu}(\Delta_\mu\phi)^2 + \log y\sum_{\mathbf{R}} m^2(\mathbf{R}) + 2\pi i\sum_{\mathbf{R}} m(\mathbf{R})\phi(\mathbf{R})\right\} \tag{B.8}$$

Assuming that $y \ll 1$, we only need to keep $m(\mathbf{R}) = 0, \pm 1$ in the summation over $m(\mathbf{R})$. Summing over $m(\mathbf{R}) = 0, \pm 1$, we get

$$Z \Rightarrow \int\prod_{\mathbf{R}} d\phi(\mathbf{R}) \exp\left\{-\frac{1}{2\beta}\sum_{\mathbf{R},\mu}(\Delta_\mu\phi)^2 + 2y\cos(2\pi\phi(\mathbf{R}))\right\}, \tag{B.9}$$

which is identical to the partition function of the Sine-Gordon model. Thus the renormalization group flow and critical behavior of XY model can be read off from the Sine-Gordon model.

APPENDIX C

N-BODY WAVEFUNCTION AND FEYNMAN'S 'NO-NODE' THEOREM

The 'no-node' theorem states that the many body wavefunction of a non-relativistic N-boson system has no nodes. This can be easily proved by ODE (ordinary differential equation) theorem.

Suppose we have a quantum many body system described by a Hamiltonian

$$H = \sum_i \left(-\frac{\hbar^2}{2m} \vec{\nabla}_i^2 + V(\mathbf{r}_i) \right) + \frac{1}{2} \sum_{i \neq j} u(\mathbf{r}_i - \mathbf{r}_j), \tag{C.1}$$

the wavefunction $\Psi(\mathbf{r}_1, \ldots, \mathbf{r}_N)$ of an eigenstate is defined by

$$H\Psi(\mathbf{r}_1, \ldots, \mathbf{r}_N) = E\Psi. \tag{C.2}$$

Let us assume the ground state wavefunction $\Psi_0(\mathbf{r}_1, \ldots, \mathbf{r}_N)$ has a nodal surface S. Then Ψ_0 minimizes the energy functional $(\Psi, H\Psi)$. It can be verified that $|\Psi_0|$ has the same energy, and thus $|\Psi_0|$ also minimizes $(\Psi, H\Psi)$. With the variational principle $|\Psi_0|$ also satisfies Eq. C.2. Further because the potential $V(\mathbf{r})$ and the interaction $u(\mathbf{r} - \mathbf{r}')$ are finite, the second derivatives of $|\Psi_0|$ are finite, which implies the first derivatives of $|\Psi_0|$ are continuous. We know the first derivative (along the normal direction of the nodal surface S) of $|\Psi_0|$ switch sign across S. So this first derivative vanishes. All other derivatives are within the nodal surface and thus vanish trivially. Now we know all first derivatives and the value of $|\Psi_0|$ vanish on the nodal surface. The ODE theorem tells us $|\Psi_0|$ vanishes in the whole space. Thus the assumption that Ψ_0 has a nodal surface breaks down.

This 'no-node' property of the groundstate wavefunction Ψ_0 also implies the ground state of a N-body quantum system is unique. Thus Ψ_0 respects all symmetries (including the permutation symmetry $\mathbf{r}_i \to \mathbf{r}_j$) of the Hamiltonian. Actually this means the wavefunction minimizing $(\Psi, H\Psi)$ describe bosons. The 'no-node' theorem is now proved.

Although this theorem is rigorously proved, what the theorem implies in the thermodynamic limit is uncertain. It was expected this theorem implies the condensate wavefunction of the superfluid phase is essentially real (up to a global phase) [12]. However the recent observation of chiral symmetry breaking in a superfluid phase [16] suggests this expectation might not be correct. The question what 'no-node' theorem implies in the thermodynamic limit is open, to the author's best knowledge.

BIBLIOGRAPHY

[1] W. Vincent Liu and Congjun Wu. Atomic matter of nonzero-momentum bose-einstein condensation and orbital current order. *Phys. Rev. A*, 74(1):013607, Jul 2006.

[2] Ulrich Schollwök. The density-matrix renormalization group in the age of matrix product states. *Annals of Physics*, 326(1):96 – 192, 2011. January 2011 Special Issue.

[3] Immanuel Bloch. Ultracold quantum gases in optical lattices. *Nature Physics*, 1:23–30, 2005.

[4] Maciej Lewenstein, Anna Sanpera, Veronica Ahufinger, Bogdan Damski, Aditi Sen, and Sen Ujjwal. Ultracold atomic gases in optical lattices: mimicking condensed matter physics and beyond. *Advances in Physics*, 56(2):243–379, 2007.

[5] Immanuel Bloch, Jean Dalibard, and Wilhelm Zwerger. Many-body physics with ultracold gases. *Rev. Mod. Phys.*, 80(3):885–964, Jul 2008.

[6] Feshbach Herman. Unified theory of nuclear reactions. *Annals of Physics*, 5:357, Dec 1958.

[7] Ian Spielman. An optical lattice of flux. *Physics*, 4:35, Apr 2011.

[8] D. Jaksch *et al.* Cold bosonic atoms in optical lattices. *Phys. Rev. Lett.*, 81(15):3108–3111, Oct 1998.

[9] Markus Greiner *et al.* Quantum phase transition from a superfluid to a mott insulator in a gas of ultracold atoms. *Nature*, 415:39, January 2002.

[10] I. B. Spielman, W. D. Phillips, and J. V. Porto. Condensate fraction in a 2d bose gas measured across the mott-insulator transition. *Phys. Rev. Lett.*, 100(12):120402, Mar 2008.

[11] Nathan Gemelke *et al.* In situ observation of incompressible mott-insulating domains in ultracold atomic gases. *Nature*, 460:995–998, August 2009.

[12] Congjun Wu. Unconventional bose-einstein condensations beyond the "no node" theorem. *Mod. Phys. Lett. B*, 23:1, 2009.

[13] Maciej Lewenstein and W. Vincent Liu. Optical lattices: Orbital dance. *Nature Physics*, 7:101, Feb 2011.

[14] Georg Wirth, Matthias Ölschläger, and Andreas Hemmerich. Evidence for orbital superfluidity in the p-band of bipartite optical square lattice. *Nature Physics*, 7:147, Dec 2011.

[15] Matthias Ölschläger, Georg Wirth, and Andreas Hemmerich. Unconventional superfluid order in the f band of a bipartite optical square lattice. *Phys. Rev. Lett.*, 106(1):015302, Jan 2011.

[16] Parvis Soltan-Panahi *et al.* Quantum phase transition to unconventional multi-orbital superfluidity in optical lattices. arXiv:1104.3456, Apr 2011.

[17] Xiaopeng Li, Erhai Zhao, and W. Vincent Liu. Effective action approach to the p-band mott insulator and superfluid transition. *Phys. Rev. A*, 83:063626, Jun 2011.

[18] Xiaopeng Li, Zixu Zhang, and W. Vincent Liu. Time-reversal symmetry breaking of p-orbital bosons in a one-dimensional optical lattice. *Phys. Rev. Lett.*, 108:175302, Apr 2012.

[19] X. Li and W. V. Liu. Orbital phases of fermions in an asymmetric optical ladder. *ArXiv e-prints*, October 2012.

[20] Chungwei Lin, Xiaopeng Li, and W. Vincent Liu. U(1) $\times$ u(1) to Z_2 kosterlitz-thouless transition of the larkin-ovchinnikov phase in an anisotropic two-dimensional system. *Phys. Rev. B*, 83:092501, Mar 2011.

[21] Michael Köhl, Henning Moritz, Thilo Stöferle, Kenneth Günter, and Tilman Esslinger. Fermionic atoms in a three dimensional optical lattice: Observing fermi surfaces, dynamics, and interactions. *Phys. Rev. Lett.*, 94:080403, Mar 2005.

[22] Martin W. Zwierlein, Andr Schirotzek, Christian H. Schunck, and Wolfgang Ketterle. Fermionic superfluidity with imbalanced spin populations. *Science*, 311(5760):492–496, 2006.

[23] Guthrie B. Partridge, Wenhui Li, Ramsey I. Kamar, Yean-an Liao, and Randall G. Hulet. Pairing and phase separation in a polarized fermi gas. *Science*, 311(5760):503–505, 2006.

[24] Yean-an Liao, Ann Sophie C. Rittner, Tobias Paprotta, Wenhui Li, Guthrie B. Partridge, Randall G. Hulet, Stefan K. Baur, and Erich J. Mueller. Spin-imbalance in a one-dimensional fermi gas. *Nature*, 467:567, Sep 2010.

[25] Adriana Moreo and D. J. Scalapino. Cold attractive spin polarized fermi lattice gases and the doped positive u hubbard model. *Phys. Rev. Lett.*, 98:216402, May 2007.

[26] Subir Sachdev. The landscape of the hubbard model. arXiv:1012.0299v5, Dec 2010.

[27] X. Li, E. Zhao, and W. V. Liu. Topological states in a ladder-like optical lattice containing ultracold atoms in higher orbital bands. *Nature Communications*, 4, Feb 2013.

[28] Matthew P. A. Fisher *et al.* Boson localization and the superfluid-insulator transition. *Phys. Rev. B*, 40(1):546–570, Jul 1989.

[29] A. Browaeys *et al.* Transport of atoms in a quantum conveyor belt. *Phys. Rev. A*, 72(5):053605, Nov 2005.

[30] Torben Müller *et al.* State preparation and dynamics of ultracold atoms in higher lattice orbitals. *Phys. Rev. Lett.*, 99(20):200405, Nov 2007.

[31] A. Isacsson and S. M. Girvin. Multiflavor bosonic hubbard models in the first excited bloch band of an optical lattice. *Phys. Rev. A*, 72(5):053604, Nov 2005.

[32] A. B. Kuklov. Unconventional strongly interacting bose-einstein condensates in optical lattices. *Phys. Rev. Lett.*, 97(11):110405, Sep 2006.

[33] Lih-King Lim, C. Morais Smith, and Andreas Hemmerich. Staggered-vortex superfluid of ultracold bosons in an optical lattice. *Phys. Rev. Lett.*, 100(13):130402, Apr 2008.

[34] A. Collin, J. Larson, and J. P. Martikainen. Quantum states of p-band bosons in optical lattices. *Phys. Rev. A*, 81(2):023605, Feb 2010.

[35] K. Sengupta and N. Dupuis. Mott-insulator–to–superfluid transition in the bose-hubbard model: A strong-coupling approach. *Phys. Rev. A*, 71(3):033629, Mar 2005.

[36] Alexander Hoffmann and Axel Pelster. Visibility of cold atomic gases in optical lattices for finite temperatures. *Phys. Rev. A*, 79(5):053623, May 2009.

[37] J. K. Freericks, H. R. Krishnamurthy, Yasuyuki Kato, Naoki Kawashima, and Nandini Trivedi. Strong-coupling expansion for the momentum distribution of the bose-hubbard model with benchmarking against exact numerical results. *Phys. Rev. A*, 79(5):053631, May 2009.

[38] R. Shankar. Renormalization-group approach to interacting fermions. *Rev. Mod. Phys.*, 66:129–192, Jan 1994.

[39] D. van Oosten, P. van der Straten, and H. T. C. Stoof. Quantum phases in an optical lattice. *Phys. Rev. A*, 63(5):053601, Apr 2001.

[40] J. M. Kosterlitz and D.J. Thouless. Ordering, metastability and phase transitions in two-dimensional systems. *J. Phys. C*, 6:1181–1203, 1973.

[41] Lars Onsager. Crystal statistics. i. a two-dimensional model with an order-disorder transition. *Phys. Rev.*, 65(3-4):117–149, Feb 1944.

[42] Vladimir M. Stojanović *et al.* Incommensurate superfluidity of bosons in a double-well optical lattice. *Phys. Rev. Lett.*, 101(12):125301, Sep 2008.

[43] Qi Zhou, J. V. Porto, and S. Das Sarma. Interaction-induced excited-band condensate in a double-well optical lattice. *Phys. Rev. A*, 84:031607, Sep 2011.

[44] Zi Cai and Congjun Wu. Complex and real unconventional bose-einstein condensations in high orbital bands. *Phys. Rev. A*, 84:033635, Sep 2011.

[45] Zi Cai, Lu-Ming Duan, and Congjun Wu. Phase-sensitive detection for unconventional bose-einstein condensations. arXiv:1110.3021, Oct 2011.

[46] Belén Paredes *et al.* Tonks-girardeau gas of ultracold atoms in an optical lattice. *Nature*, 429:277, May 2004.

[47] U. Schollwöck. The density-matrix renormalization group. *Rev. Mod. Phys.*, 77(1):259–315, Apr 2005.

[48] Steven R. White. Density matrix renormalization group algorithms with a single center site. *Phys. Rev. B*, 72(18):180403, Nov 2005.

[49] Steven R. White. Density matrix formulation for quantum renormalization groups. *Phys. Rev. Lett.*, 69(19):2863–2866, Nov 1992.

[50] T. D. Kühner and H. Monien. Phases of the one-dimensional bose-hubbard model. *Phys. Rev. B*, 58(22):R14741–R14744, Dec 1998.

[51] Till D. Kühner, Steven R. White, and H. Monien. One-dimensional bose-hubbard model with nearest-neighbor interaction. *Phys. Rev. B*, 61(18):12474–12489, May 2000.

[52] T. Giamarchi and H. J. Schulz. Anderson localization and interactions in one-dimensional metals. *Phys. Rev. B*, 37(1):325–340, Jan 1988.

[53] F. D. M. Haldane. Effective harmonic-fluid approach to low-energy properties of one-dimensional quantum fluids. *Phys. Rev. Lett.*, 47(25):1840–1843, Dec 1981.

[54] Thierry Giamarchi. *Quantum Physics in One Dimension.* Oxford, Oxford, 2003.

[55] Simon Fölling *et al.* Spatial quantum noise interferometry in expanding ultracold atom clouds. *Nature*, 434:481, March 2005.

[56] Immanuel Bloch. Quantum coherence and entanglement with ultracold atoms in optical lattices. *Nature*, 453:1016–1022, June 2008.

[57] Maciej Lewenstein, Anna Sanpera, and Verònica Ahufinger. *Ultracold atoms in optical lattices: Simulating Quantum Many-body systems.* Oxford University Press, Oxford, 2012.

[58] J. Sebby-Strabley, M. Anderlini, P. S. Jessen, and J. V. Porto. Lattice of double wells for manipulating pairs of cold atoms. *Phys. Rev. A*, 73:033605, Mar 2006.

[59] Marco Anderlini, Patricia J. Lee, Benjamin L. Brown, Jennifer Sebby-Strabley, William D. Phillips, and J. V. Porto. Controlled exchange interaction between pairs of neutral atoms in an optical lattice. *Nature*, 448:452–456, Jul 2007.

[60] S. Trotzky, P. Cheinet, S. Fölling, M. Feld, U. Schnorrberger, A. M. Rey, A. Polkovnikov, E. A. Demler, M. D. Lukin, and I. Bloch. Time-resolved observation and control of superexchange interactions with ultracold atoms in optical lattices. *Science*, 319(5861):295–299, 2008.

[61] P. Soltan-Panahi, J. Struck, P. Hauke, A. Bick, W. Plenkers, G. Meineke, C. Becker, P. Windpassinger, M. Lewenstein, and K. Sengstock. Multi-component quantum gases in spin-dependent hexagonal lattices. *Nat Phys*, 7:434–440, May 2011.

[62] Gyu-Boong Jo, Jennie Guzman, Claire K. Thomas, Pavan Hosur, Ashvin Vishwanath, and Dan M. Stamper-Kurn. Ultracold atoms in a tunable optical kagome lattice. *Phys. Rev. Lett.*, 108:045305, Jan 2012.

[63] Leticia Tarruell, Daniel Greif, Thomas Uehlinger, Gregor Jotzu, and Tilman Esslinger. Creating, moving and merging dirac points with a fermi gas in a tunable honeycomb lattice. *Nature*, 483(7389):302–305, 2012.

[64] Zixu Zhang *et al.* Modulated pair condensate of p-orbital ultracold fermions. *Phys. Rev. A*, 82(3):033610, Sep 2010.

[65] Qi Zhou, J. V. Porto, and S. Das Sarma. Condensates induced by interband coupling in a double-well lattice. *Phys. Rev. B*, 83:195106, May 2011.

[66] Kai Sun, W. Vincent Liu, Andreas Hemmerich, and S. Das Sarma. Topological semimetal in a fermionic optical lattice. *Nature Phys.*, 8(1):67–70, 2012.

[67] M. Popp, B. Paredes, and J. I. Cirac. Adiabatic path to fractional quantum hall states of a few bosonic atoms. *Phys. Rev. A*, 70:053612, Nov 2004.

[68] Congjun Wu. Orbital analogue of the quantum anomalous hall effect in p-band systems. *Phys. Rev. Lett.*, 101:186807, Oct 2008.

[69] N. Goldman, I. Satija, P. Nikolic, A. Bermudez, M. A. Martin-Delgado, M. Lewenstein, and I. B. Spielman. Realistic time-reversal invariant topological insulators with neutral atoms. *Phys. Rev. Lett.*, 105:255302, Dec 2010.

[70] Masatoshi Sato, Yoshiro Takahashi, and Satoshi Fujimoto. Non-abelian topological order in s-wave superfluids of ultracold fermionic atoms. *Phys. Rev. Lett.*, 103:020401, Jul 2009.

[71] Liang Jiang, Takuya Kitagawa, Jason Alicea, A. R. Akhmerov, David Pekker, Gil Refael, J. Ignacio Cirac, Eugene Demler, Mikhail D. Lukin, and Peter Zoller. Majorana fermions in equilibrium and in driven cold-atom quantum wires. *Phys. Rev. Lett.*, 106:220402, Jun 2011.

[72] Roman M. Lutchyn, Jay D. Sau, and S. Das Sarma. Majorana fermions and a topological phase transition in semiconductor-superconductor heterostructures. *Phys. Rev. Lett.*, 105:077001, Aug 2010.

[73] Yuval Oreg, Gil Refael, and Felix von Oppen. Helical liquids and majorana bound states in quantum wires. *Phys. Rev. Lett.*, 105:177002, Oct 2010.

[74] A Yu Kitaev. Unpaired majorana fermions in quantum wires. *Physics-Uspekhi*, 44:131, 2001.

[75] Janne Ruostekoski, Gerald V. Dunne, and Juha Javanainen. Particle number fractionalization of an atomic fermi-dirac gas in an optical lattice. *Phys. Rev. Lett.*, 88:180401, Apr 2002.

[76] Akbar Jaefari and Eduardo Fradkin. Pair-density-wave superconducting order in two-leg ladders. *Phys. Rev. B*, 85:035104, Jan 2012.

[77] Xiao-Gang Wen. Symmetry-protected topological phases in noninteracting fermion systems. *Phys. Rev. B*, 85:085103, Feb 2012.

[78] Andreas P. Schnyder, Shinsei Ryu, Akira Furusaki, and Andreas W. W. Ludwig. Classification of topological insulators and superconductors in three spatial dimensions. *Phys. Rev. B*, 78:195125, Nov 2008.

[79] Xiao-Liang Qi, Taylor L. Hughes, and Shou-Cheng Zhang. Topological field theory of time-reversal invariant insulators. *Phys. Rev. B*, 78:195424, Nov 2008.

[80] A. Kitaev and C. Laumann. Topological phases and quantum computation. *ArXiv e-prints*, April 2009.

[81] N. Gemelke, E. Sarajlic, and S. Chu. Rotating Few-body Atomic Systems in the Fractional Quantum Hall Regime. *ArXiv e-prints*, July 2010.

[82] Juha Javanainen and Janne Ruostekoski. Optical detection of fractional particle number in an atomic fermi-dirac gas. *Phys. Rev. Lett.*, 91:150404, Oct 2003.

[83] W. S. Bakr, A. Peng, M. E. Tai, R. Ma, J. Simon, J. I. Gillen, S. Fölling, L. Pollet, and M. Greiner. Probing the superfluid-to-mott insulator transition at the single-atom level. *Science*, 329(5991):547–550, 2010.

[84] Jacob F. Sherson, Christof Weitenberg, Manuel Endres, Marc Cheneau, Immanuel Bloch, and Stefan Kuhr. Single-atom-resolved fluorescence imaging of an atomic mott insulator. *Nature*, 467:68–72, 2010.

[85] Christopher N. Varney, Kai Sun, Marcos Rigol, and Victor Galitski. Interaction effects and quantum phase transitions in topological insulators. *Phys. Rev. B*, 82:115125, Sep 2010.

[86] Kai Sun, Zhengcheng Gu, Hosho Katsura, and S. Das Sarma. Nearly flatbands with nontrivial topology. *Phys. Rev. Lett.*, 106:236803, Jun 2011.

[87] Jean Dalibard, Fabrice Gerbier, Gediminas Juzeliūnas, and Patrik Öhberg. *Colloquium* : Artificial gauge potentials for neutral atoms. *Rev. Mod. Phys.*, 83:1523–1543, Nov 2011.

[88] N. R. Cooper. Optical flux lattices for ultracold atomic gases. *Phys. Rev. Lett.*, 106:175301, Apr 2011.

[89] W. P. Su, J. R. Schrieffer, and A. J. Heeger. Solitons in polyacetylene. *Phys. Rev. Lett.*, 42:1698–1701, Jun 1979.

[90] C. W. J. Beenakker. Search for Majorana fermions in superconductors. *ArXiv e-prints*, December 2011.

[91] J. Alicea. New directions in the pursuit of Majorana fermions in solid state systems. *ArXiv e-prints*, February 2012.

[92] Jay D. Sau, Roman M. Lutchyn, Sumanta Tewari, and S. Das Sarma. Generic new platform for topological quantum computation using semiconductor heterostructures. *Phys. Rev. Lett.*, 104:040502, Jan 2010.

[93] Jason Alicea, Yuval Oreg, Gil Refael, Felix von Oppen, and Matthew P. A. Fisher. Non-abelian statistics and topological quantum information processing in 1d wire networks. *Nature Phys.*, 7(5):412–417, 2011.

[94] Y. Tokura and N. Nagaosa. Orbital physics in transition-metal oxides. *Science*, 288(5465):462–468, 2000.

[95] T. Rom, Th. Best, D. van Oosten, U. Schneider, S. Folling, B. Paredes, and I. Bloch. Free fermion antibunching in a degenerate atomic fermi gas released from an optical lattice. *Nature*, 444(7120):733–736, Dec 2006.

[96] A. F. Ho, M. A. Cazalilla, and T. Giamarchi. Quantum simulation of the hubbard model: The attractive route. *Phys. Rev. A*, 79:033620, Mar 2009.

[97] Y.-J. Lin, R. L. Compton, K. Jimenez-Garcia, J. V. Porto, and I. B. Spielman. Synthetic magnetic fields for ultracold neutral atoms. *Nature*, 462(7273):628–632, Dec 2009.

[98] Pengjun Wang, Zeng-Qiang Yu, Zhengkun Fu, Jiao Miao, Lianghui Huang, Shijie Chai, Hui Zhai, and Jing Zhang. Spin-orbit coupled degenerate fermi gases. *Phys. Rev. Lett.*, 109:095301, Aug 2012.

[99] Lawrence W. Cheuk, Ariel T. Sommer, Zoran Hadzibabic, Tarik Yefsah, Waseem S. Bakr, and Martin W. Zwierlein. Spin-injection spectroscopy of a spin-orbit coupled fermi gas. *Phys. Rev. Lett.*, 109:095302, Aug 2012.

[100] Matthias Ölschläger, Georg Wirth, Thorge Kock, and Andreas Hemmerich. Topologically induced avoided band crossing in an optical checkerboard lattice. *Phys. Rev. Lett.*, 108:075302, Feb 2012.

[101] Erhai Zhao and W. Vincent Liu. Orbital order in mott insulators of spinless p-band fermions. *Phys. Rev. Lett.*, 100(16):160403, Apr 2008.

[102] Congjun Wu. Orbital ordering and frustration of p-band mott insulators. *Phys. Rev. Lett.*, 100:200406, May 2008.

[103] Hsiang-Hsuan Hung, Wei-Cheng Lee, and Congjun Wu. Frustrated cooper pairing and f-wave supersolidity in cold-atom optical lattices. *Phys. Rev. B*, 83:144506, Apr 2011.

[104] Zi Cai, Yupeng Wang, and Congjun Wu. Stable fulde-ferrell-larkin-ovchinnikov pairing states in two-dimensional and three-dimensional optical lattices. *Phys. Rev. A*, 83:063621, Jun 2011.

[105] Hoi-Yin Hui, Ryan Barnett, J. V. Porto, and S. Das Sarma. Loop-structure stability of a double-well-lattice bose-einstein condensate. *Phys. Rev. A*, 86:063636, Dec 2012.

[106] K.-K. Ni *et al.* A high phase-space-density gas of polar molecules. *Science*, 322(5899):231, October 2008.

[107] Mingwu Lu, Seo Ho Youn, and Benjamin L. Lev. Trapping ultracold dysprosium: A highly magnetic gas for dipolar physics. *Phys. Rev. Lett.*, 104:063001, Feb 2010.

[108] M. H. G. de Miranda, A. Chotia, B. Neyenhuis, D. Wang, G. Quemener, S. Ospelkaus, J. L. Bohn, J. Ye, and D. S. Jin. Controlling the quantum stereodynamics of ultracold bimolecular reactions. *Nat Phys*, 7(6):502–507, Jun 2011.

[109] Amodsen Chotia, Brian Neyenhuis, Steven A. Moses, Bo Yan, Jacob P. Covey, Michael Foss-Feig, Ana Maria Rey, Deborah S. Jin, and Jun Ye. Long-lived dipolar molecules and feshbach molecules in a 3d optical lattice. *Phys. Rev. Lett.*, 108:080405, Feb 2012.

[110] Cheng-Hsun Wu, Jee Woo Park, Peyman Ahmadi, Sebastian Will, and Martin W. Zwierlein. Ultracold fermionic feshbach molecules of $^{23}Na^{40}K$. *Phys. Rev. Lett.*, 109:085301, Aug 2012.

[111] Erez Berg, Eduardo Fradkin, and Steven A. Kivelson. Charge-4e superconductivity from pair-density-wave order in certain high-temperature superconductors. *Nat Phys*, 5:830, Nov 2009.

[112] Ran Wei and Erich J. Mueller. Pair density waves and vortices in an elongated spin-1/2 fermi gas. *Phys. Rev. Lett.*, 108:245301, Jun 2012.

[113] N. J. Robinson, F. H. L. Essler, E. Jeckelmann, and A. M. Tsvelik. Finite wave vector pairing in doped two-leg ladders. *Phys. Rev. B*, 85:195103, May 2012.

[114] Benjamin K. Stuhl, Matthew T. Hummon, Mark Yeo, Goulven Quemener, John L. Bohn, and Jun Ye. Evaporative cooling of the dipolar hydroxyl radical. *Nature*, 492:396–400, Dec 2012.

[115] X.-L. Deng, D. Porras, and J. I. Cirac. Effective spin quantum phases in systems of trapped ions. *Phys. Rev. A*, 72:063407, Dec 2005.

[116] D. Sénéchal. An introduction to bosonization. *arXiv:cond-mat/9908262*, August 1999.

[117] M. Fabrizio. Role of transverse hopping in a two-coupled-chains model. *Phys. Rev. B*, 48:15838–15860, Dec 1993.

[118] Leon Balents and Matthew P. A. Fisher. Weak-coupling phase diagram of the two-chain hubbard model. *Phys. Rev. B*, 53:12133–12141, May 1996.

[119] Hsiu-Hau Lin, Leon Balents, and Matthew P. A. Fisher. n-chain hubbard model in weak coupling. *Phys. Rev. B*, 56:6569–6593, Sep 1997.

[120] Urs Ledermann and Karyn Le Hur. Phases of the two-band model of spinless fermions in one dimension. *Phys. Rev. B*, 61:2497–2505, Jan 2000.

[121] J. T. Stewart, J. P. Gaebler, and D. S. Jin. Using photoemission spectroscopy to probe a strongly interacting fermi gas. *Nature*, 454:744–747, Aug 2008.

[122] Qijin Chen and K. Levin. Momentum resolved radio frequency spectroscopy in trapped fermi gases. *Phys. Rev. Lett.*, 102:190402, May 2009.

[123] Matthew Killi, Stefan Trotzky, and Arun Paramekanti. Anisotropic quantum quench in the presence of frustration or background gauge fields: A probe of bulk currents and topological chiral edge modes. *Phys. Rev. A*, 86:063632, Dec 2012.

[124] Erez Berg, Eduardo Fradkin, and Steven A. Kivelson. Theory of the striped superconductor. *Phys. Rev. B*, 79(6):064515, Feb 2009.

[125] D. F. Agterberg and H. Tsunetsugu. Dislocations and vortices in pair-density-wave superconductors. *Nat. Phys.*, 4:639, 2008.

[126] Leo Radzihovsky and Ashvin Vishwanath. Quantum liquid crystals in an imbalanced fermi gas: Fluctuations and fractional vortices in larkin-ovchinnikov states. *Phys. Rev. Lett.*, 103(1):010404, Jul 2009.

[127] E. Berg, E. Fradkin, and S. A. Kivelson. Charge-4e superconductivity from pair-density-wave order in certain high-temperature superconductors. *Nat. Phys.*, 5:830, Nov 2009.

[128] Congjun Wu. Competing orders in one-dimensional spin-3/2 fermionic systems. *Phys. Rev. Lett.*, 95(26):266404, Dec 2005.

[129] Peter Fulde and Richard A. Ferrell. Superconductivity in a strong spin-exchange field. *Phys. Rev.*, 135(3A):A550–A563, Aug 1964.

[130] A. I. Larkin and Y. N. Ovchinnikov. Nonuniform state of superconductors. *Zh. Eksp. Teor. Fiz.*, 47:1136–1146, 1964.

[131] H. A. Radovan, N. A. Fortune, T. P. Murphy, S. T. Hannahs, E. C. Palm, S. W. Tozer, and D. Hall. Magnetic enhancement of superconductivity from electron spin domains. *Nature*, 425:51–55, 2003.

[132] A. Bianchi, R. Movshovich, C. Capan, P. G. Pagliuso, and J. L. Sarrao. Possible fulde-ferrell-larkin-ovchinnikov superconducting state in $cecoin_5$. *Phys. Rev. Lett.*, 91(18):187004, Oct 2003.

[133] Meera M. Parish, Stefan K. Baur, Erich J. Mueller, and David A. Huse. Quasi-one-dimensional polarized fermi superfluids. *Phys. Rev. Lett.*, 99(25):250403, Dec 2007.

[134] E. W. Carlson, D. Orgad, S. A. Kivelson, and V. J. Emery. Dimensional crossover in quasi-one-dimensional and high-T_c superconductors. *Phys. Rev. B*, 62:3422–3437, Aug 2000.

[135] S. Biermann, A. Georges, A. Lichtenstein, and T. Giamarchi. Deconfinement transition and luttinger to fermi liquid crossover in quasi-one-dimensional systems. *Phys. Rev. Lett.*, 87:276405, Dec 2001.

[136] A. F. Ho, M. A. Cazalilla, and T. Giamarchi. Deconfinement in a 2d optical lattice of coupled 1d boson systems. *Phys. Rev. Lett.*, 92:130405, Apr 2004.

[137] C. Kollath, Julia S. Meyer, and T. Giamarchi. Dipolar bosons in a planar array of one-dimensional tubes. *Phys. Rev. Lett.*, 100:130403, Apr 2008.

[138] P. M. Chaikin and T. C. Lubensky. *Principles of Condensed Matter Physics*. Cambridge University Press, 1995.

[139] Frank Krüger and Stefan Scheidl. Nonuniversal ordering of spin and charge in stripe phases. *Phys. Rev. Lett.*, 89(9):095701, Aug 2002.

[140] K. V. Samokhin. Goldstone modes in larkin-ovchinnikov-fulde-ferrell superconductors. *Phys. Rev. B*, 81(22):224507, Jun 2010.

[141] John Bardeen, R. Kümmel, A. E. Jacobs, and L. Tewordt. Structure of vortex lines in pure superconductors. *Phys. Rev.*, 187(2):556–569, Nov 1969.

[142] Shigemasa Matsuo, Seiji Higashitani, Yasushi Nagato, and Katsuhiko Nagai. Phase diagram of the fulde-ferrell-larkin-ovchinnikov state in a three-dimensional superconductor. *J.Phys.Soc.Jpn.*, 67:280–289, 1998.

[143] G. Orso. Attractive fermi gases with unequal spin populations in highly elongated traps. *Phys. Rev. Lett.*, 98(7):070402, Feb 2007.

[144] Nobukatsu Yoshida and S.-K. Yip. Larkin-ovchinnikov state in resonant fermi gas. *Phys. Rev. A*, 75(6):063601, Jun 2007.

[145] Erhai Zhao and W. Vincent Liu. Theory of quasi-one-dimensional imbalanced fermi gases. *Phys. Rev. A*, 78(6):063605, Dec 2008.

[146] Oliver Penrose and Lars Onsager. Bose-einstein condensation and liquid helium. *Phys. Rev.*, 104(3):576–584, Nov 1956.

[147] M. W. Meisel. Supersolid 4he: an overview of past searches and future possibilities. *Physica B*, pages 121–128, 1992.

[148] C. N. Yang. Concept of off-diagonal long-range order and the quantum phases of liquid he and of superconductors. *Rev. Mod. Phys.*, 34:694–704, Oct 1962.

[149] G. V. Chester. Speculations on bose-einstein condensation and quantum crystals. *Phys. Rev. A*, 2:256–258, Jul 1970.

[150] A. J. Leggett. Can a solid be "superfluid"? *Phys. Rev. Lett.*, 25:1543–1546, Nov 1970.

[151] Tony Leggett. Superfluidity in a crystal? *Science*, 305(5692):1921, Sep 2004.

[152] E. Kim and M. H. W. Chan. Observation of superflow in solid helium. *Science*, 305:1941, January 2004.

[153] E. Kim and M. H. W. Chan. Probable observation of a supersolid helium phase. *Nature*, 427:225, January 2004.

[154] Nikolay Prokof'ev. What makes a crystal supersolid. *Advances in Physics*, 56(2):381–402, March 2007.

[155] A. Micheli *et al.* Cold molecules in two-dimensional traps. *Phys. Rev. A*, 76(4):043604, Oct 2007.

[156] F. Cinti, P. Jain, M. Boninsegni, A. Micheli, P. Zoller, and G. Pupillo. Supersolid droplet crystal in a dipole-blockaded gas. *Phys. Rev. Lett.*, 105(13):135301, Sep 2010.

[157] G. Pupillo *et al.* Strongly correlated gases of rydberg-dressed atoms: Quantum and classical dynamics. *Phys. Rev. Lett.*, 104(22):223002, Jun 2010.

[158] M. W. Mancini, G. D. Telles, A. R. L. Caires, V. S. Bagnato, and L. G. Marcassa. Observation of ultracold ground-state heteronuclear molecules. *Phys. Rev. Lett.*, 92:133203, Apr 2004.

[159] D. Wang *et al.* Photoassociative production and trapping of ultracold krb molecules. *Phys. Rev. Lett.*, 93(24):243005, Dec 2004.

[160] C. Ospelkaus *et al.* Ultracold heteronuclear molecules in a 3d optical lattice. *Phys. Rev. Lett*, 97(12):120402, Sep 2006.

[161] S. Ospelkaus, A. Pe/'er, K.-K. Ni, J. J. Zirbel, B. Neyenhuis, S. Kotochigova, P. S. Julienne, J. Ye, and D. S. Jin. Efficient state transfer in an ultracold dense gas of heteronuclear molecules. *Nature Physics*, 4:622, Aug 2008.

[162] D. Wang, B. Neyenhuis, M. H. G. de Miranda, K.-K. Ni, S. Ospelkaus, D. S. Jin, and J. Ye. Direct absorption imaging of ultracold polar molecules. *Phys. Rev. A*, 81:061404, Jun 2010.

[163] T. Lahaye, C. Menotti, L. Santos, M. Lewenstein, and T. Pfau. The physics of dipolar bosonic quantum gases. *Rep. Prog. Phys*, 72(12):126401, Nov. 2009.

[164] Yves Pomeau and Sergio Rica. Dynamics of a model of supersolid. *Phys. Rev. Lett.*, 72(15):2426–2429, Apr 1994.

[165] S. Giovanazzi, D. O'Dell, and G. Kurizki. Density modulations of bose-einstein condensates via laser-induced interactions. *Phys. Rev. Lett.*, 88(13):130402, Mar 2002.

[166] Uwe R. Fischer. Stability of quasi-two-dimensional bose-einstein condensates with dominant dipole-dipole interactions. *Phys. Rev. A*, 73(3):031602, Mar 2006.

[167] O. Dutta, R. Kanamoto, and P. Meystre. Fermionic stabilization and density-wave ground state of a polar condensate. *Phys. Rev. Lett.*, 99(11):110404, Sep 2007.

[168] O. Dutta, R. Kanamoto, and P. Meystre. Stability of the density-wave state of a dipolar condensate in a pancake-shaped trap. *Phys. Rev. A*, 78(4):043608, Oct 2008.

[169] Leo Radzihovsky and Sungsoo Choi. p-wave resonant bose gas: A finite-momentum spinor superfluid. *Phys. Rev. Lett.*, 103(9):095302, Aug 2009.

[170] N. Henkel, R. Nath, and T. Pohl. Three-dimensional roton excitations and supersolid formation in rydberg-excited bose-einstein condensates. *Phys. Rev. Lett.*, 104(19):195302, May 2010.

[171] Kaushik Mitra, C. J. Williams, and C. A. R. Sa de Melo. Hexatic, wigner crystal, and superfluid phases of dipolar bosons,arxiv:cond-mat/0903.4655v1. arXiv:0903.4655, Mar 2009.

[172] Xiaopeng Li, W. Vincent Liu, and Chungwei Lin. Bose-einstein supersolid phase for a type of momentum-dependent interaction. *Phys. Rev. A*, 83:021602, Feb 2011.

[173] V. N. Popov. *Functional Integrals and Collective Excitations*. Cambridge University Press, Cambridge, 1987.

[174] Xiao-Gang Wen. *Quantum Field Theory of Many-Body Systems*. Oxford, Oxford, 2007.

[175] E. J. Mueller *et al.* Fragmentation of bose-einstein condensates. *Phys. Rev.A*, 74(3):033612, Sep 2006.

[176] Kazumi Maki and Xenophon Zotos. Static and dynamic properties of a two-dimensional wigner crystal in a strong magnetic field. *Phys. Rev. B*, 28(8):4349–4356, Oct 1983.

[177] A. A. Koulakov, M. M. Fogler, and B. I. Shklovskii. Charge density wave in two-dimensional electron liquid in weak magnetic field. *Phys. Rev. Lett.*, 76(3):499–502, Jan 1996.

[178] P. Nozieres and F. Gallet. The roughening transition of crystal surfaces. i. static and dynamic renormalization theory, crystal shape and facet growth. *Journal Physics France*, 48:353–367, 1987.

[179] John B. Kogut. An introduction to lattice gauge theory and spin systems. *Rev. Mod. Phys.*, 51:659–713, Oct 1979.